Electronic Supplementary Material (ESI) for Dalton Transactions.

Supporting Information

Facile generation of iridium $PC_{carbene}P$ pincer complexes via water elimination from an alcohol proligand

Simon Sung, Rowan D. Young*

[a] *Department of Chemistry, National University of Singapore, 3 Science Drive 3, Singapore 117543*

**Corresponding Author*

Table of Contents

Experimental

General information

All syntheses were carried out in N_2 atmosphere using a glovebox or with standard Schlenk techniques. All reactions were performed in glassware that was oven-dried for at least 12 h. Ligand **1**,[1] **1-H$_2$**,[2] **1a**,[3] **1b**,[3] $[IrCl(COD)]_2$,[4] $[IrCl(COD)(PPh_3)]$,[5] and $Na[BAr^F_4]$[6] were prepared according to reported methods. $[Ir(COD)_2][BAr^F_4]$ was prepared using a similar method for the synthesis of analogous rhodium complexes.[7] Toluene, DCM, and *n*-hexane were dried over activated alumina using a LC Technology Solutions Inc. SP-1 solvent purification system and then deoxygenated prior to use. CD_2Cl_2 and C_6D_6 used was stirred over CaH_2 at room temperature under a nitrogen atmosphere overnight prior to distillation under reduced pressure and storage over 4 Å molecular sieves. NMR spectra were recorded using a Bruker AV500 spectrometer. All chemical shifts are quoted in parts per million (ppm) relative to $SiMe_4$ (^{1}H, ^{13}C) or H_3PO_4 (85%) (^{31}P). Coupling constant *J* values are given in Hz. ^{13}C and ^{31}P NMR analyses were performed with ^{1}H decoupling. HRMS (ESI-TOF) spectra were obtained using an Agilent Technologies 6230 TOF LC/MS. Single crystal was measured at low temperature (T = 100K) on a four circles goniometer Kappa geometry Bruker AXS D8 Venture equipped with a Photon 100 CMOS active pixel sensor detector using Copper (λ = 1.54178 Å) or Molybdenum (λ = 0.71073 Å) monochromatized X-Ray radiation sources.

Reaction between complex 7a and Na[BAr$^F_4$] that formed [Ir(CO)(PPh$_3$)$_3$][BAr$^F_4$]

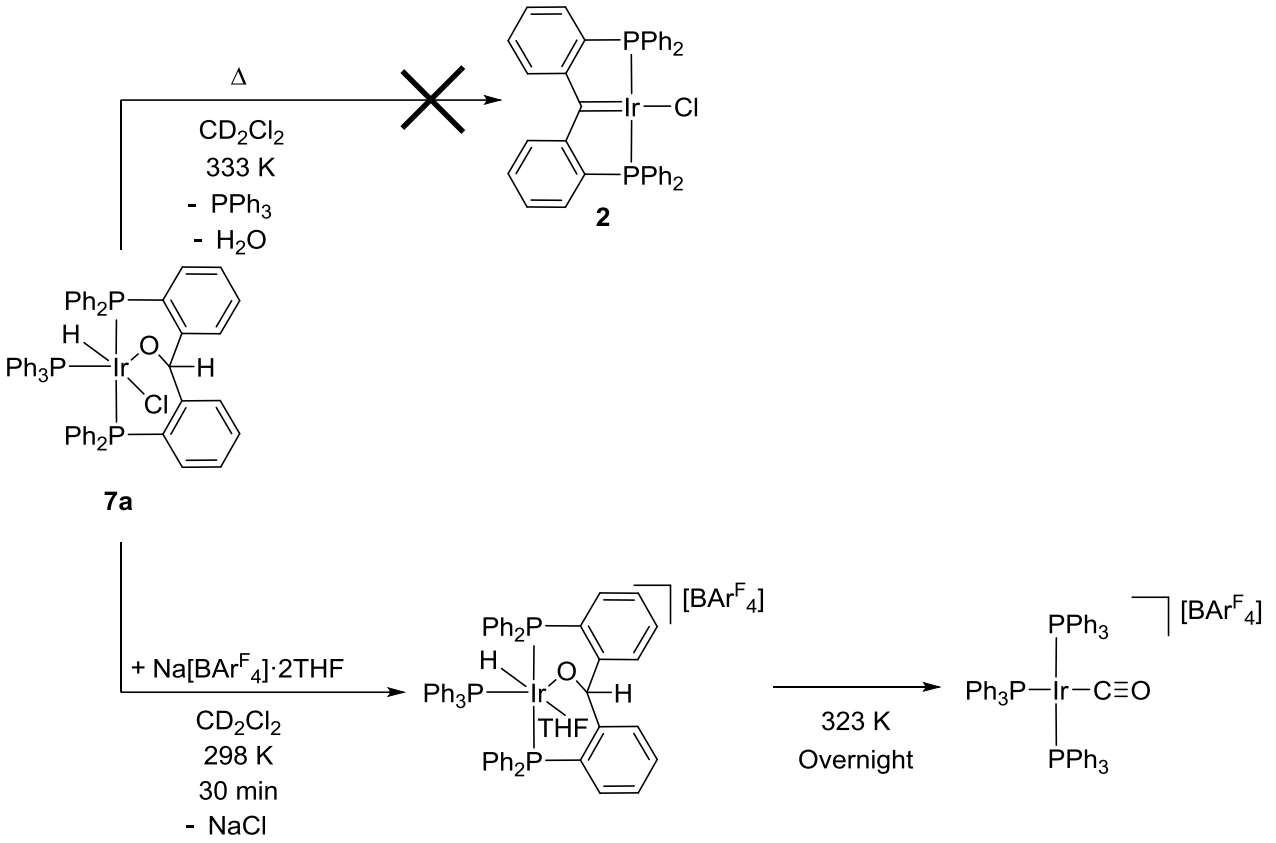

A solution of complex **7a** (10.4 mg, 0.01 mmol) in CD_2Cl_2 (0.6 mL) in a screw cap NMR tube was heated to 333 K for 18 h. Analysis by $^{31}P\{^1H\}$ NMR spectroscopy indicated that no conversion of **7a** had occurred. The NMR tube was taken into a glovebox and Na[BAr$^F_4$]·2THF (10.3 mg, 0.01 mmol) was then added at room temperature and shaken well to mix. $^{31}P\{^1H\}$ NMR analyses after 30 min at room temperature revealed the formation of a single species, which was not the desired complex **3** (presumably the corresponding chloride abstracted cationic hydrido Ir complex was present:

δ_H (500 MHz, CD_2Cl_2, 298 K) -19.02 (1H, td, $J_{2,\,H\text{-}P}$ 18.1, $J_{2,\,H\text{-}P}$ 15.3, Ir-*H*), 5.06 (1H, d, $J_{4,\,H\text{-}P}$ 12.8, 1H, methine C-*H*), 6.60 – 7.96 (55H, m, Ar-*H*).

δ_P (202 MHz, CD_2Cl_2, 298 K) -1.6 (1P, t, $J_{2,\,P\text{-}P}$ 12.3, *P*Ph$_3$), 0.7 (2P, d, $J_{2,\,P\text{-}P}$ 12.3, POP pincer *P*'s).

When heated the solution was at 323 K overnight, this species was quantitatively converted to [Ir(CO)(PPh$_3$)$_3$][BAr$^F_4$], with $^{31}P\{^1H\}$ NMR spectroscopic evidence in agreement with the literature for [Ir(CO)(PPh$_3$)$_3$][OTf].[8]

δ_H (500 MHz, CD_2Cl_2, 298 K) 6.93 – 7.10 (12H, m, Ar-*H*), 7.22 – 7.31 (14H, m, Ar-*H*), 7.34 – 7.46 (18H, m, Ar-*H*), 7.56 (4H, s, [BAr^F_4] Ar-*H*), 7.73 (8H, s, [BAr^F_4] Ar-*H*).

δ_P (202 MHz, CD_2Cl_2, 298 K) 15.4 (2P, d, $J_{2,\,P\text{-}P}$ 29.6, *P*Ph_3), 18.0 (1P, t, $J_{2,\,P\text{-}P}$ 29.6, *P*Ph_3).

Attempted conversion of complex 7b to complexes 2 and 3

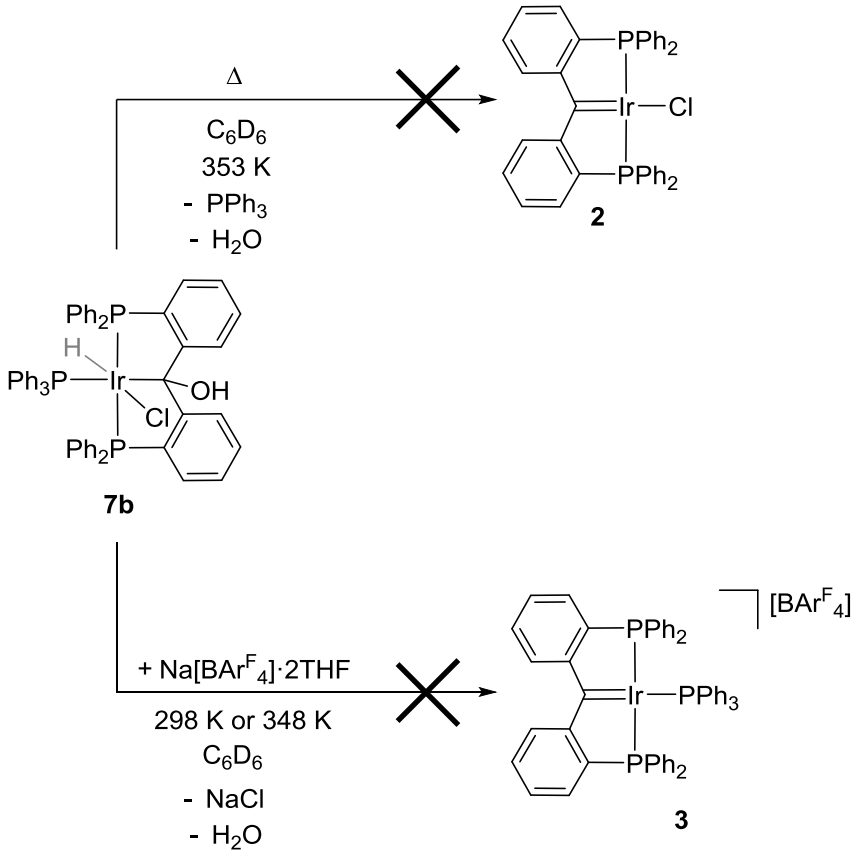

A solution of complex **7b** (10.4 mg, 0.01 mmol) in C_6D_6 (0.6 mL) in a screw cap NMR tube was heated to 353 K for 5 h. Analysis by ^{1}H and ^{31}P{^{1}H} NMR spectroscopy indicated that no conversion of **7b** had occurred. The NMR tube was taken into a glovebox and Na[BAr^F_4]·2THF (10.3 mg, 0.01 mmol) was then added at room temperature and shaken well to mix. NMR analyses after allowing the mixture to react at room temperature and also with heating to 348 K revealed the formation of several unknown species, none of which were the desired product **3**.

NMR spectroscopic analyses of reaction intermediates in the formation of 2

[IrCl(COD)]$_2$ (13.4 mg, 0.020 mmol) and compound **1**, **1a**, **1b** or **1-H₂** (22.1 mg, 0.040 mmol) were added into a J. Young valve NMR tube (see Figure S30 and Figure S28 for the structures of **1a** and **1b** respectively).

CD_2Cl_2 (0.6 mL) was vacuum transferred into the NMR tube using a liquid nitrogen bath, and then the NMR tube was filled with a N_2 or H_2 (≈ 4 atm) atmosphere. The CD_2Cl_2 solvent was thawed immediately prior to placing the NMR tube into a NMR spectrometer set at the desired temperature for analyses. Intermediates **I**, **II**, **VI** and **VII** were all characterised by NMR spectroscopy but only **VII** was isolated.

Intermediate **I**:

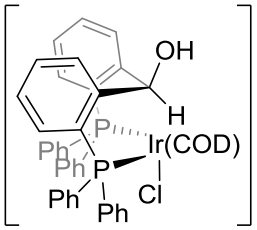

I

δ_H (500 MHz, CD_2Cl_2, 263 K) 1.32 – 1.62 (4H, m, COD *H*), 2.02 (4H, s, COD *H*), 3.52 (4H, s, COD *H*), 5.91 (1H, d, $J_{3,\ H\text{-}H}$ 3.4, methine C-*H*), 6.58 (2H, t, *J* 8.0, Ar-*H*), 6.65 (3H, t, *J* 8.1, Ar-*H*), 7.03 (2H, t, *J* 7.4, Ar-*H*), 7.14 – 7.36 (13H, m, Ar-*H*), 7.44 – 7.48 (5H, m, Ar-*H*), 7.64 – 7.73 (4H, m, Ar-*H*), 11.07 (1H, d, $J_{3,\ H\text{-}H}$ 3.4, O-*H*).

δ_P (202 MHz, CD_2Cl_2, 263 K) -6.1 (2P, s, PCP pincer *P*).

Intermediate **II**:

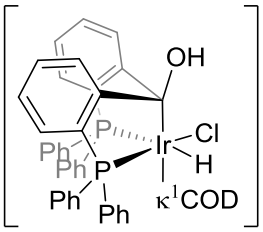

II

Selected δ_H (500 MHz, CD_2Cl_2, 268 K) -8.18 (1H, ddd, $J_{2,\ H\text{-}P}$ 93.3, $J_{2,\ H\text{-}P}$ 9.8, $J_{4,\ H\text{-}H}$ 2.5 Hz, Ir-*H*), 0.82 – 0.93 (1H, m, COD *H*), 2.22 – 2.49 (6H, m, COD *H*), 3.07 – 3.19 (1H, m, COD *H*), 4.07 – 4.15 (1H, m, COD *H*), 4.29 – 4.43 (1H, m, COD *H*), 5.00 – 5.11 (1H, m, COD *H*), 6.09 – 6.19 (1H, m, COD *H*), 6.52 (2H, dd, *J* 10.3, *J* 7.7, Ar-*H*), 8.03 (1H, dd, *J* 8.0, *J* 2.7, Ar-*H*), 8.28 (1H, dd, *J* 7.9, *J* 3.4, Ar-*H*).

δ_P (202 MHz, CD_2Cl_2, 268 K) 7.5 (1P, d, $J_{2,\ P\text{-}P}$ 17.2, *P trans* to Ir-H), 19.2 (1P, d, $J_{2,\ P\text{-}P}$ 17.2, *P cis* to Ir-H).

Intermediate **VI**:

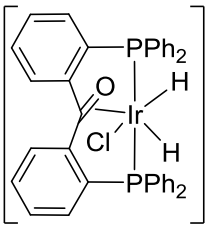

VI

Selected δ_H (500 MHz, CD_2Cl_2, 259 K) -12.57 (2H, t, $J_{2,\,H\text{-}P}$ 12.3, Ir-*H*).

Selected δ_C from HMBC (126 MHz, CD_2Cl_2, 259 K) 132.1.

δ_P (202 MHz, CD_2Cl_2, 259 K) 18.8 (2P, s, PCP pincer *P*).

Complex **VII·CH_2Cl_2**:

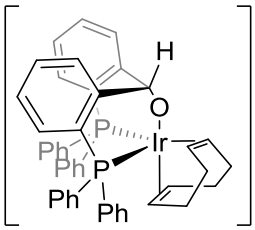

VII

Within one hour of mixing $[IrCl(COD)]_2$ and compound **1** or **1b** in CH_2Cl_2 or CD_2Cl_2 respectively, as described above, X-ray quality crystals had precipitated. To isolate, the crystals of **VII·CH_2Cl_2** were filtered, washed with small quantities of DCM (2 x 2 mL) and then dried under vacuum (23 mg, 61% yield when ligand **1** was used). When ligand **1b** was used in the reaction, the quantity of crystals appeared to be greater than when ligand **1** was used. This indicated that pathway B may be more favoured than pathway A in the presence of a methine C-D bond in the pincer ligand, which suggests a notable kinetic isotope effect was present for the activation of this bond.

Found: C, 59.4; H, 4.5. Calc. for $C_{105}H_{70}BF_{24}IrP_4\cdot CH_2Cl_2$: C, 59.0; H, 4.6%.

δ_H (500 MHz, $CDCl_3$, 298 K) 1.54 – 1.82 (6H, m, COD *H*), 2.31 – 2.47 (2H, m, COD *H*), 2.78 (2H, s (br), COD *H*), 3.13 – 3.31 (2H, m, COD *H*), 5.21 (1H, s, methine C-*H*), 5.30 (2H, s, CH_2Cl_2 solvate), 6.49 – 6.57 (2H, m, Ar-*H*), 6.83 – 6.92 (6H, m, Ar-*H*), 7.03 – 7.08 (2H, m, Ar-*H*), 7.10 – 7.24 (8H, m, Ar-*H*), 7.32 – 7.39 (6H, m, Ar-*H*), 7.57 – 7.66 (4H, m, Ar-*H*).

δ_P (202 MHz, CD_2Cl_2, 298 K) -11.1 (2P, s, PCP pincer *P*).

δ_C (126 MHz, CD_2Cl_2, 298 K) 30.3 (s, COD *C*), 35.7 (s, COD *C*), 53.5 (s, CH_2Cl_2 solvate), 61.6 (d, *J* 12.5, COD *C*), 62.0 (s, COD *C*), 79.6 (t, $J_{3,\,C\text{-}P}$ 5.7, methine *C*), 125.8 (t, *J* 2.7, Ar-*C*), 127.6 (t, *J* 4.5, Ar-*C*), 128.6

(t, *J* 5.8, Ar-*C*), 129.1 (s, Ar-*C*), 129.9 (t, *J* 4.1, Ar-*C*), 132.9 (t, *J* 5.3, Ar-*C*), 133.4 (t, *J* 5.9, Ar-*C*), 133.4 (s), 152.5 (d, *J* 6.2, Ar-*C*).

HRMS (ESI-TOF) m/z: $[M]^+$ Calcd for $C_{45}H_{41}IrOP_2$ 852.2259; Found 852.2263.

Addition of HCl to complex VII·CH_2Cl_2

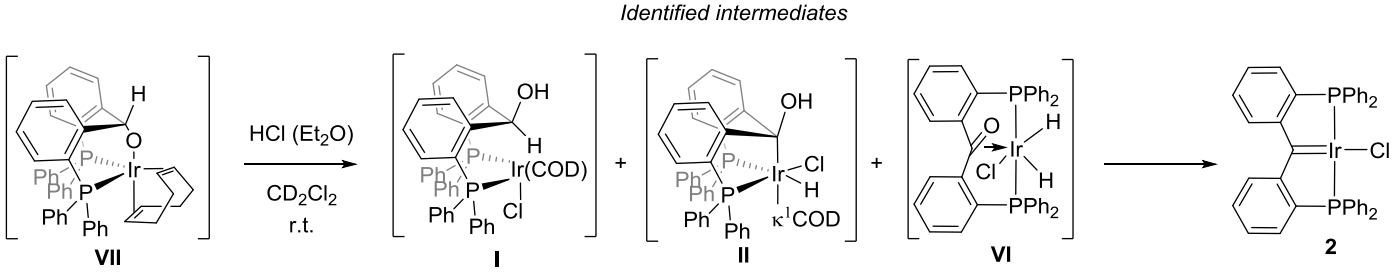

Complex **VII·CH_2Cl_2** (8.5 mg, 0.009 mmol) and CD_2Cl_2 (0.6 mL) were added into a NMR tube, sealed with a septum and opentop screw cap and brought outside the glovebox. HCl in Et_2O (5 µL, 0.010 mmol, 2 M) was added through the septum at room temperature, the NMR tube was shaken vigourously and then immediately analysed by ^1H and $^{31}P\{^1H\}$ NMR spectroscopy.

NMR Spectra of complex 2

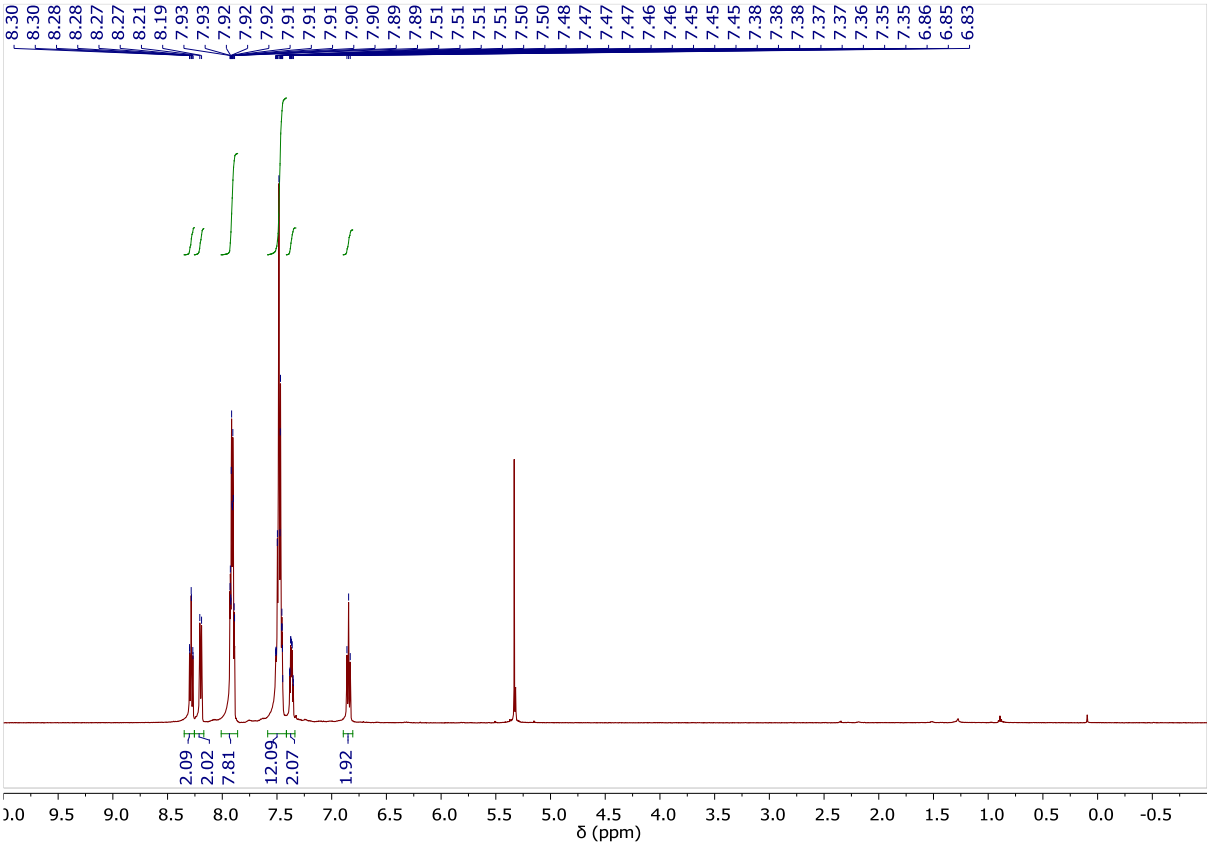

Figure S1 ^{1}H NMR of complex **2** in CD_2Cl_2 at 298 K.

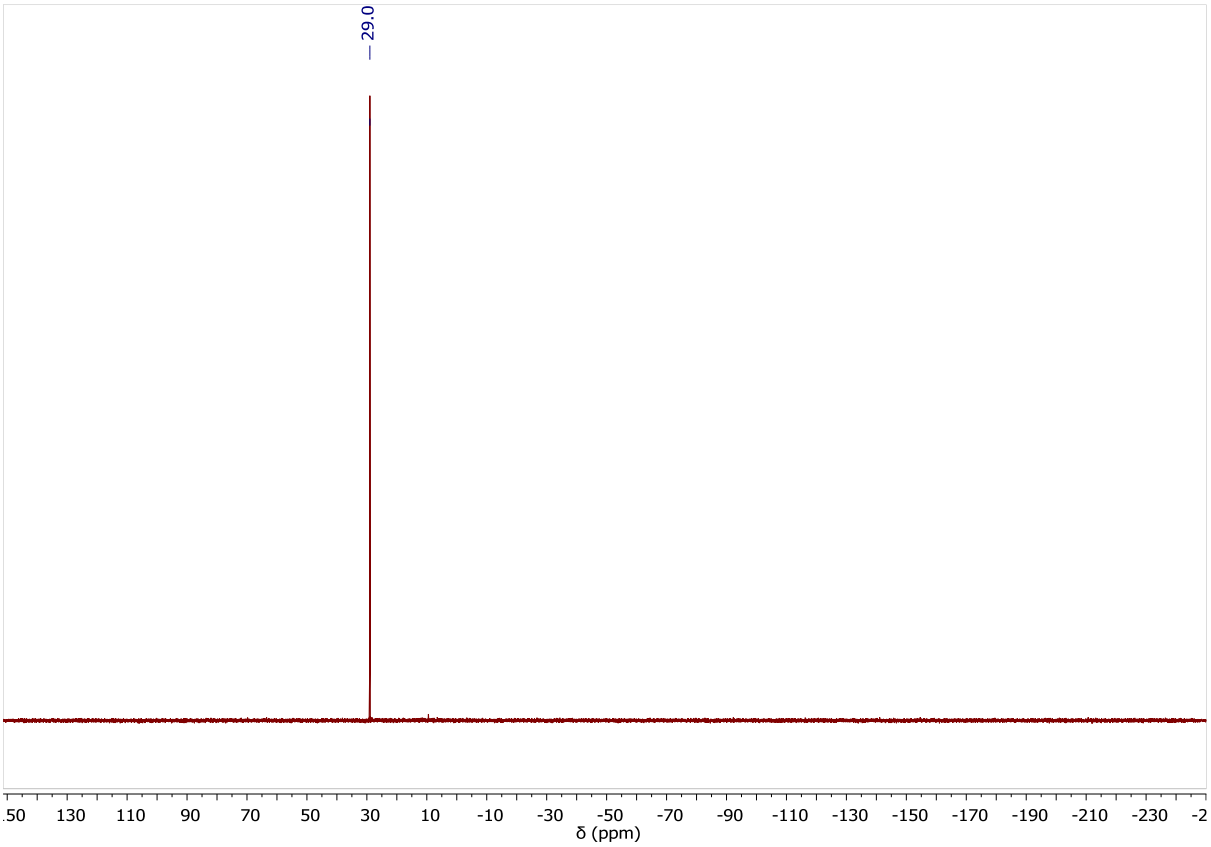

Figure S2 $^{31}P\{^{1}H\}$ NMR of complex **2** in CD_2Cl_2 at 298 K.

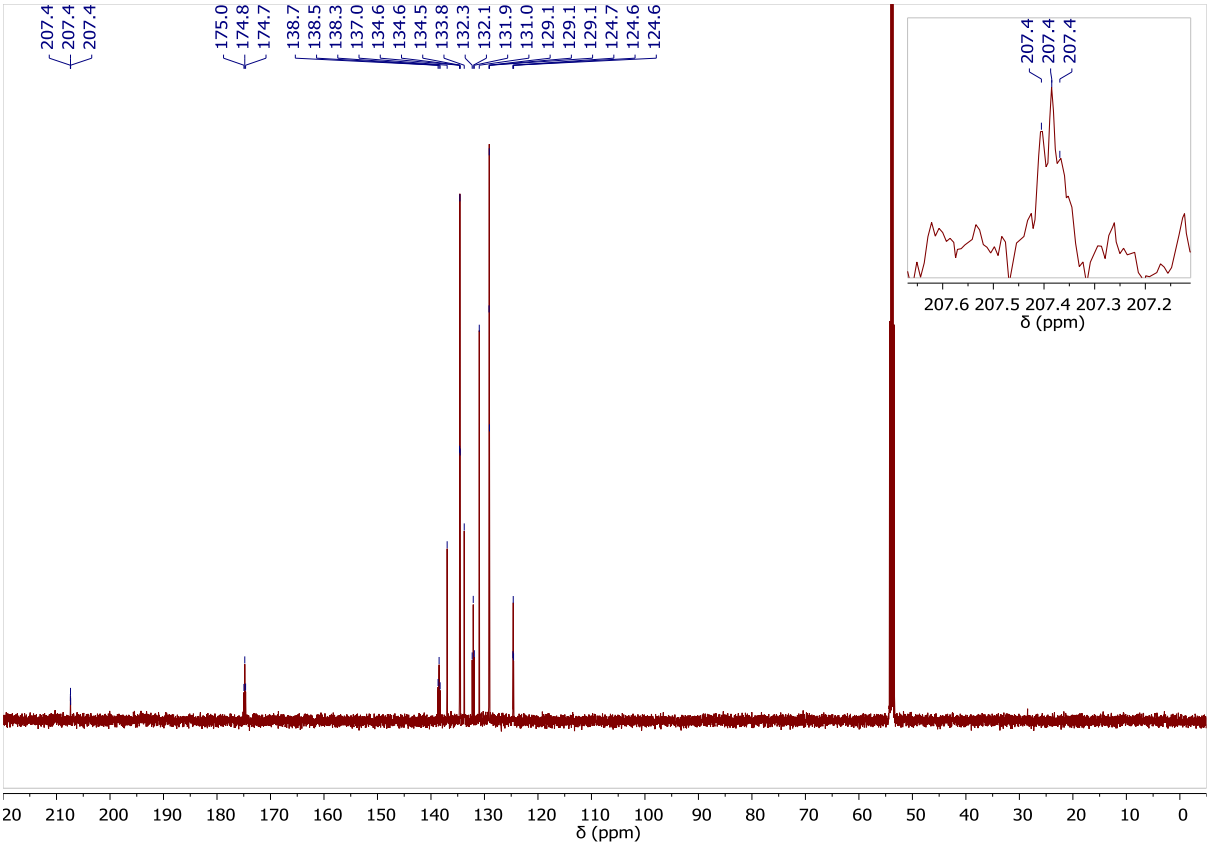

Figure S3 $^{13}C\{^{1}H\}$ NMR of complex **2** in CD_2Cl_2 at 298 K. Inset shows zoomed in spectrum of the Ir=*C* resonance.

NMR Spectra of complex 3

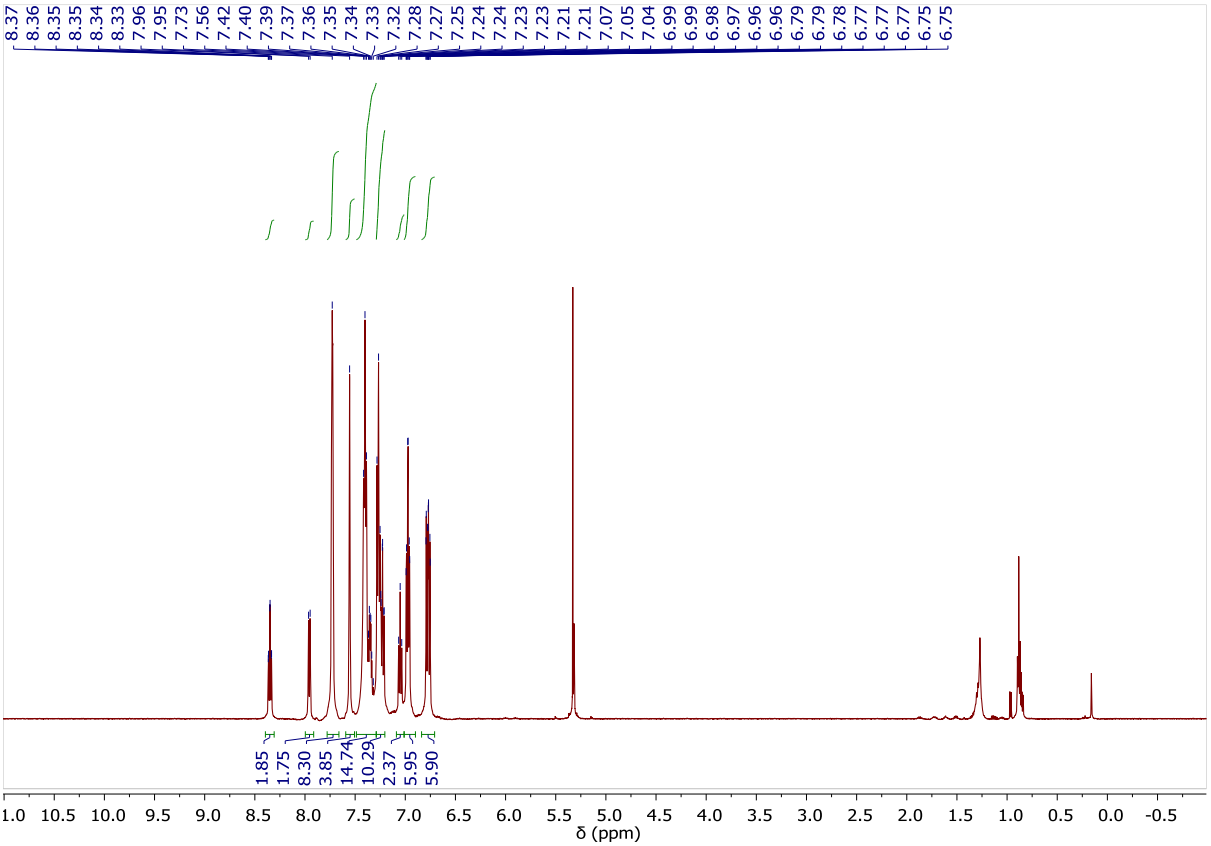

Figure S4 ^{1}H NMR of complex **3** in CD_2Cl_2 at 298 K. *n*-Hexane and silicone grease contaminants present.

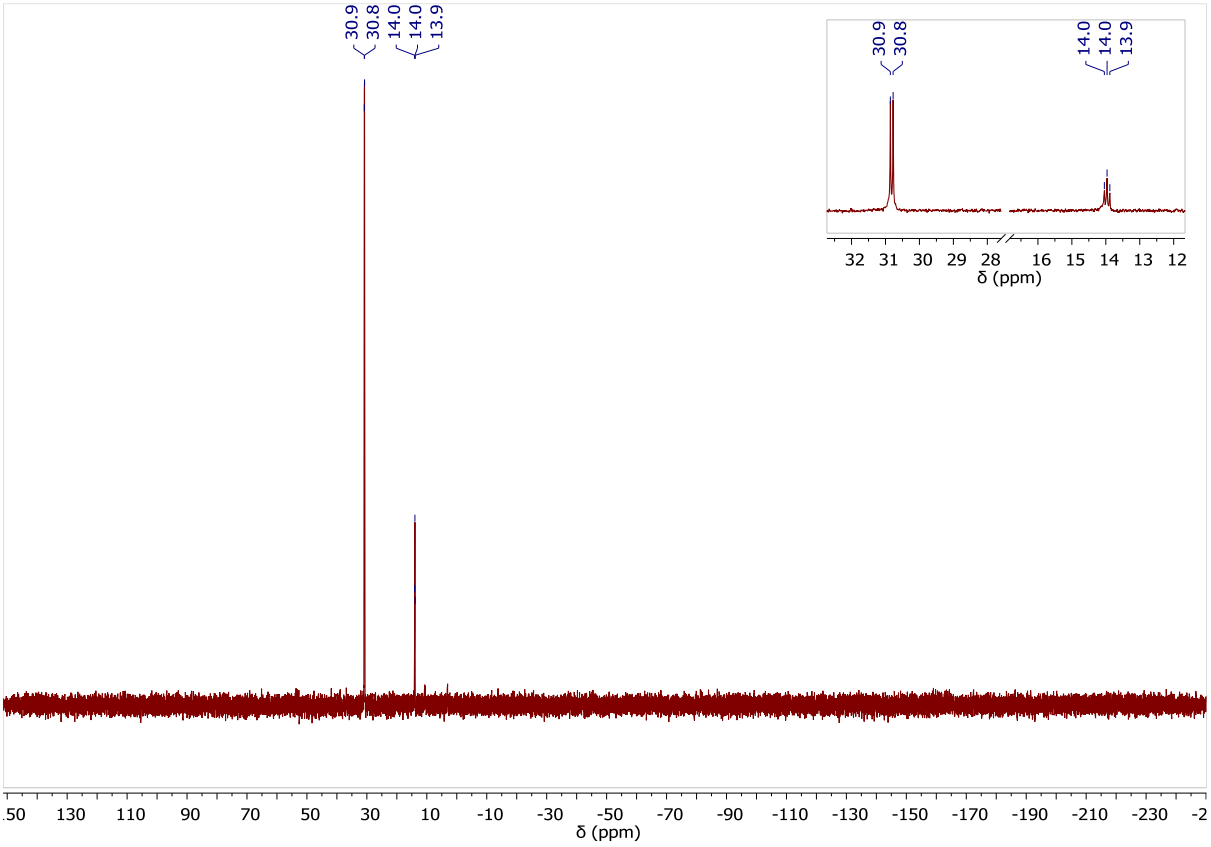

Figure S5 $^{31}P\{^{1}H\}$ NMR of complex **3** in CD_2Cl_2 at 298 K. Inset shows zoomed in spectrum.

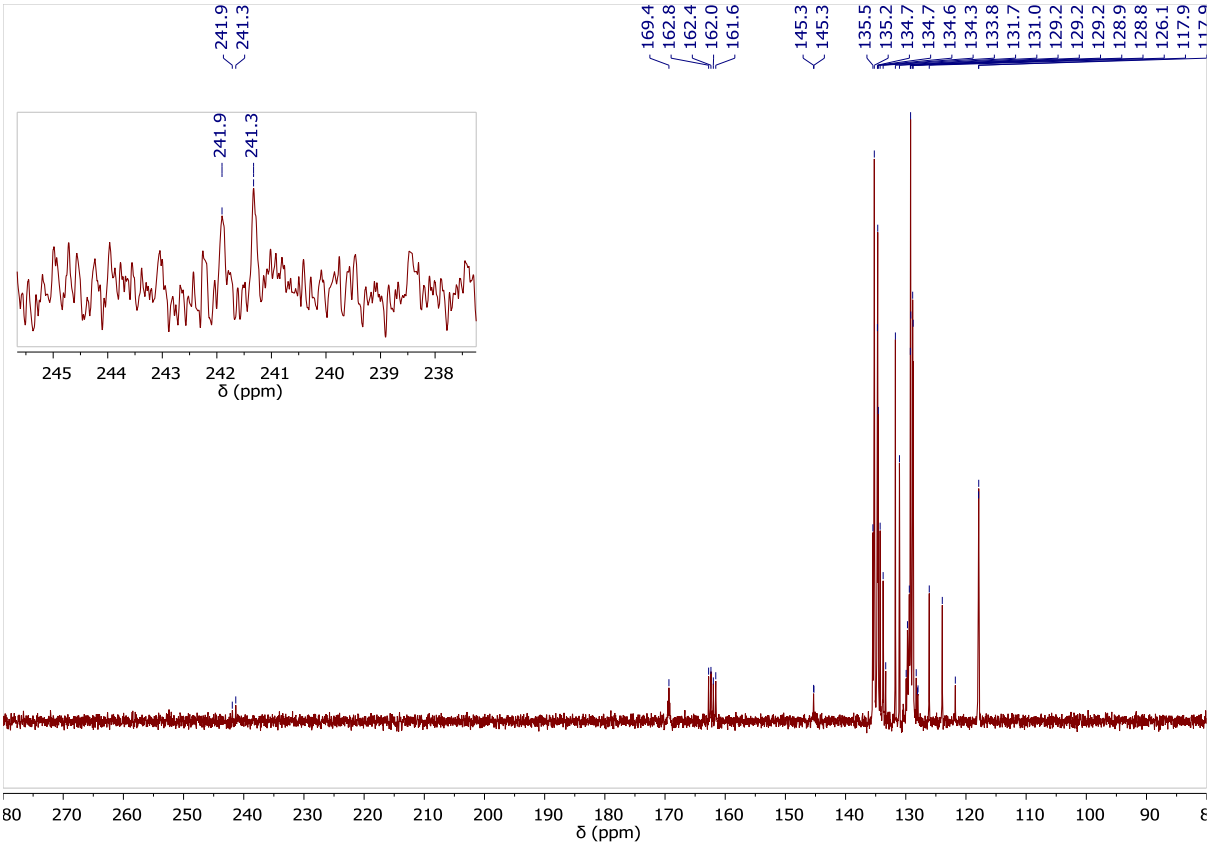

Figure S6 $^{13}C\{^{1}H\}$ NMR of complex **3** in CD_2Cl_2 at 298 K. Inset shows zoomed in spectrum of the Ir=*C* resonance

NMR Spectra of complex 4

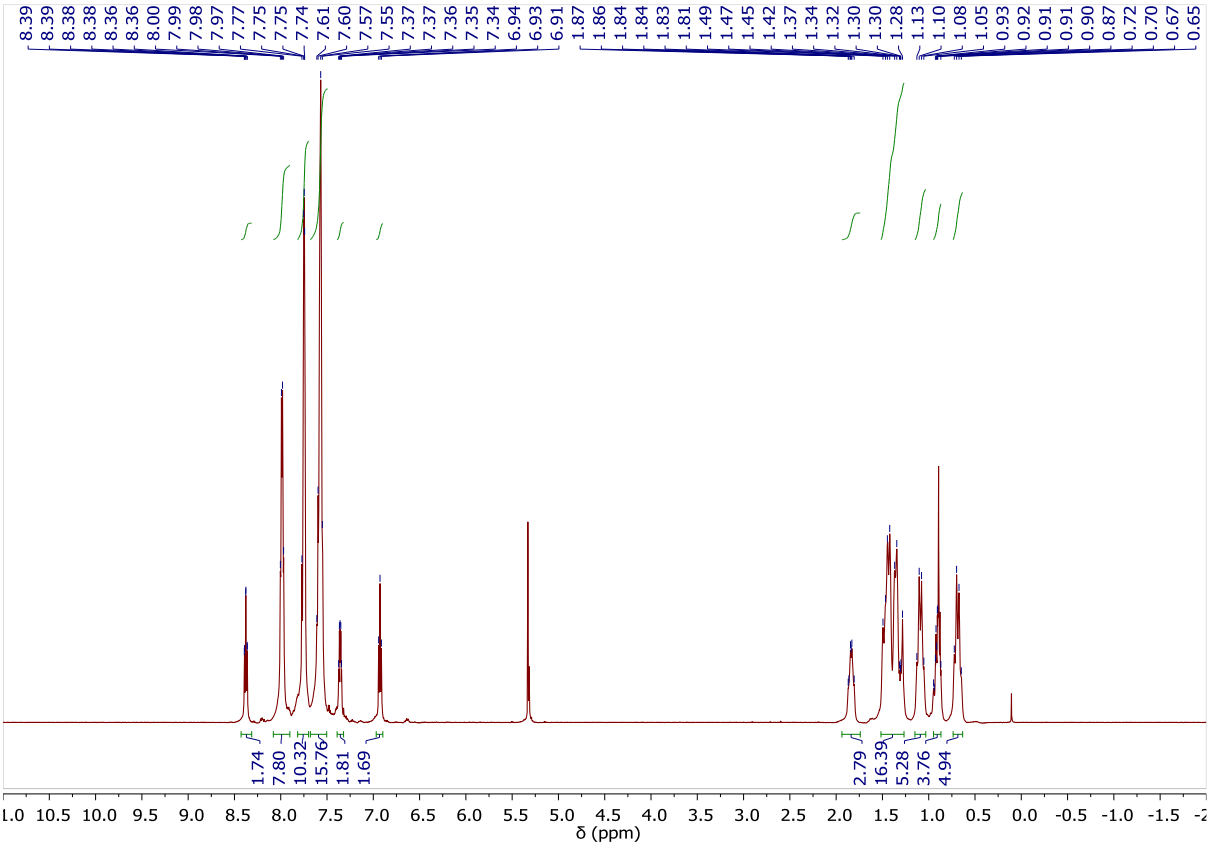

Figure S7 ^{1}H NMR of complex **4** in CD_2Cl_2 at 298 K. Silicone grease contaminant present.

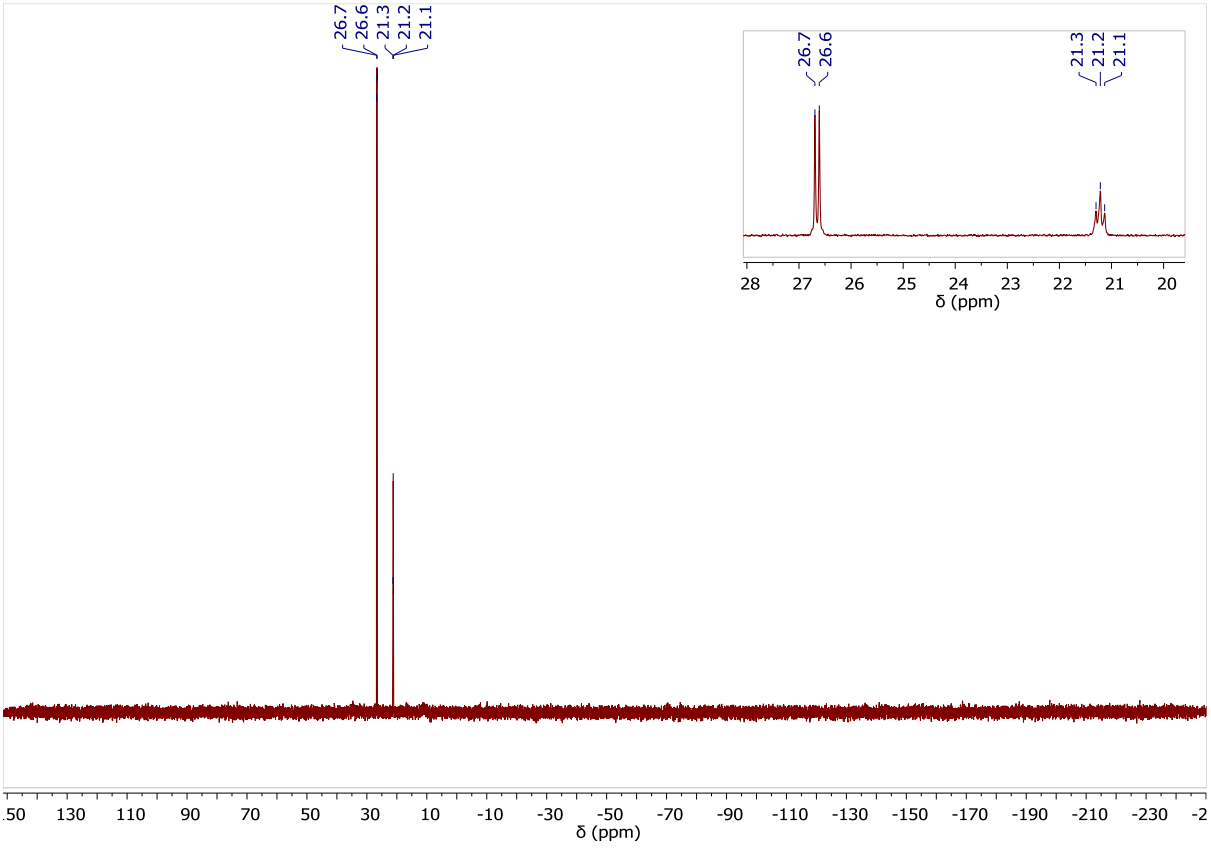

Figure S8 $^{31}P\{^{1}H\}$ NMR of complex **4** in CD_2Cl_2 at 298 K. Inset shows zoomed in spectrum.

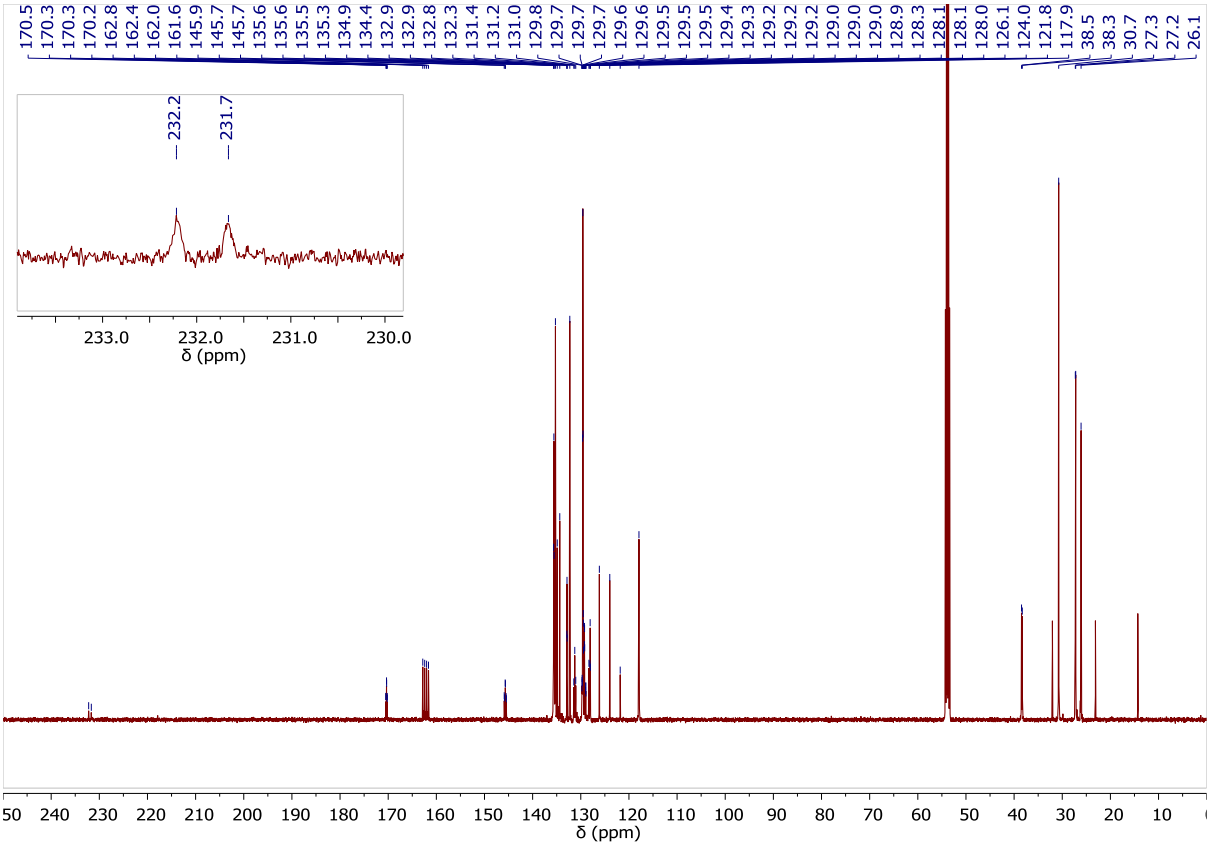

Figure S9 $^{13}C\{^{1}H\}$ NMR of complex **4** in CD_2Cl_2 at 298 K. *n*-Hexane contaminant present. Inset shows zoomed in spectrum of the Ir=*C* resonance

NMR Spectra of complex 5

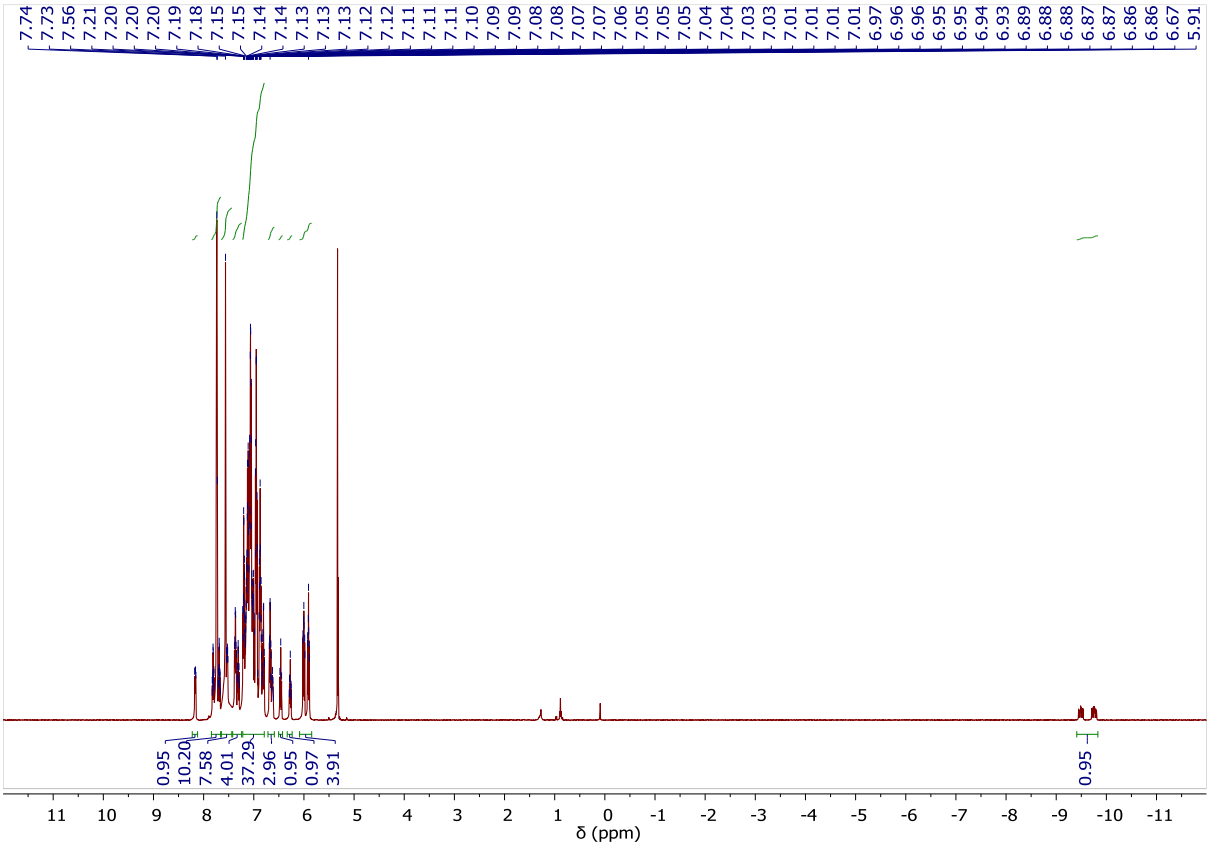

Figure S10 ^{1}H NMR of complex **5** in CD_2Cl_2 at 298 K. *n*-Hexane and silicone grease contaminants present.

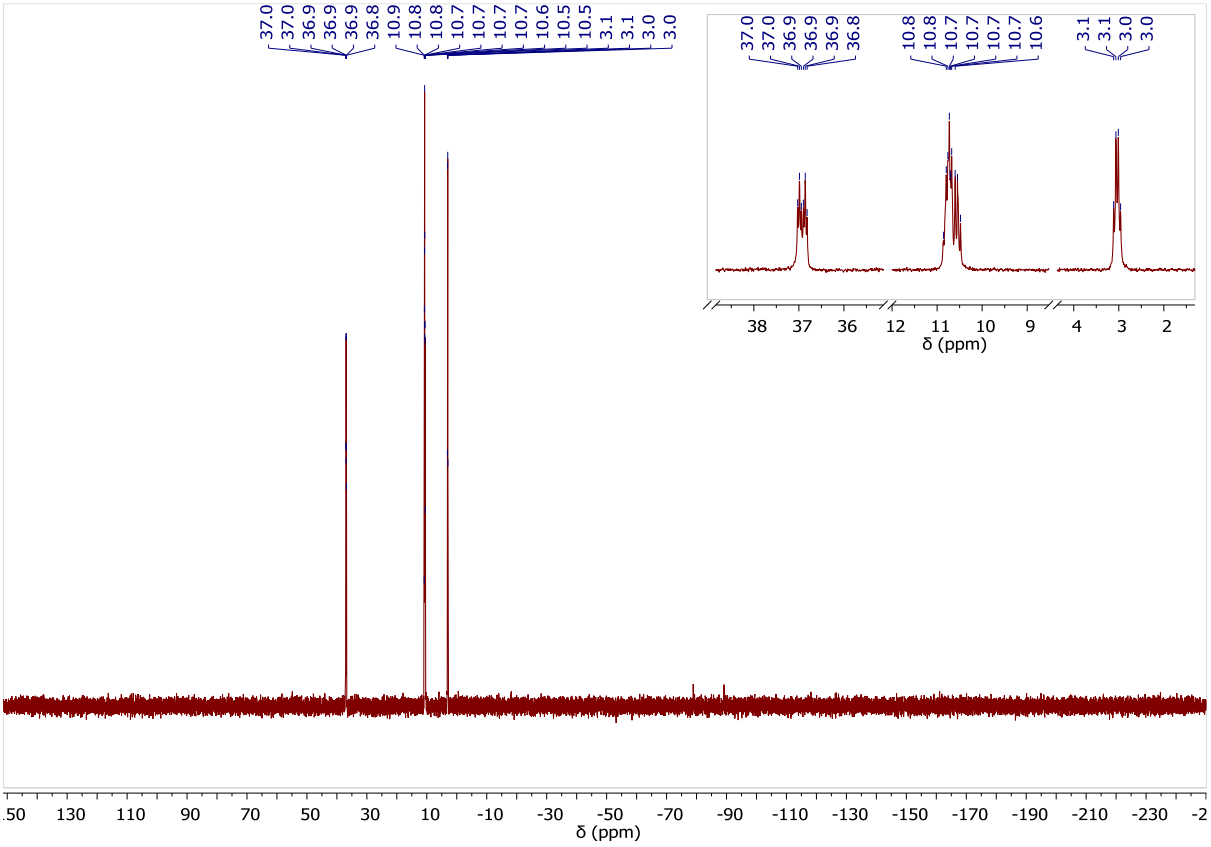

Figure S11 $^{31}P\{^{1}H\}$ NMR of complex **5** in CD_2Cl_2 at 298 K. Inset shows zoomed in spectrum.

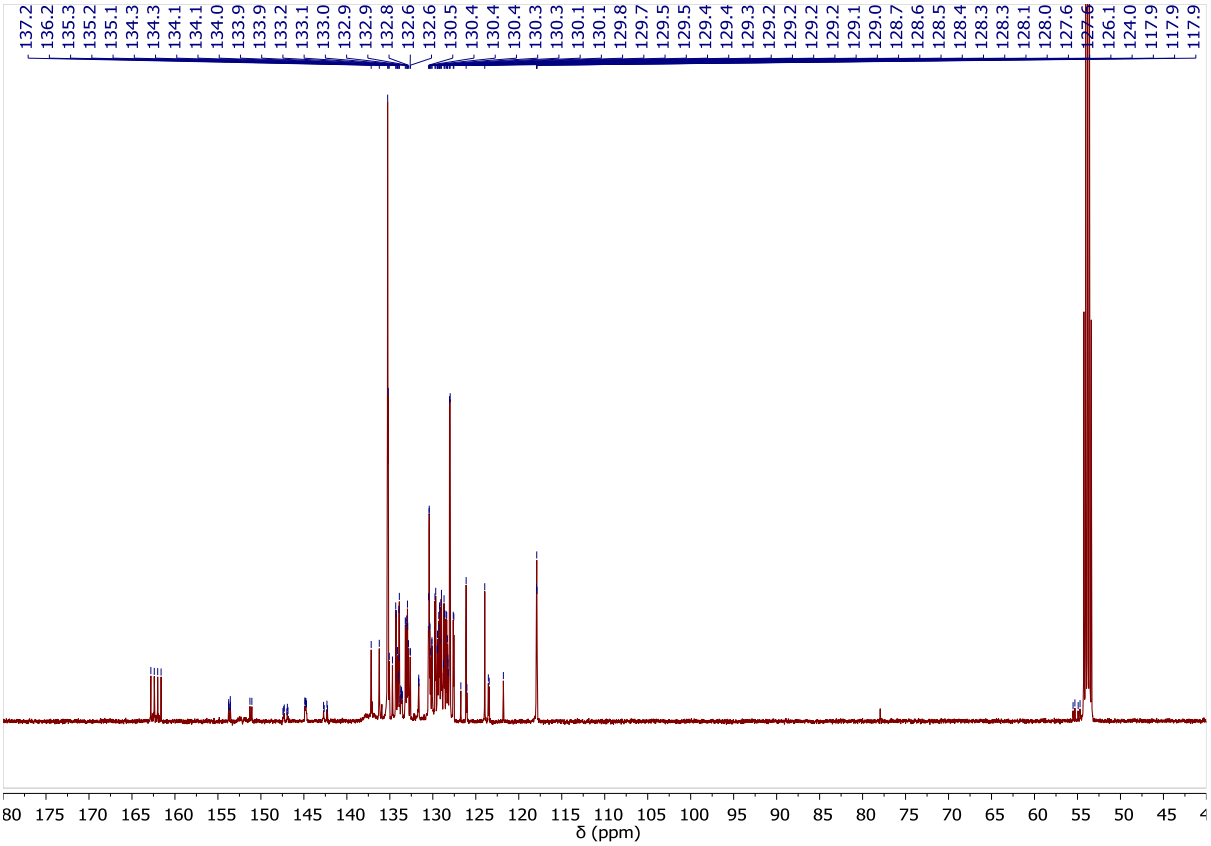

Figure S12 $^{13}C\{^{1}H\}$ NMR of complex **5** in CD_2Cl_2 at 298 K.

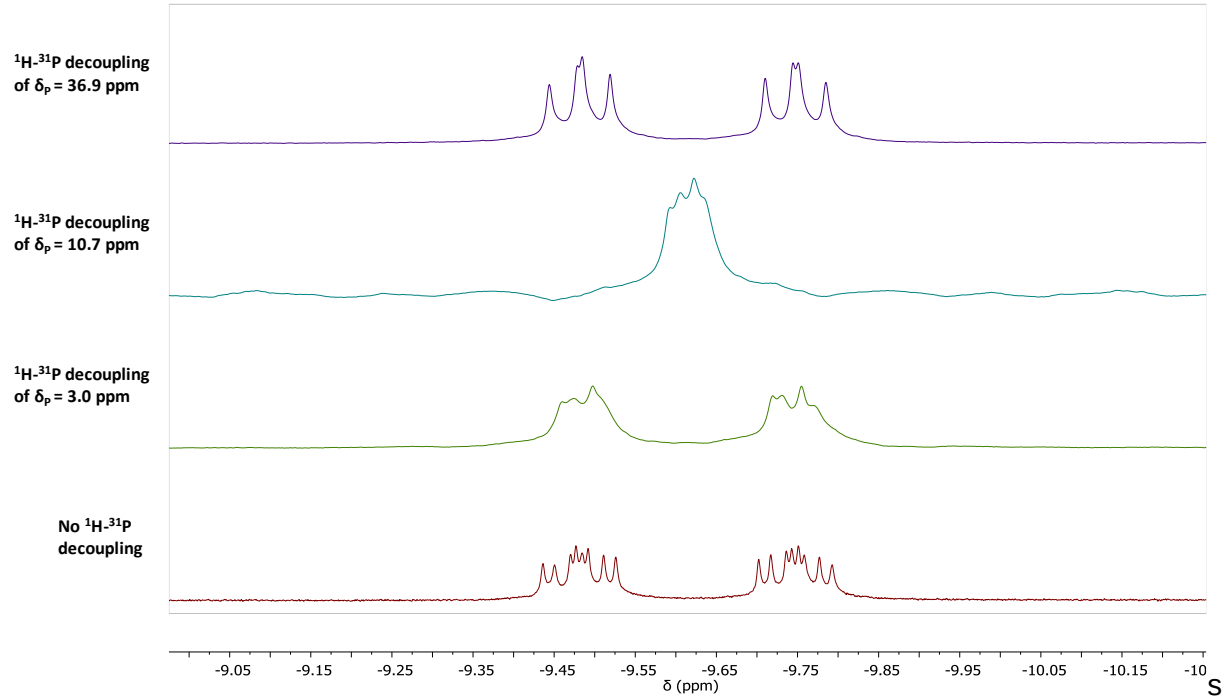

Figure S13 Comparison of ^{1}H and $^{1}H\{^{31}P\}$ NMR spectra of the hydride resonance of complex **5** in CD_2Cl_2 at 298 K.

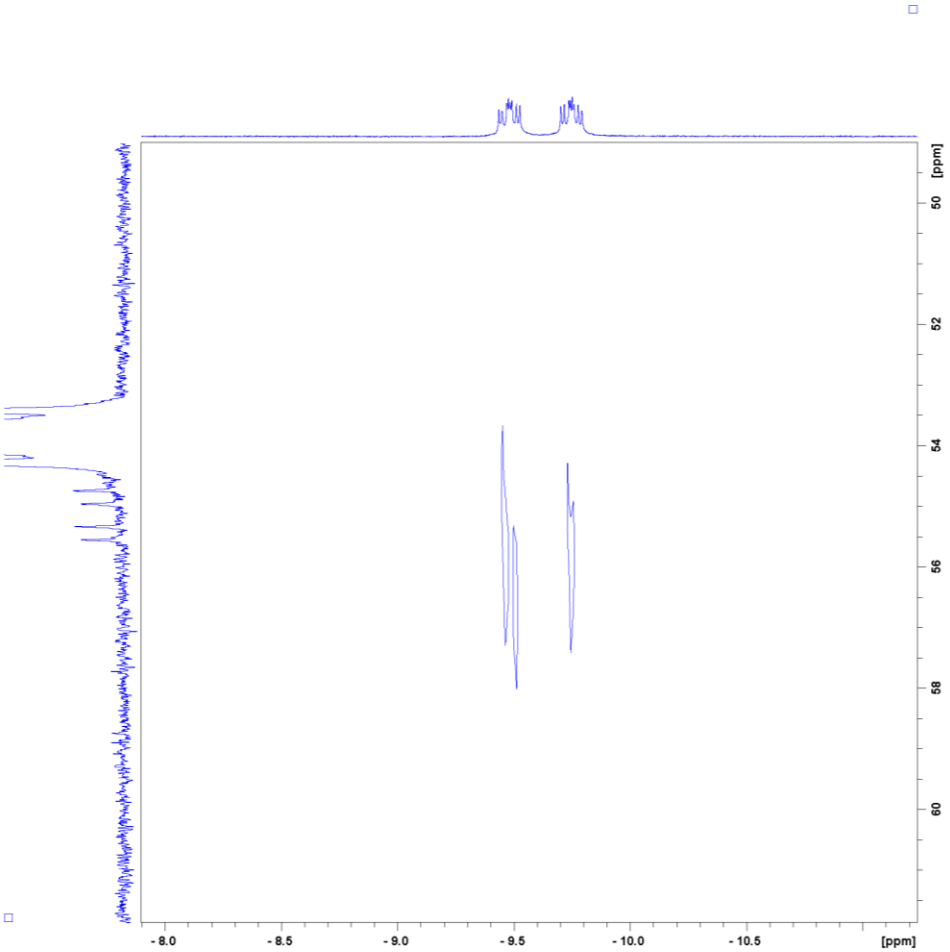

Figure S14 ^{1}H-^{13}C HMBC NMR spectrum of complex **5** in CD_2Cl_2 at 298 K. Highlights the correlation between the Ir-H resonance at δ_H -9.61 ppm and Ir-C(sp^3) resonance at δ_C 55.11 ppm.

NMR Spectra of complex 6

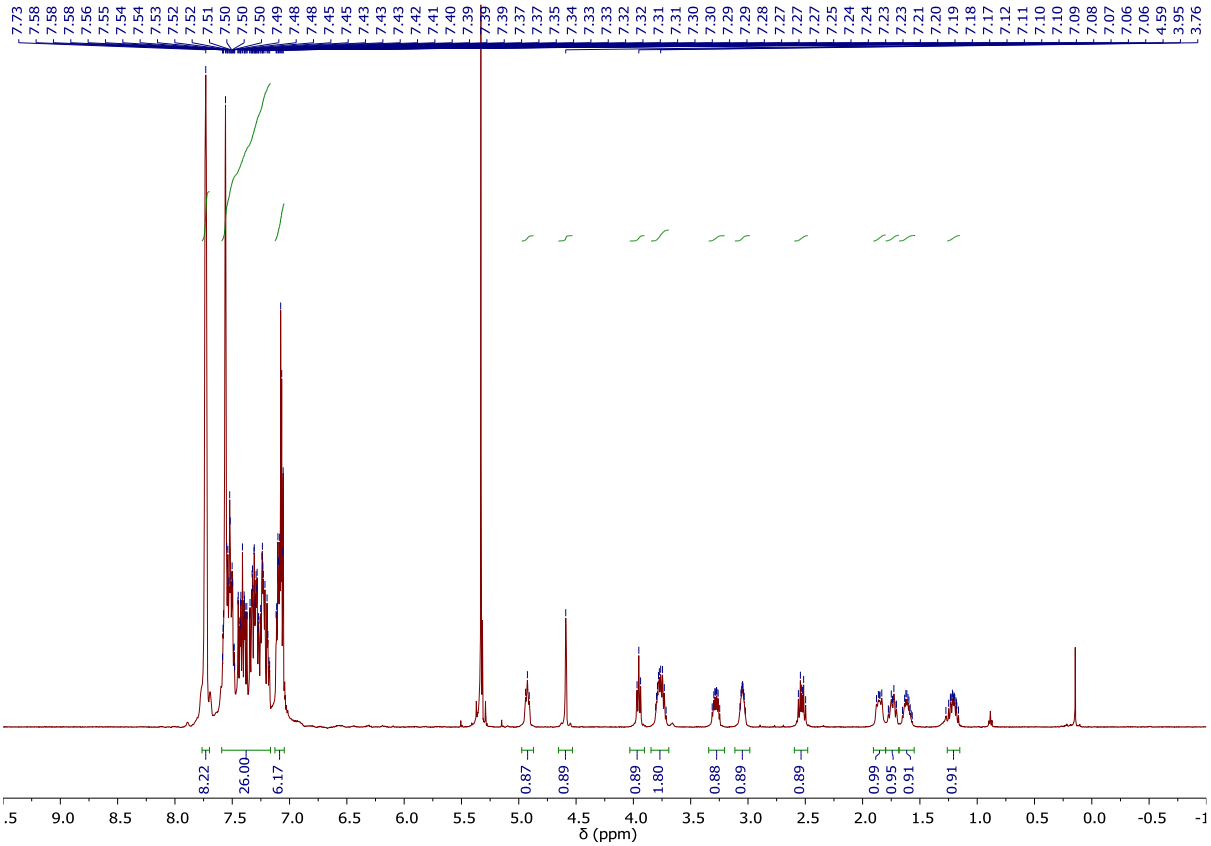

Figure S15 ^{1}H NMR of complex **6** in CD_2Cl_2 at 298 K. *n*-Hexane and silicone grease contaminants present.

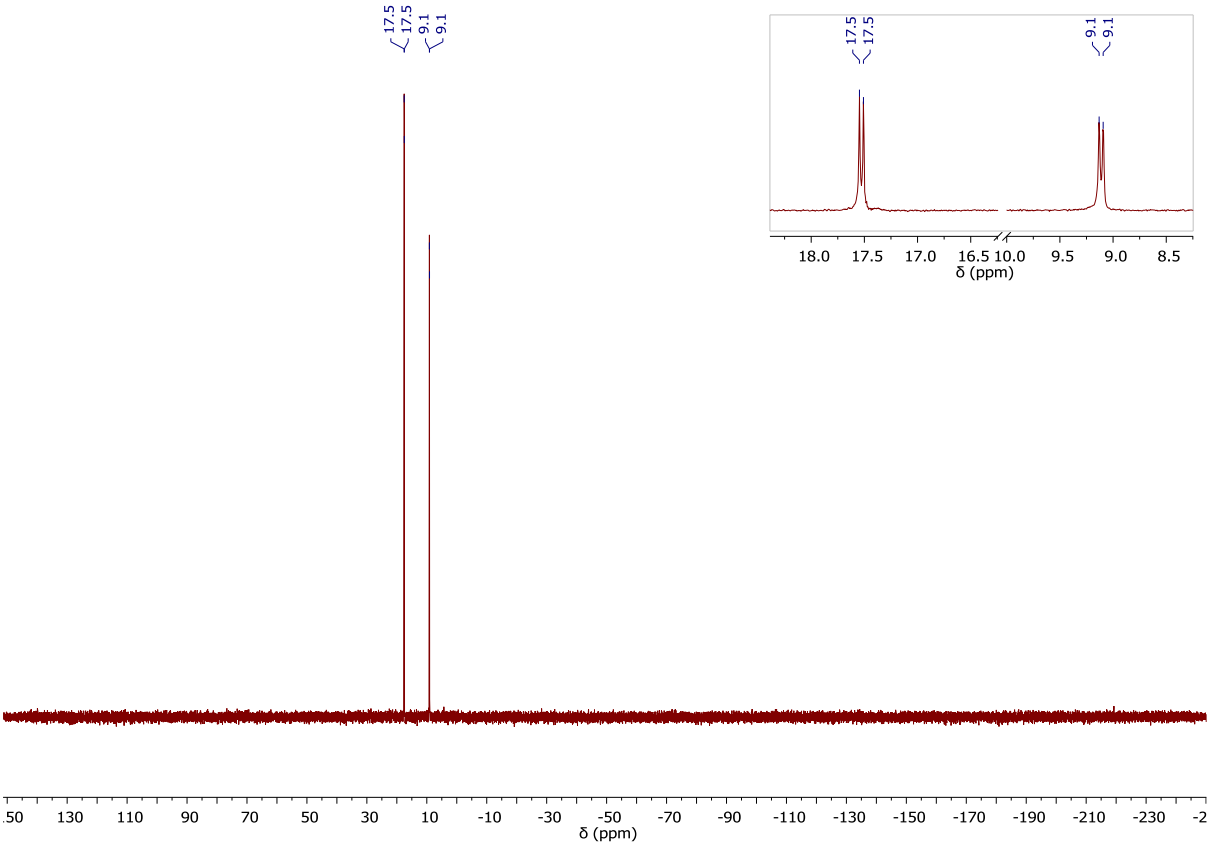

Figure S16 $^{31}P\{^{1}H\}$ NMR of complex **6** in CD_2Cl_2 at 298 K. Inset shows zoomed in spectrum.

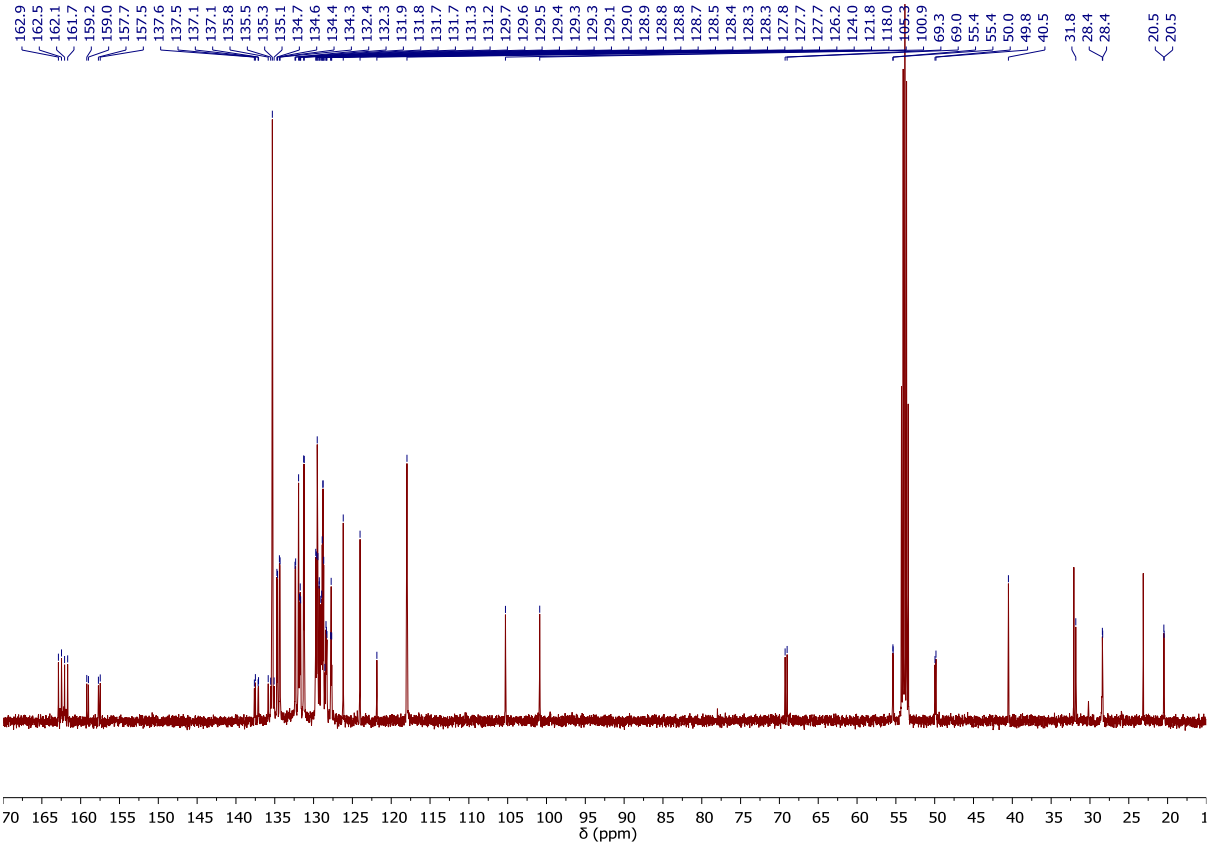

Figure S17 $^{13}C\{^{1}H\}$ NMR of complex **6** in CD_2Cl_2 at 298 K. *n*-Hexane contaminant present.

NMR Spectra of complex 7a

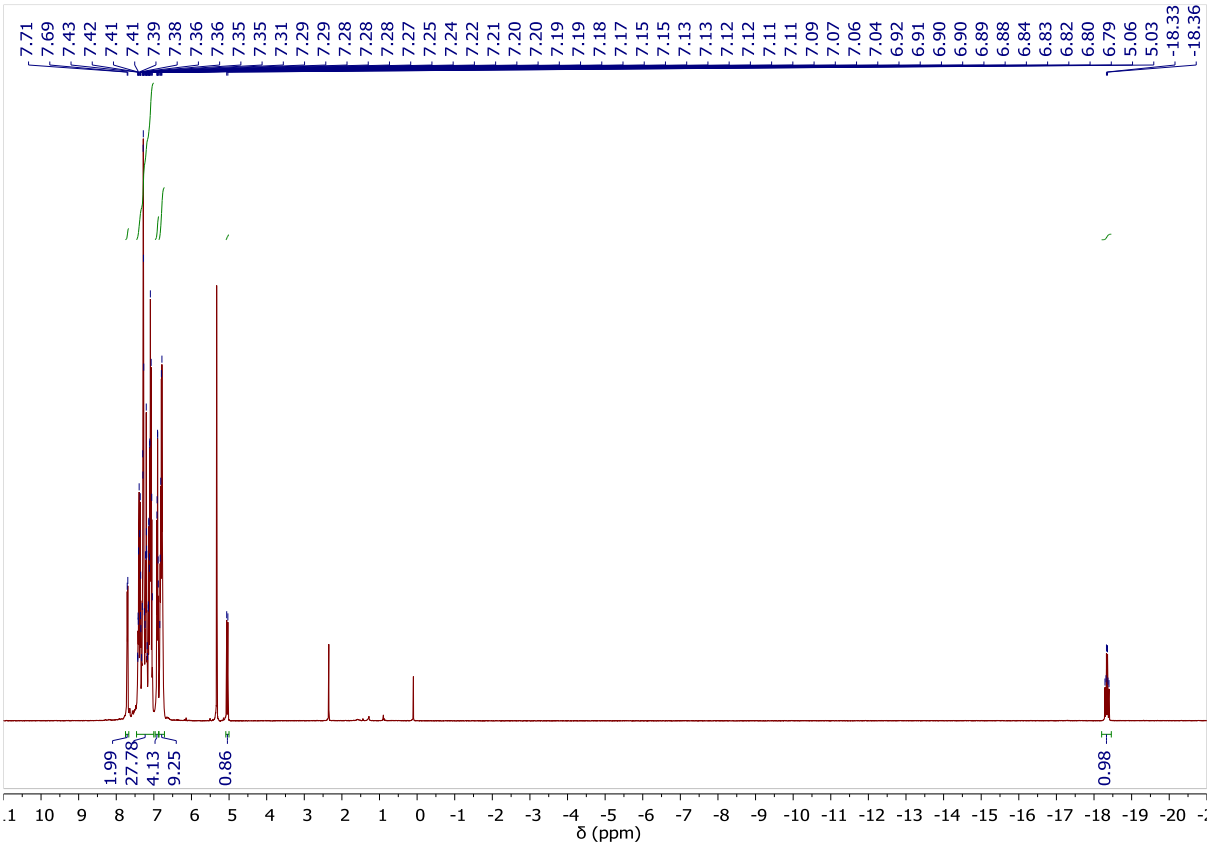

Figure S18 ^{1}H NMR of complex **7a** in CD_2Cl_2 at 298 K. Toluene and silicone grease contaminants present.

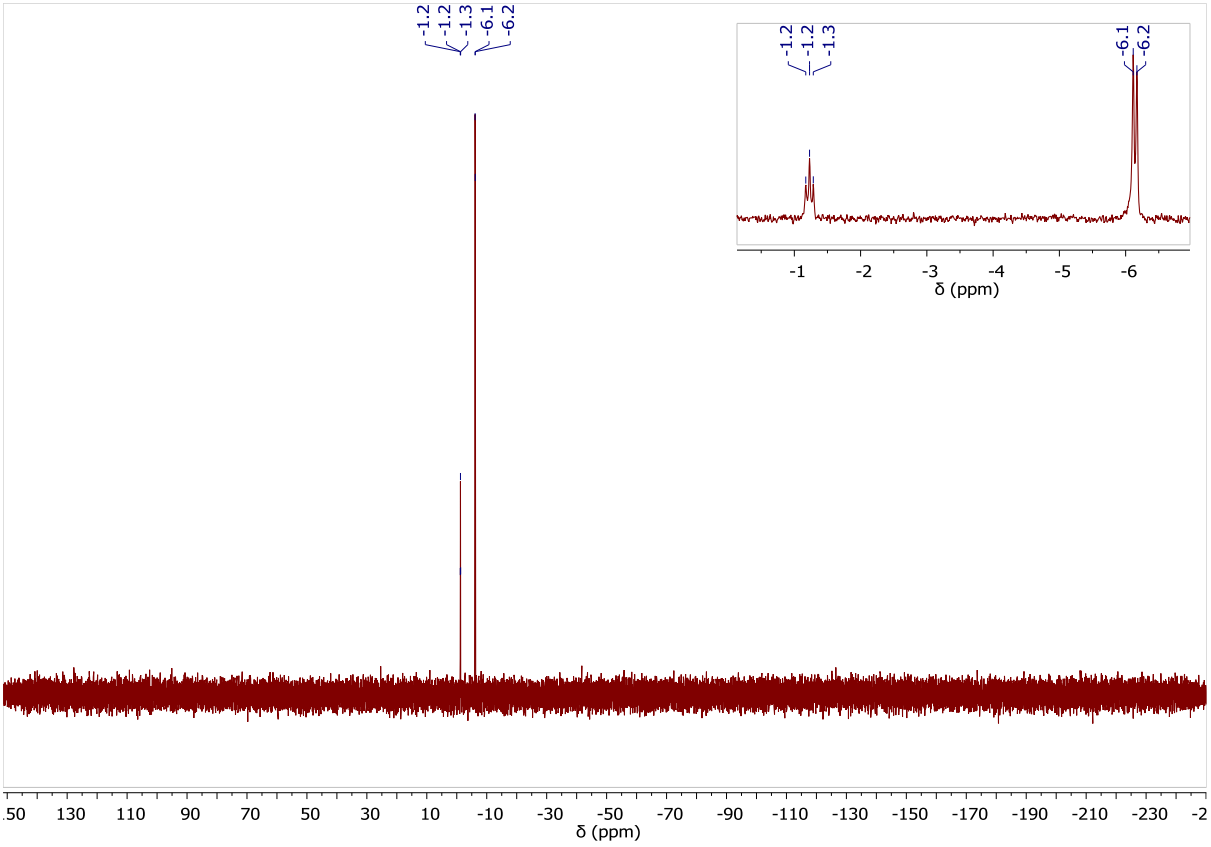

Figure S19 $^{31}P\{^{1}H\}$ NMR of complex **7a** in CD_2Cl_2 at 298 K. Inset shows zoomed in spectrum.

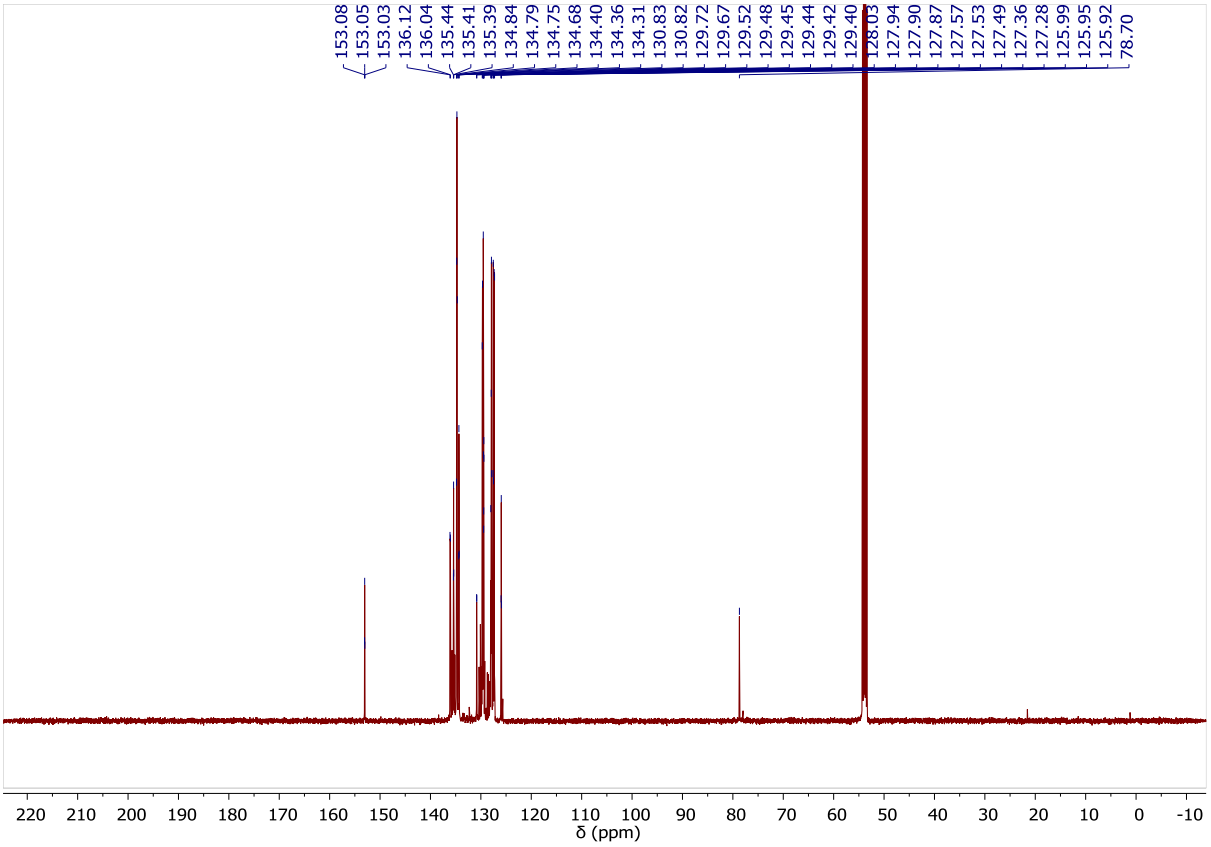

Figure S20 $^{13}C\{^{1}H\}$ NMR of complex **7a** in CD_2Cl_2 at 298 K.

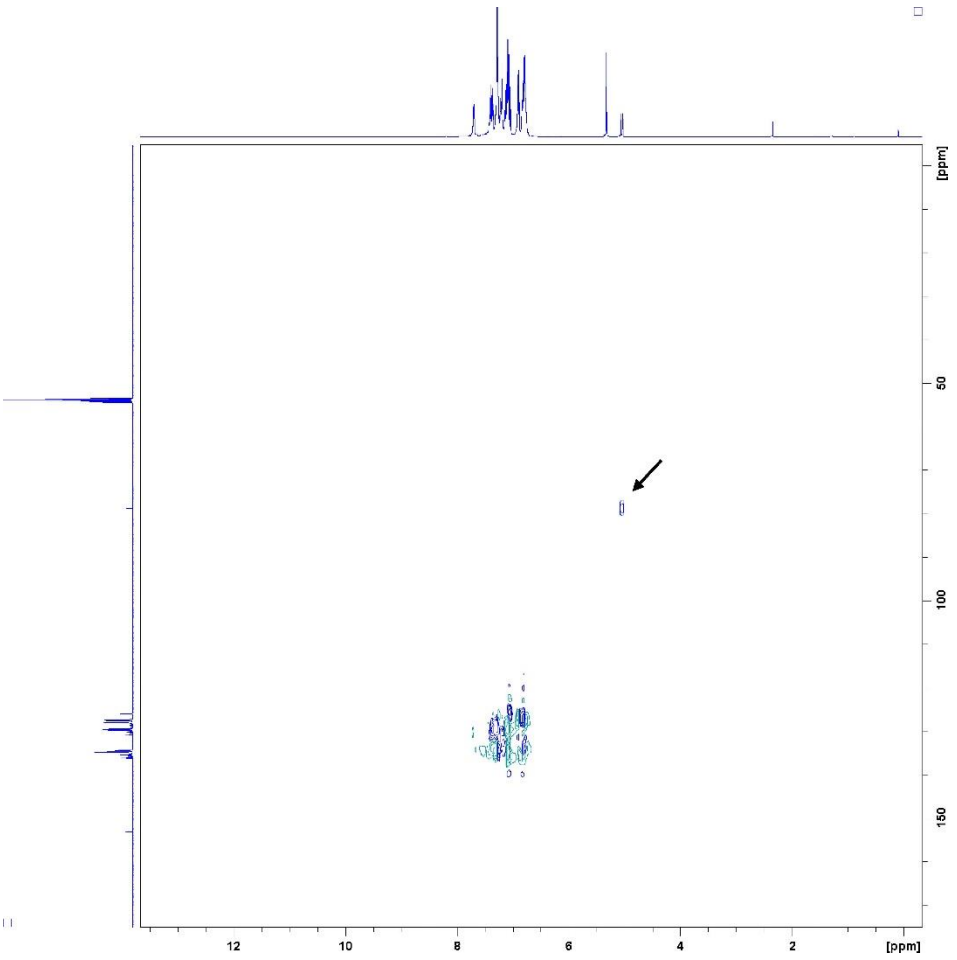

Figure S21 ^{1}H-^{13}C HMQC NMR spectrum of complex **7a** in CD_2Cl_2 at 298 K that shows correlation at δ_H 5.05 and δ_C 78.6 – 78.8 ppm confirming the presence of a methine C-H.

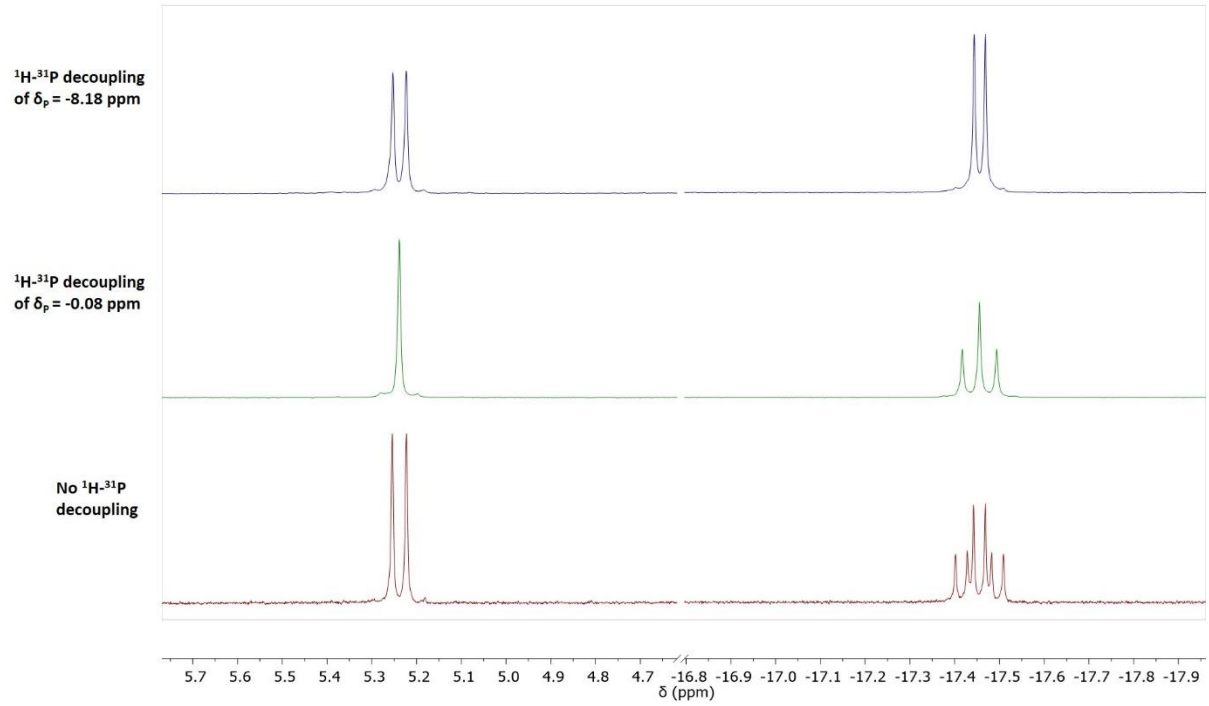

Figure S22 Comparison of ^{1}H and $^{1}H\{^{31}P\}$ NMR spectra of complex **7a** in C_6D_6 at 298 K showing methine C-H and Ir-H resonances at δ_H 5.05 and -18.34 ppm respectively. Highlights the long range $^{4}J_{HP}$ coupling between the PPh_3 ligand (δ_P -0.08 ppm) and methane C-H, and coupling between the pincer phosphines (δ_P -8.18 ppm) and PPh_3 with the Ir-H.

NMR Spectra of complex 7b

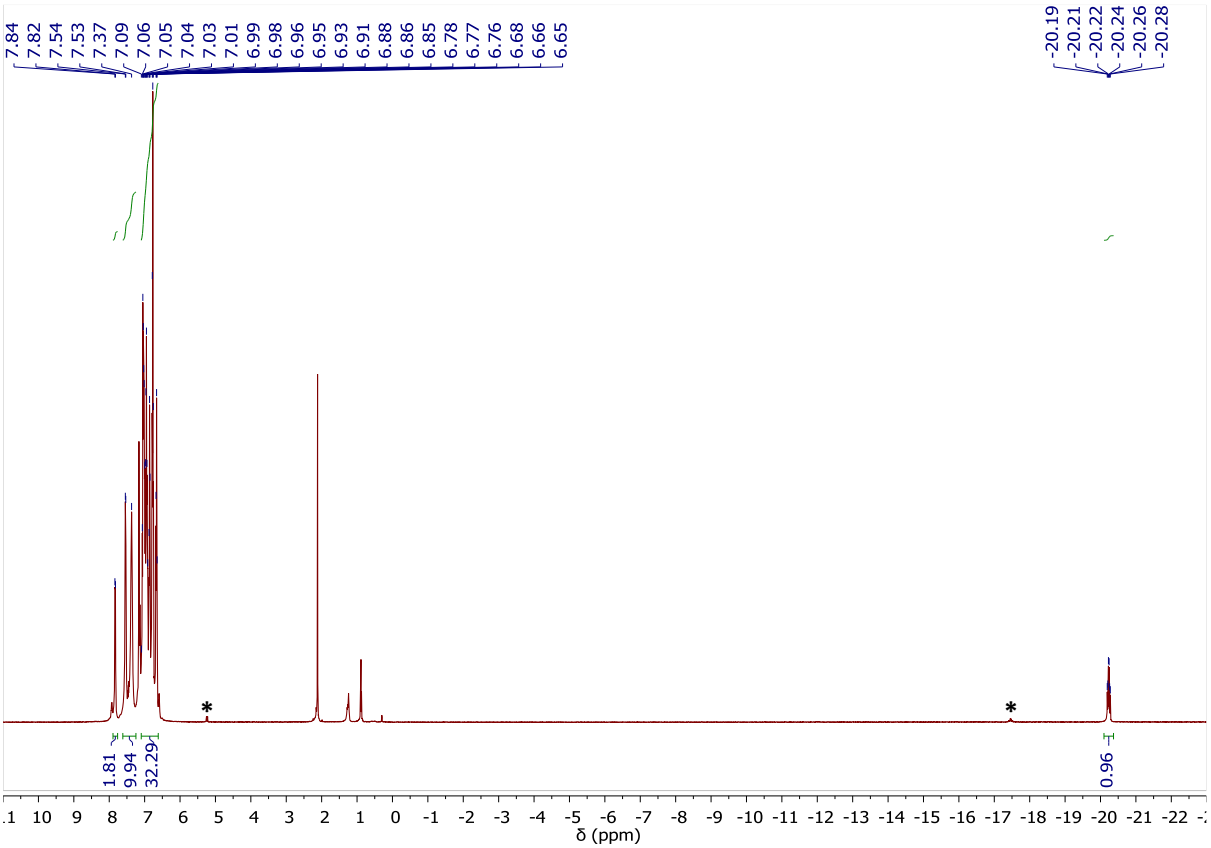

Figure S23 ^{1}H NMR of complex **7b** in C_6D_6 at 298 K. Toluene, *n*-hexane contaminants present. * Minor quantity of **7a** is also present.

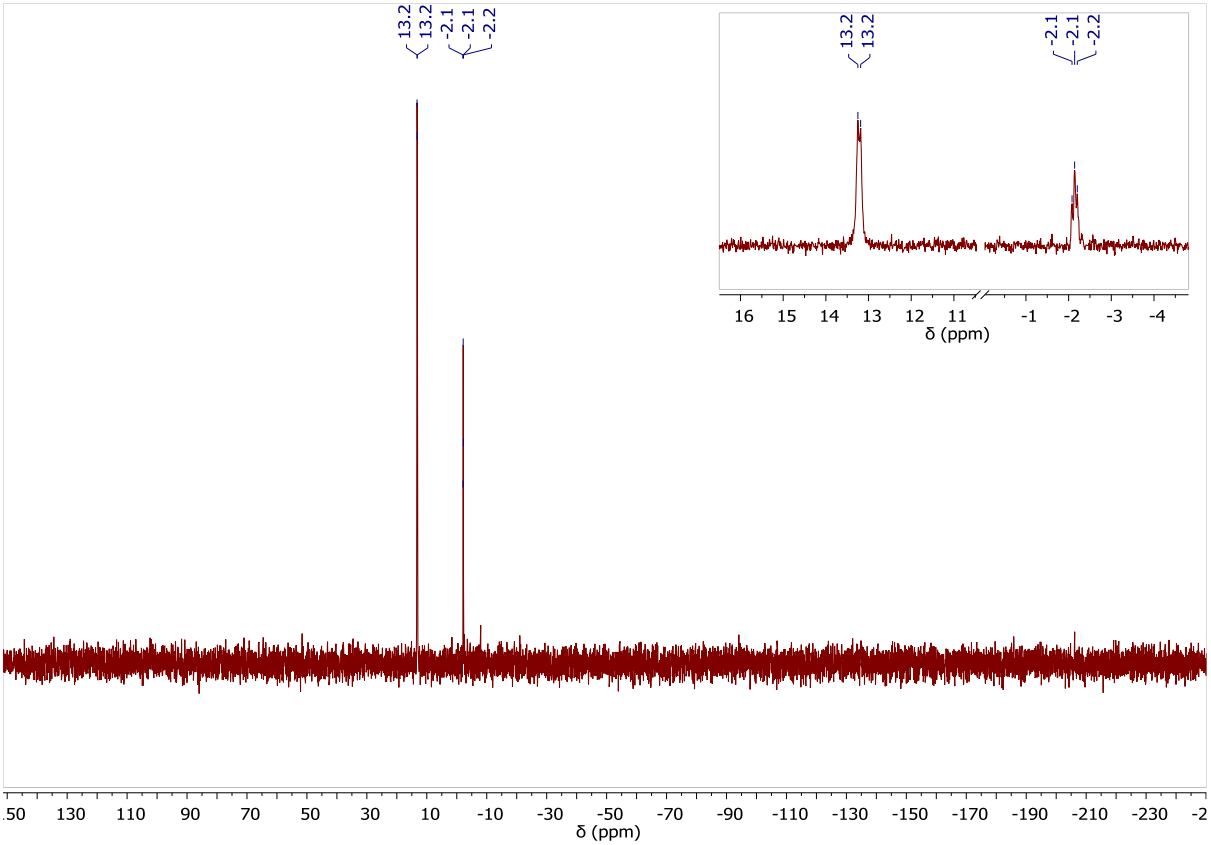

Figure S24 $^{31}P\{^{1}H\}$ NMR of complex **7b** in C_6D_6 at 298 K. Inset shows zoomed in spectrum.

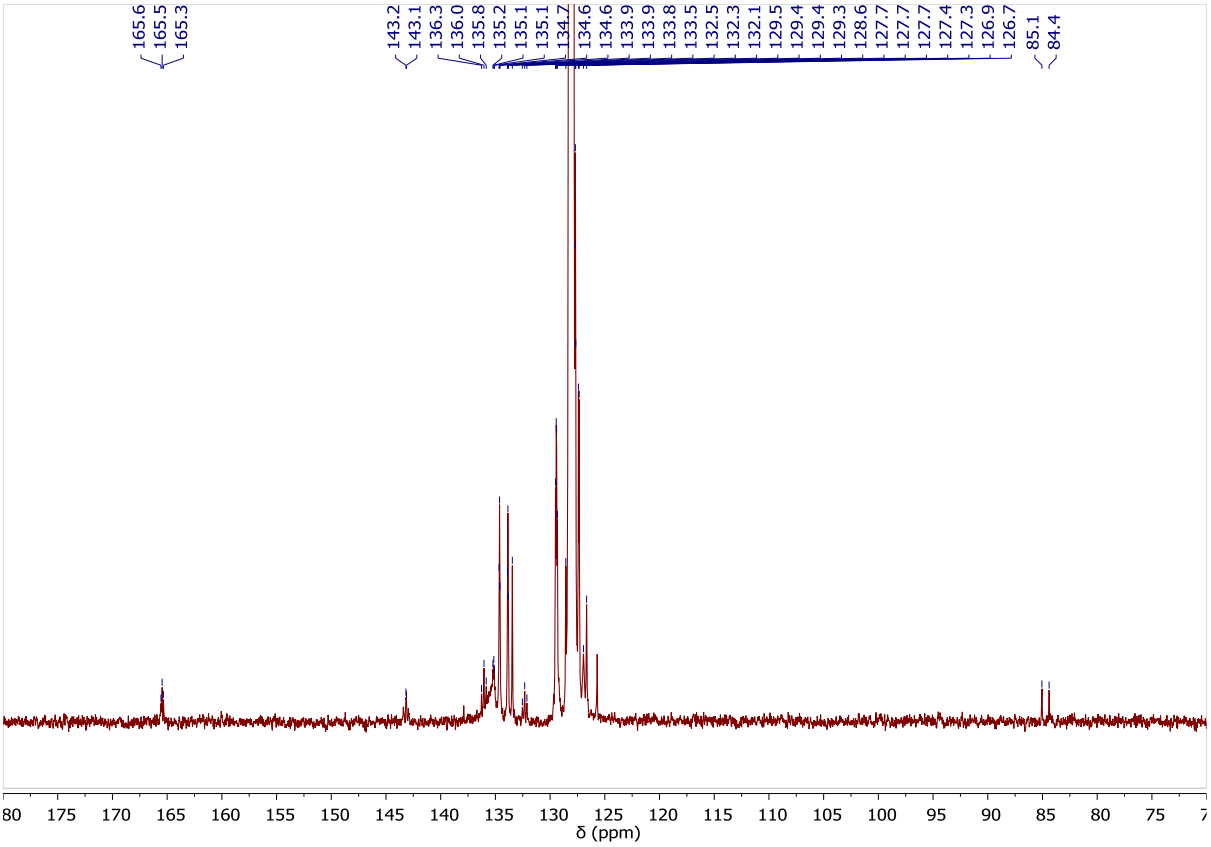

Figure S25 $^{13}C\{^{1}H\}$ NMR of complex **7b** in C_6D_6 at 298 K.

Reaction between complex 7a and Na[BAr$^F_4$] that formed [Ir(CO)(PPh$_3$)$_3$][BAr$^F_4$]

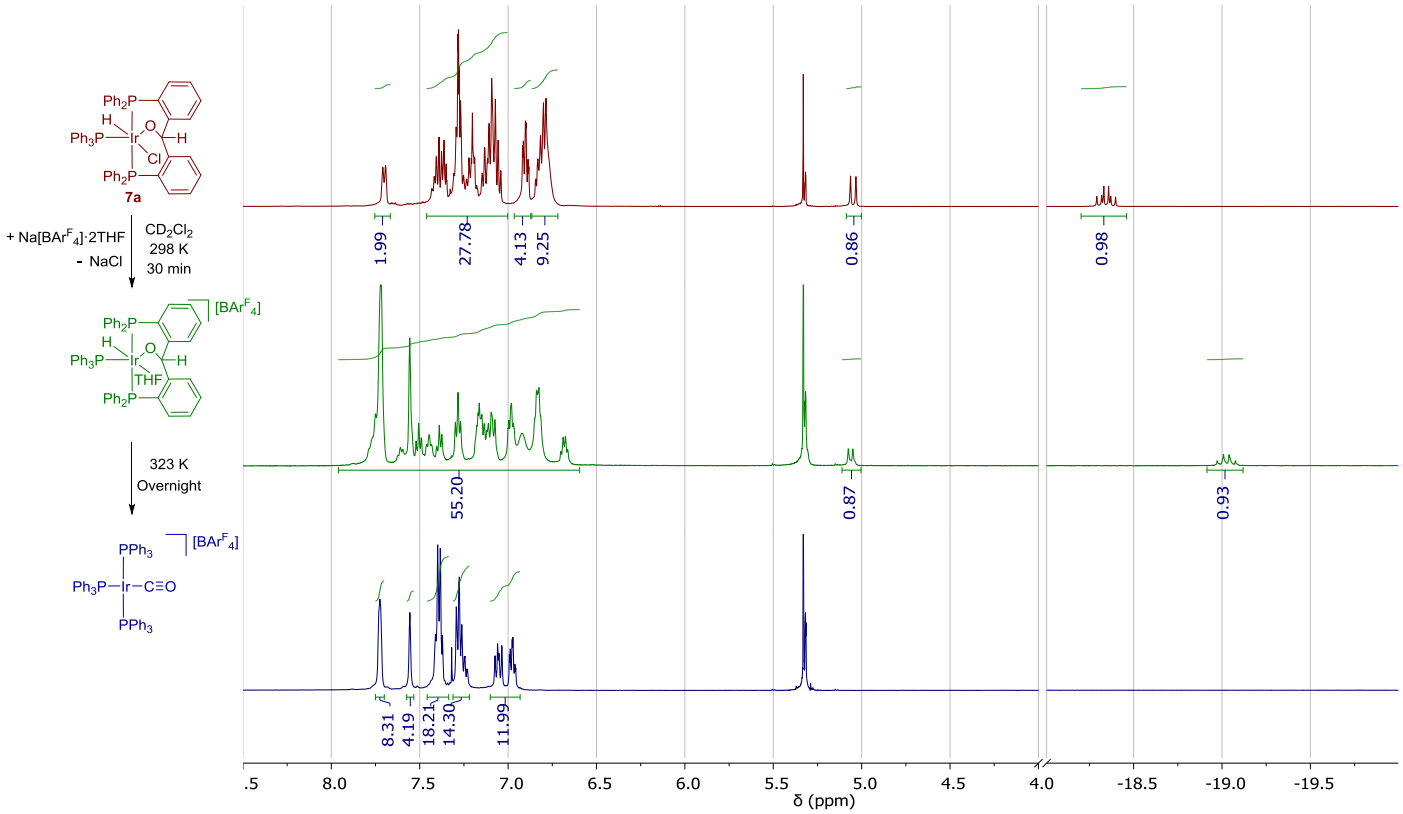

Figure S26 ^{1}H NMR spectra in CD_2Cl_2 taken at 298 K showing the species formed on addition of Na[BAr$^F_4$]·2THF to complex **7a** at room temperature and after heating at 323 K.

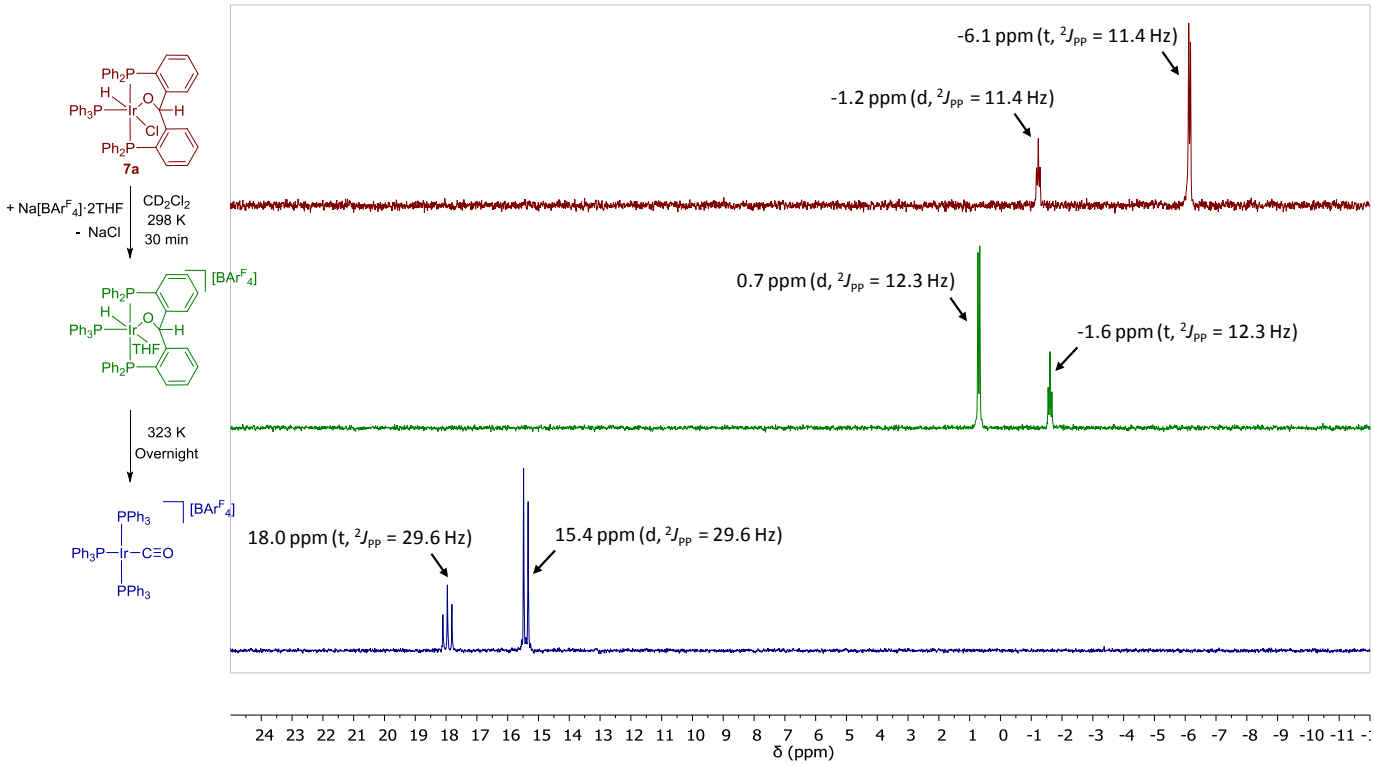

Figure S27 ^{31}P{^{1}H} NMR spectra in CD_2Cl_2 taken at 298 K showing the species formed on addition of Na[BAr$^F_4$]·2THF to complex **7a** at room temperature and after heating at 323 K.

NMR Spectra of intermediate I

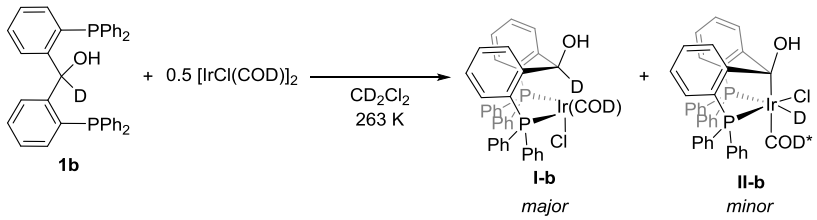

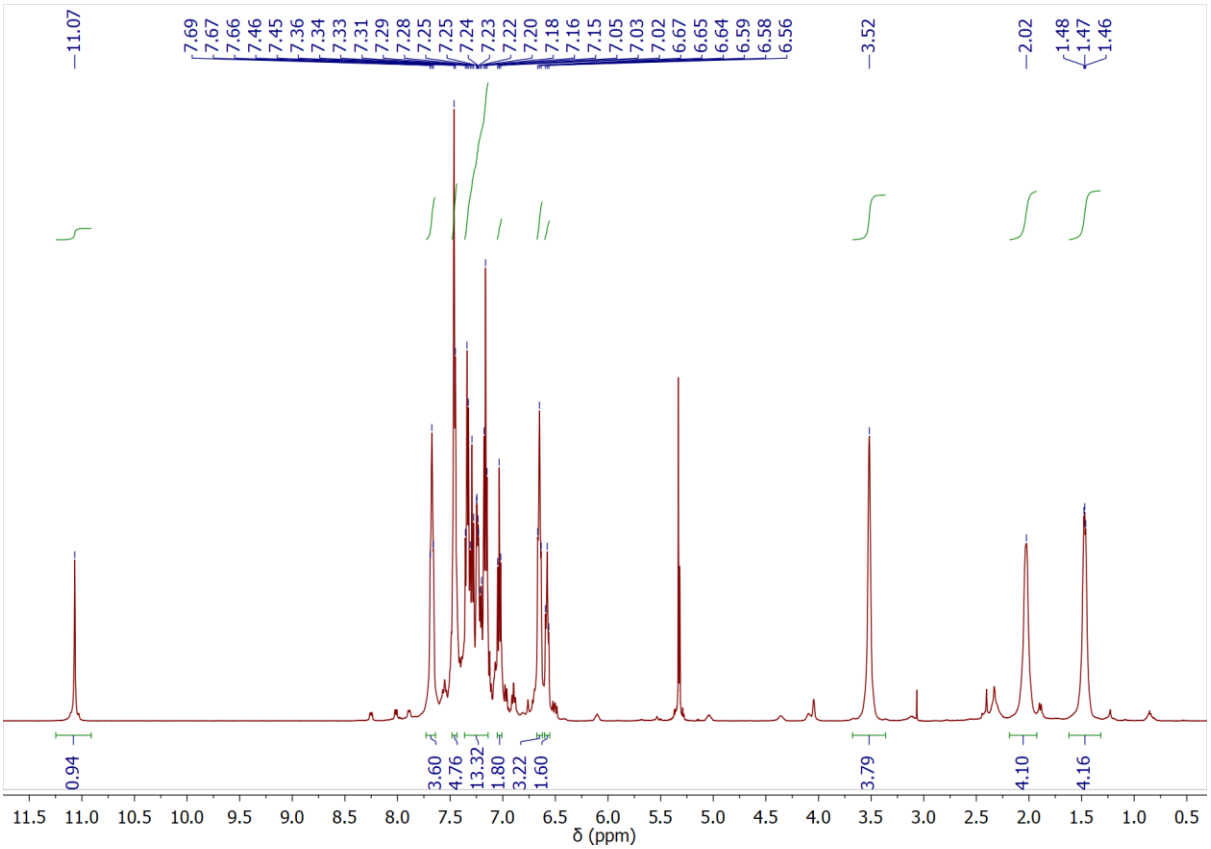

Figure S28 ^{1}H NMR spectrum showing major intermediate **I-b** made using C-D labelled ligand **1b** in CD_2Cl_2 at 263 K. Methine resonance at 5.91 ppm not present. Minor quantity of Intermediate **II-b** also present. * in the reaction scheme denotes κ^1-COD coordination.

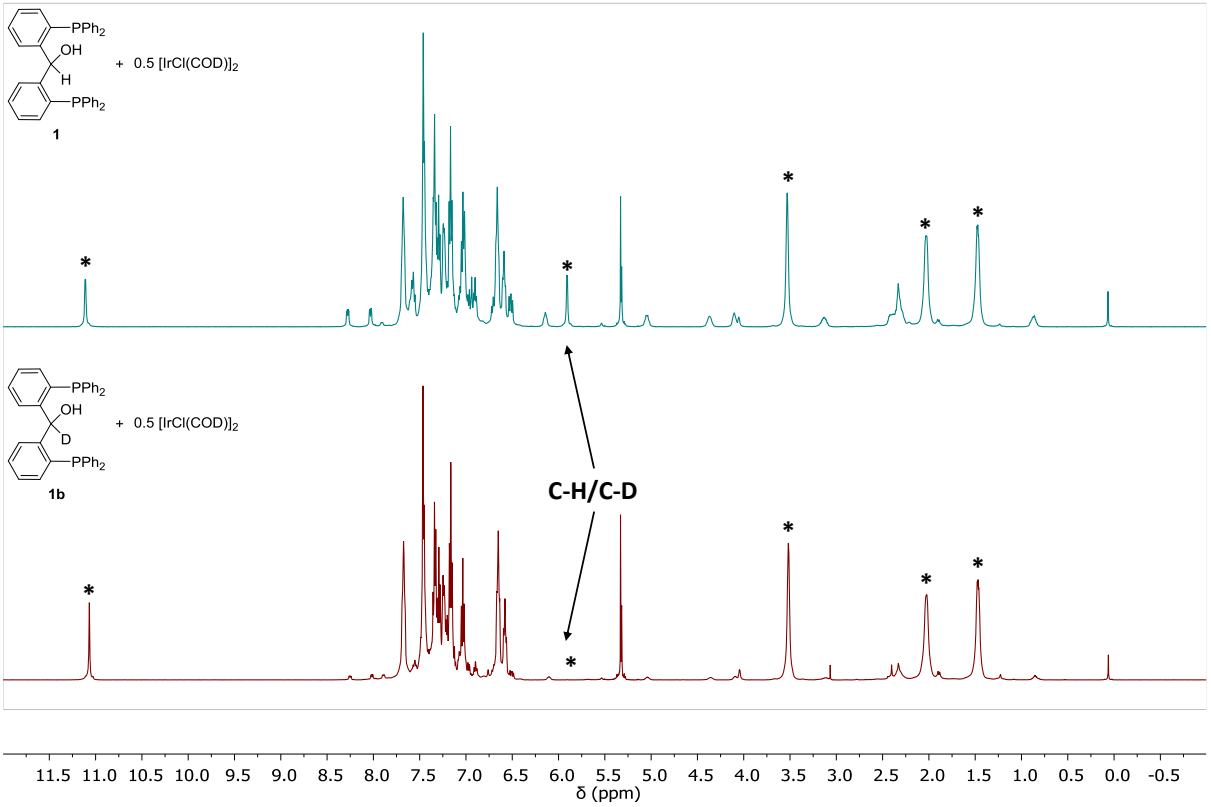

Figure S29 Comparison of ^{1}H NMR spectra in CD_2Cl_2 at 263 K highlighting the presence and absence of the methine resonance in intermediate **I** and **I-b** when ligand **1** (top) or C-D labelled ligand **1b** (bottom) were used respectively. Intermediate **II** or **II-b** also present in both spectra. * indicates resonance from intermediate **I** and **I-b**.

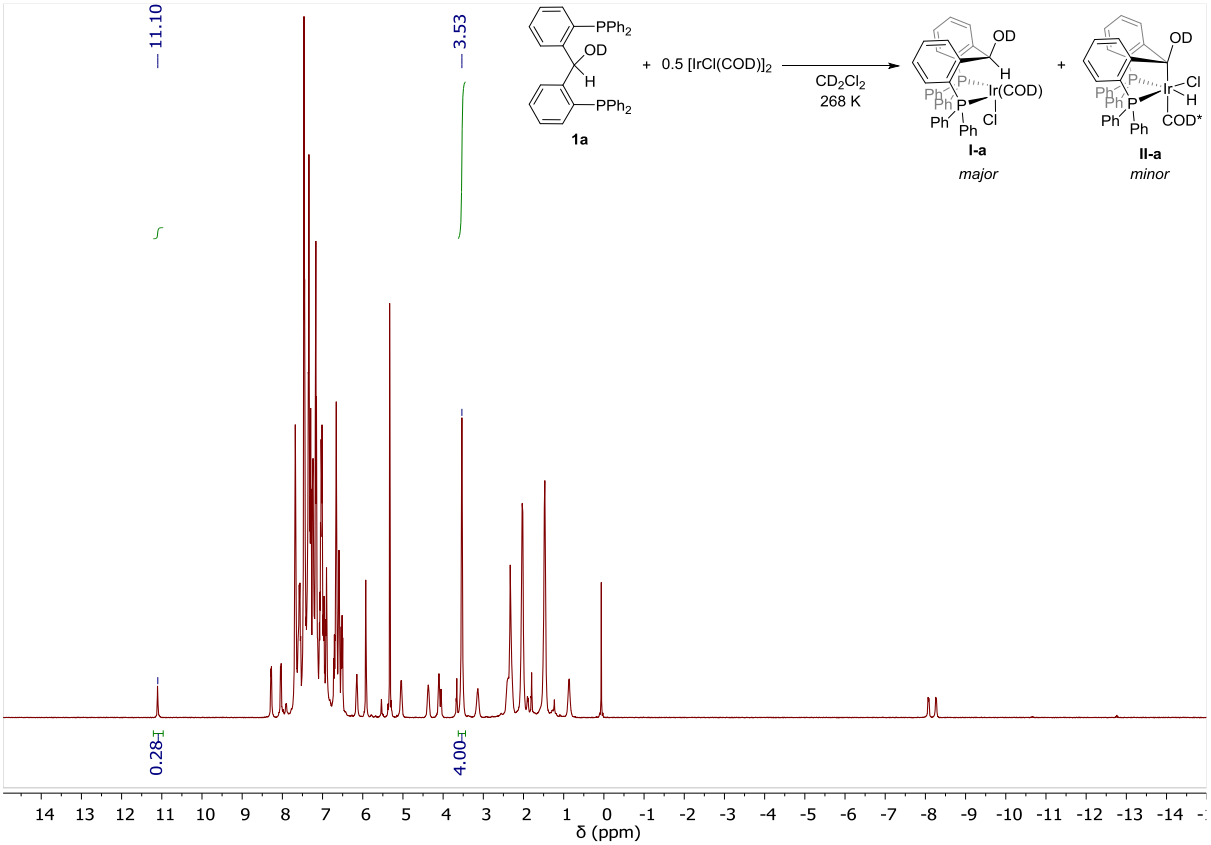

Figure S30 ^{1}H NMR spectrum showing intermediate **I-a** made using O-D labelled ligand **1a** (72% deuteration) in CD_2Cl_2 at 268 K highlighting the reduced integration for the O-H resonance at δ_H 11.10 ppm. Intermediate **II-a** also present. * in the reaction scheme denotes κ^1-COD coordination.

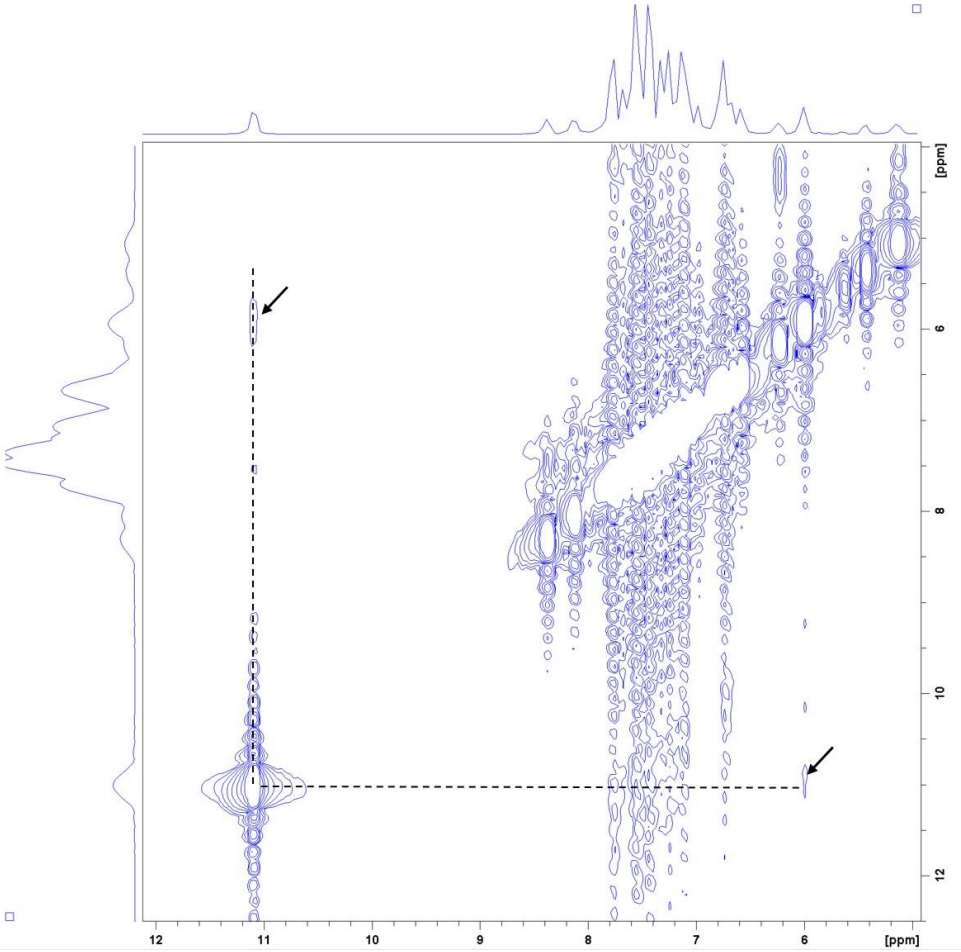

Figure S31 ^{1}H-^{1}H COSY NMR spectrum of intermediate **I** in CD_2Cl_2 at 253 K showing the correlation between the O-H and C-H resonances at δ_H 11.10 and 5.91 ppm respectively.

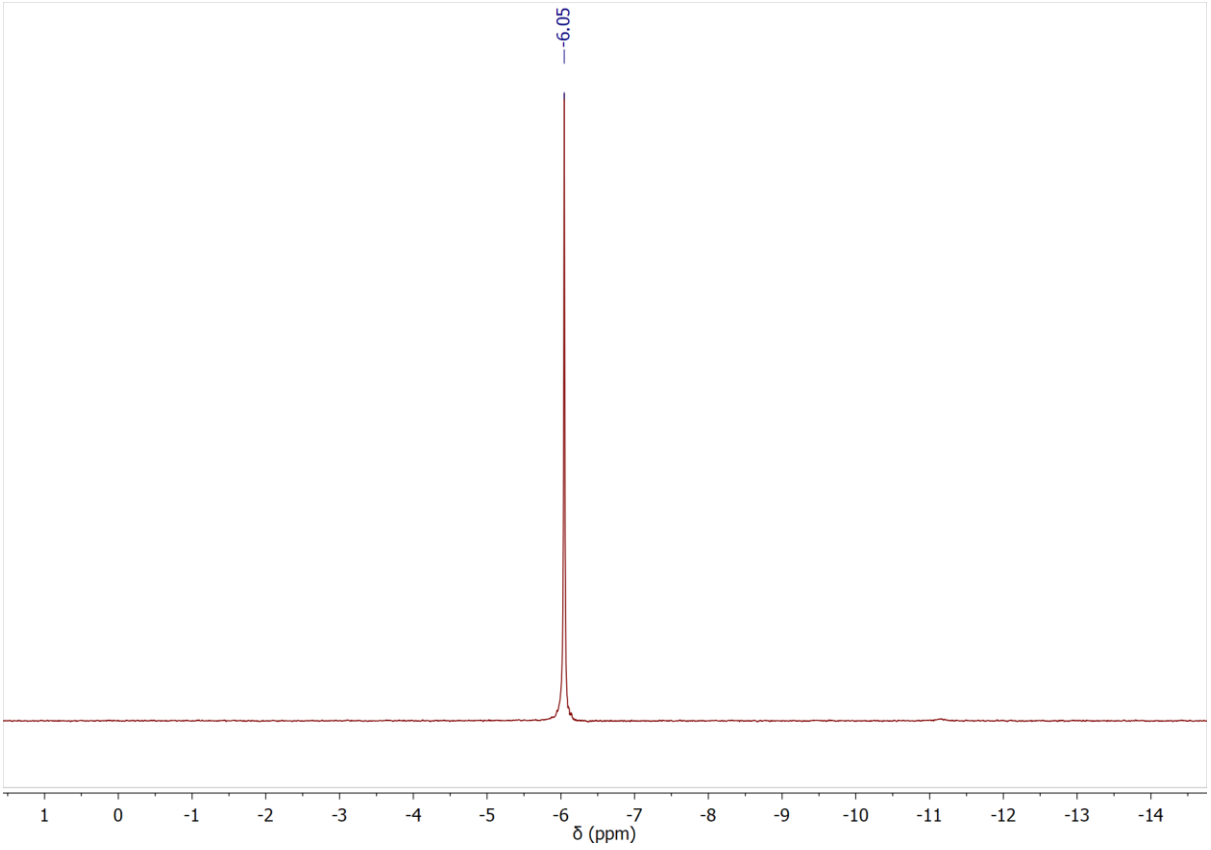

Figure S32 $^{31}P\{^{1}H\}$ NMR spectrum of intermediate **I** in CD_2Cl_2 at 263 K.

NMR Spectra of intermediate II

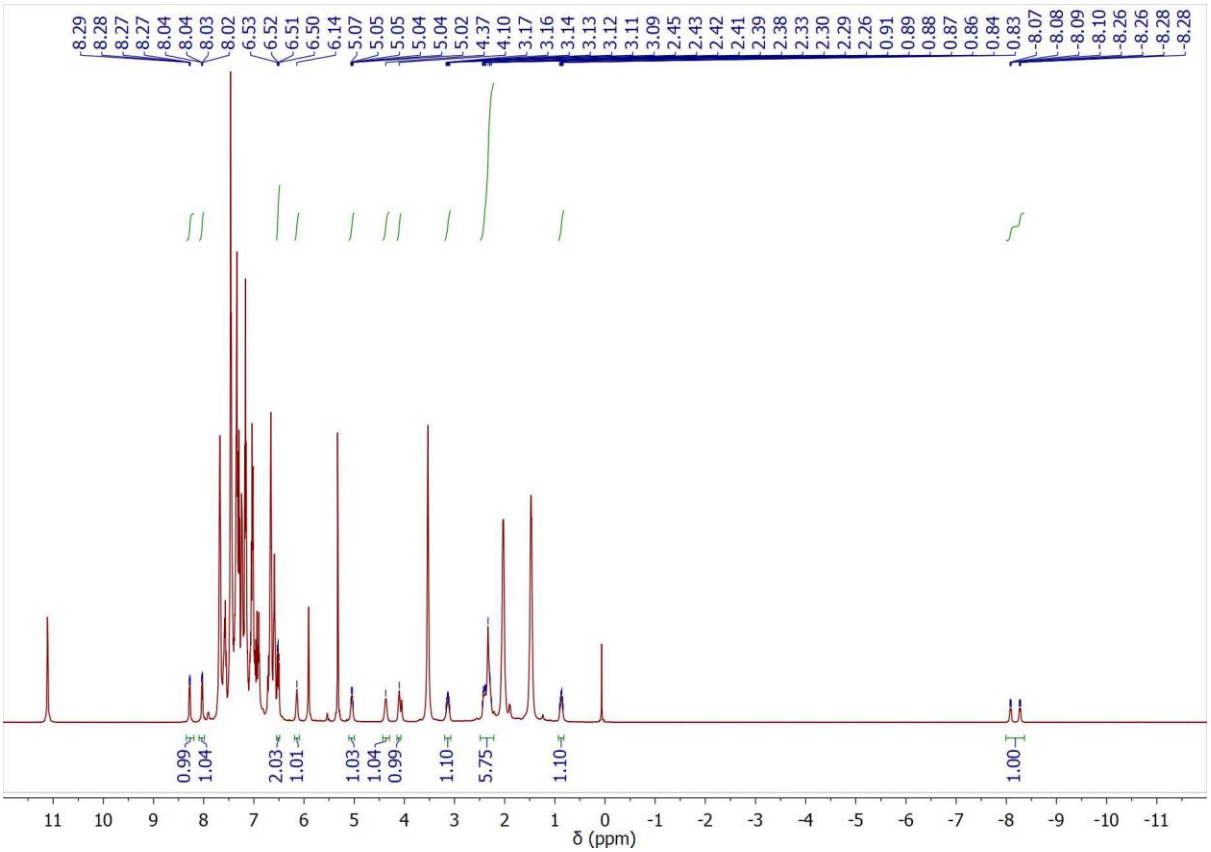

Figure S33 ^{1}H NMR spectrum highlighting the identified resonances of intermediate **II** in CD_2Cl_2 at 263 K. Intermediate **I** also present.

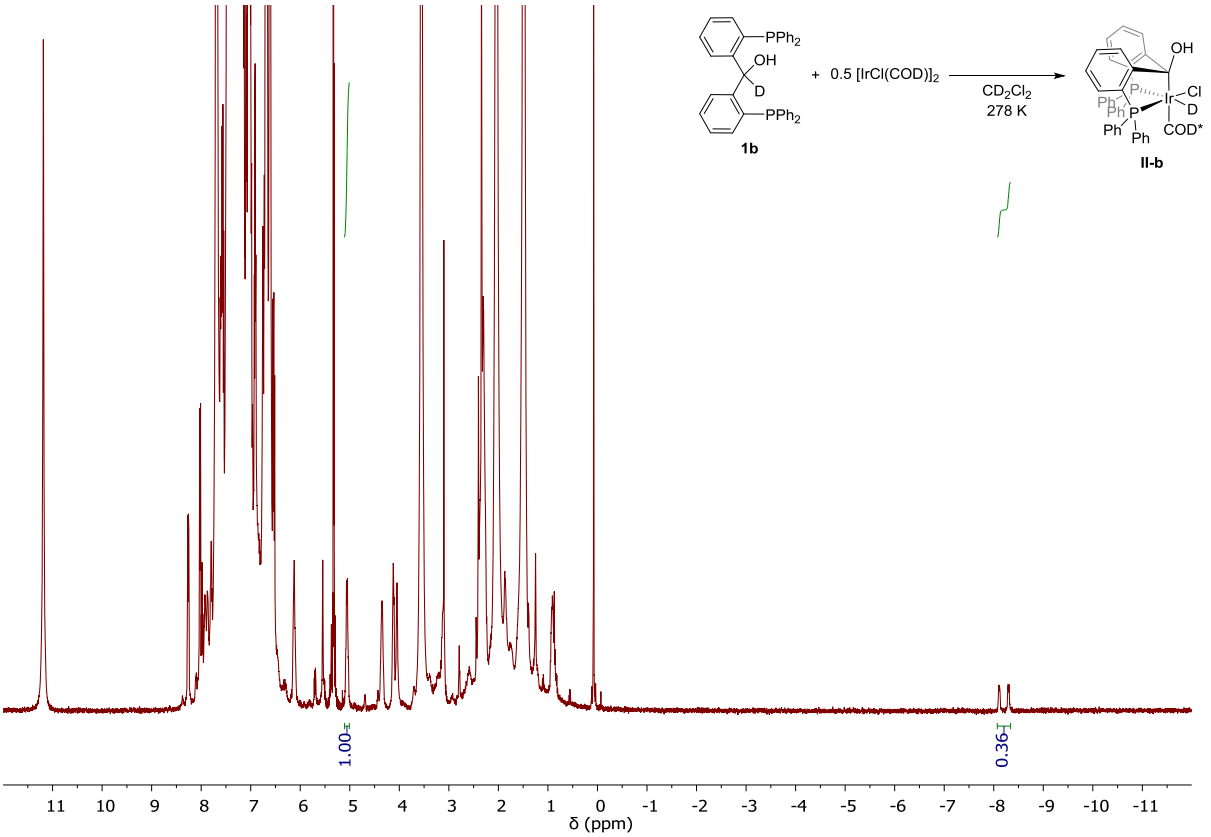

Figure S34 ^{1}H NMR spectrum showing intermediate **II-b** made using C-D labelled ligand **1b** (99% deuterated) in CD_2Cl_2 at 278 K highlighting the reduced integration for the Ir-H resonance at δ_H -8.18 ppm relative to in **II**. Intermediate **I-b** also present. Given that the C-D group in ligand **1b** used was 99% deuterated, the slightly higher than expected integration

for the Ir-H resonance (0.36 observed vs. 0.01 expected) indicates that a H-D exchange process had occurred. The mechanism for the H-D exchange likely involved intermediate **VI** and may be analogous to that described by Piers *et al* for a similar Ir complex.[9]

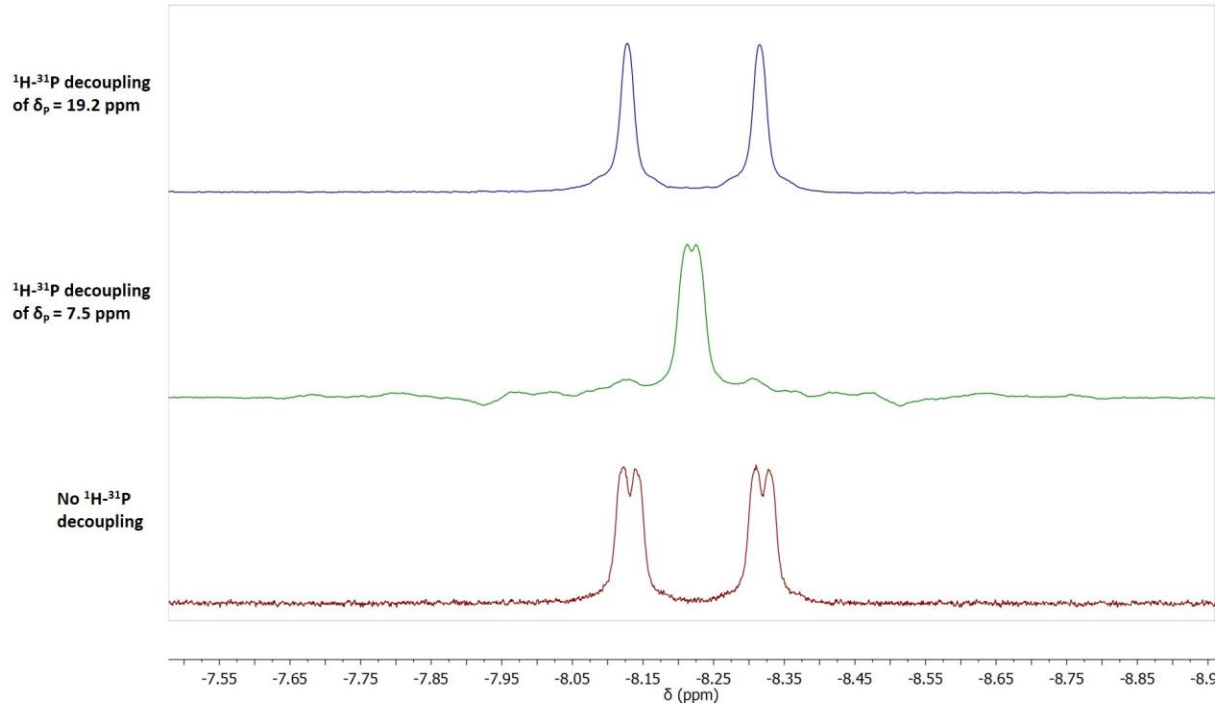

Figure S35 Comparison of ^{1}H and $^{1}H\{^{31}P\}$ NMR spectra of intermediate **II** in CD_2Cl_2 at 273 K showing the Ir-H resonance at δ_H -8.18 ppm. Confirms the hydride ligand is *trans* and *cis* disposed to the two phosphine groups of a *facially* coordinated PCP pincer ligand.

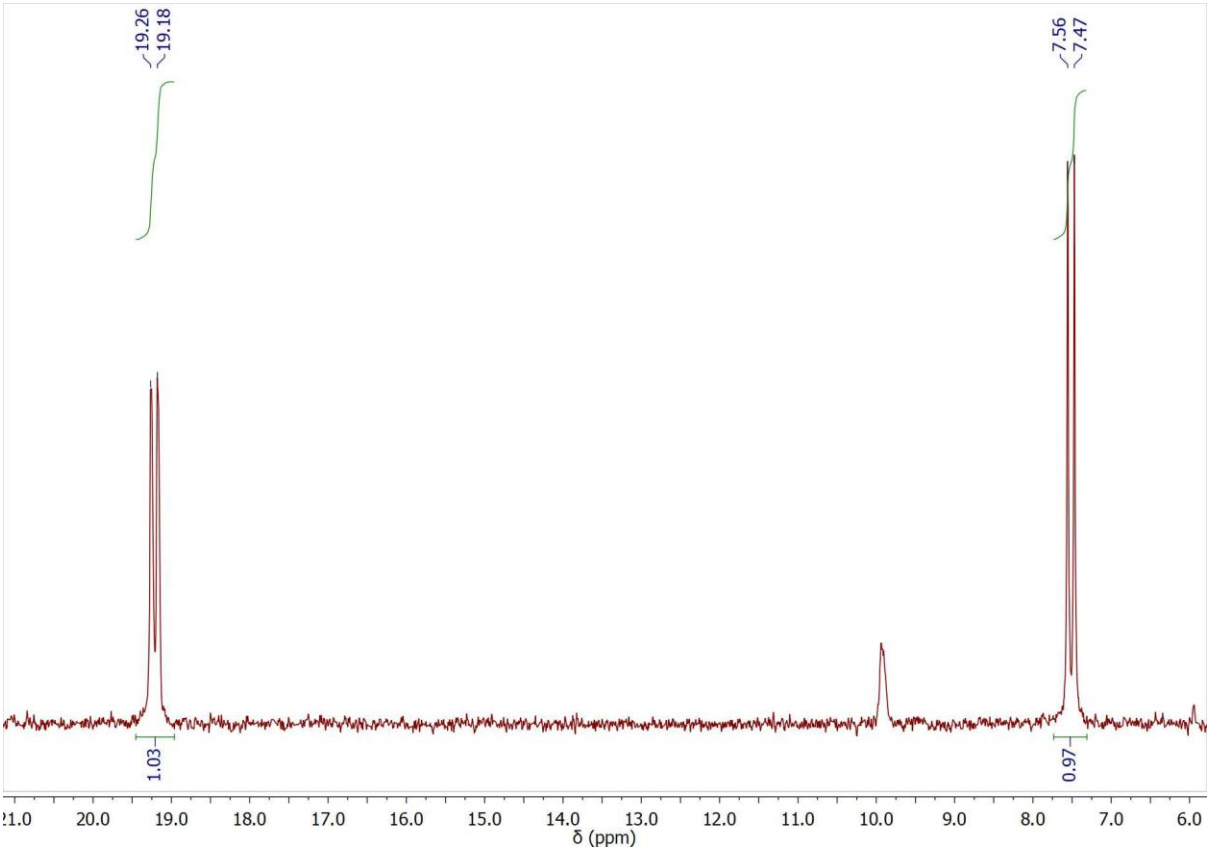

Figure S36 $^{31}P\{^{1}H\}$ NMR spectrum of intermediate **II** in CD_2Cl_2 at 268 K. Unknown species at δ_P 9.9 ppm.

NMR Spectra of intermediate VI

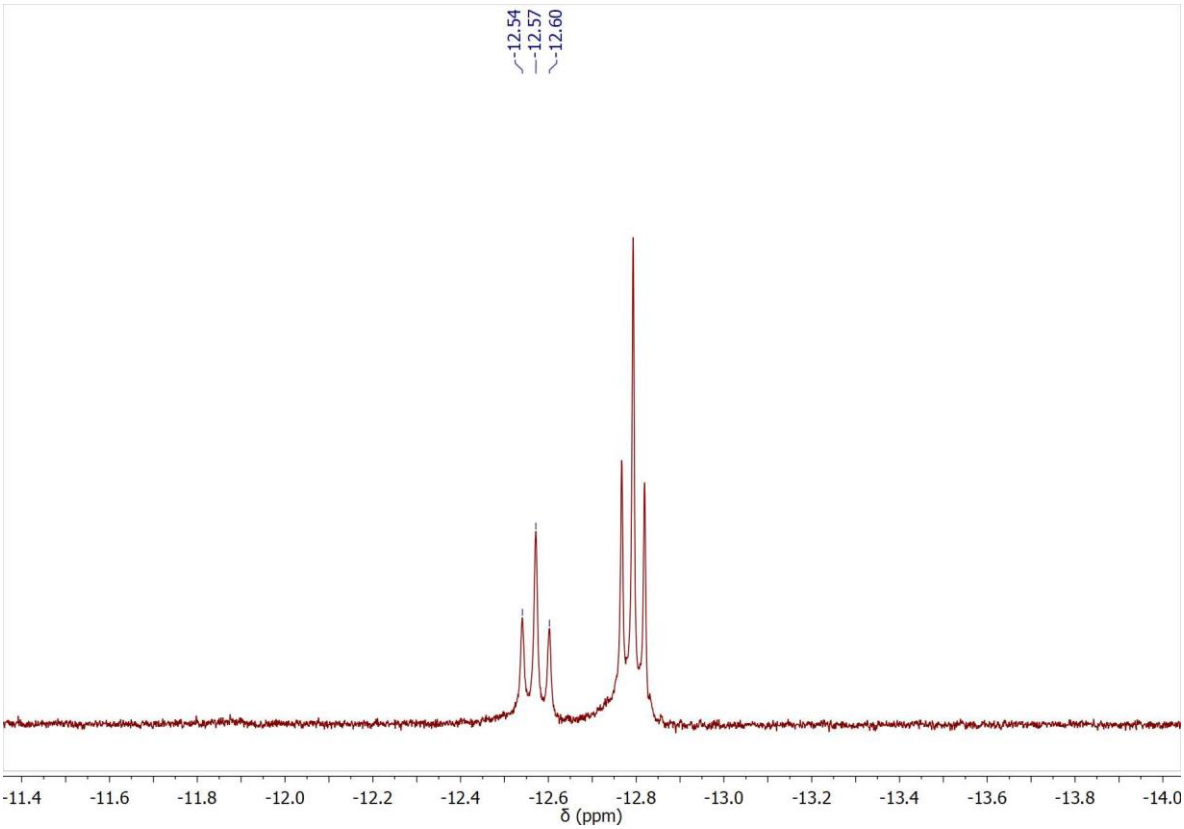

Figure S37 ^{1}H NMR spectrum at 259 K from the reaction between $[IrCl(COD)]_2$ and ligand **1** in CD_2Cl_2 highlighting intermediate **VI**.

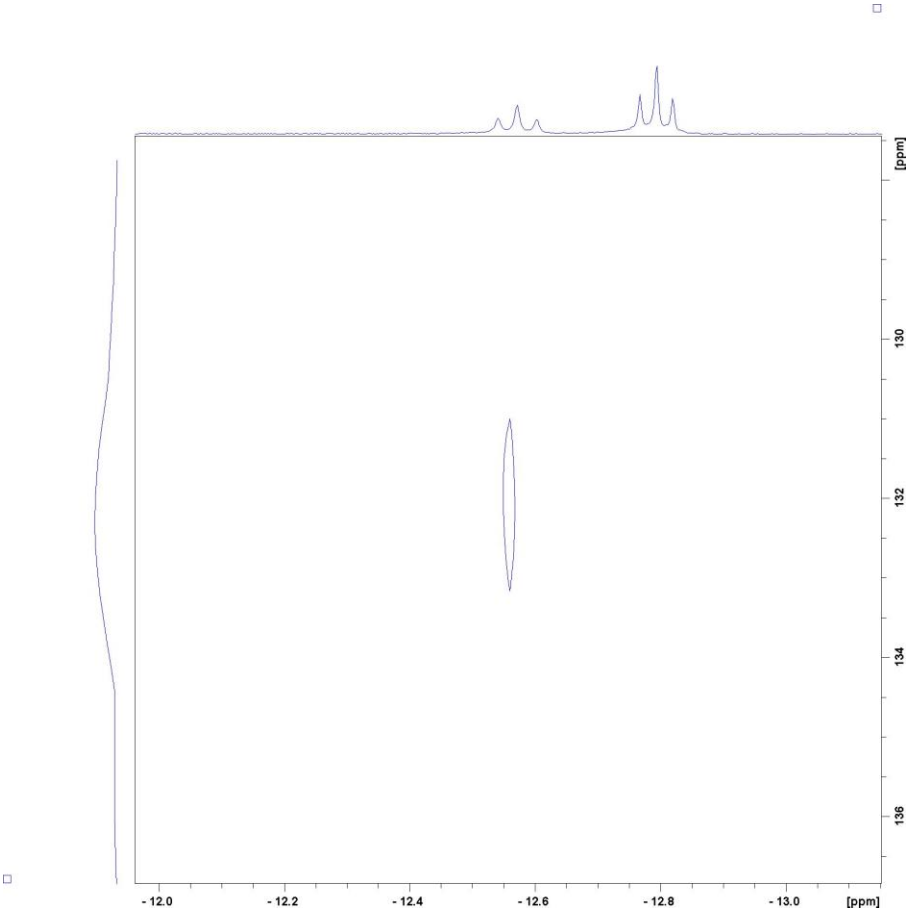

Figure S38 ^{1}H-^{13}C HMBC NMR spectrum of intermediate **VI** in CD_2Cl_2 at 259 K showing the correlation between the Ir-H resonance and a ^{13}C signal at 132.1 ppm, typical of a bound η^2-carbonyl with the same pincer ligand.[10]

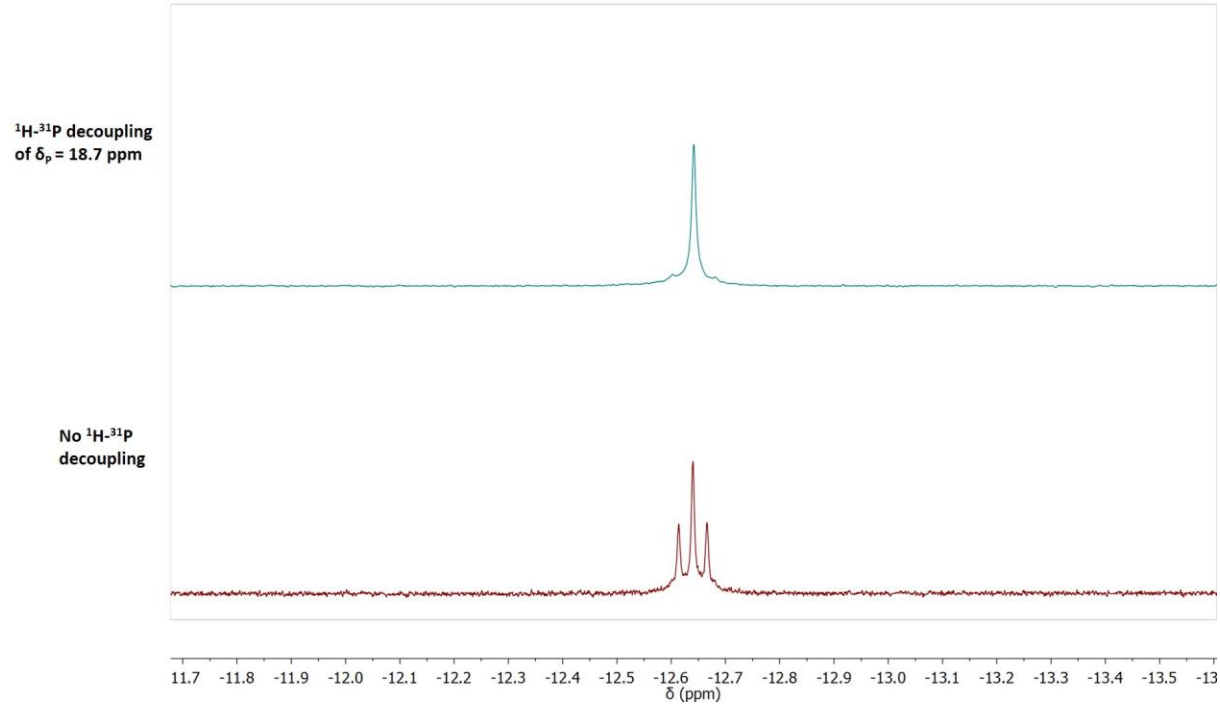

Figure S39 Comparison of ^{1}H and $^{1}H\{^{31}P\}$ NMR spectra of intermediate **VI** formed by reaction between intermediate **VII** and HCl in CD_2Cl_2 at 298 K, showing the Ir-H resonance at δ_H -12.64 ppm.

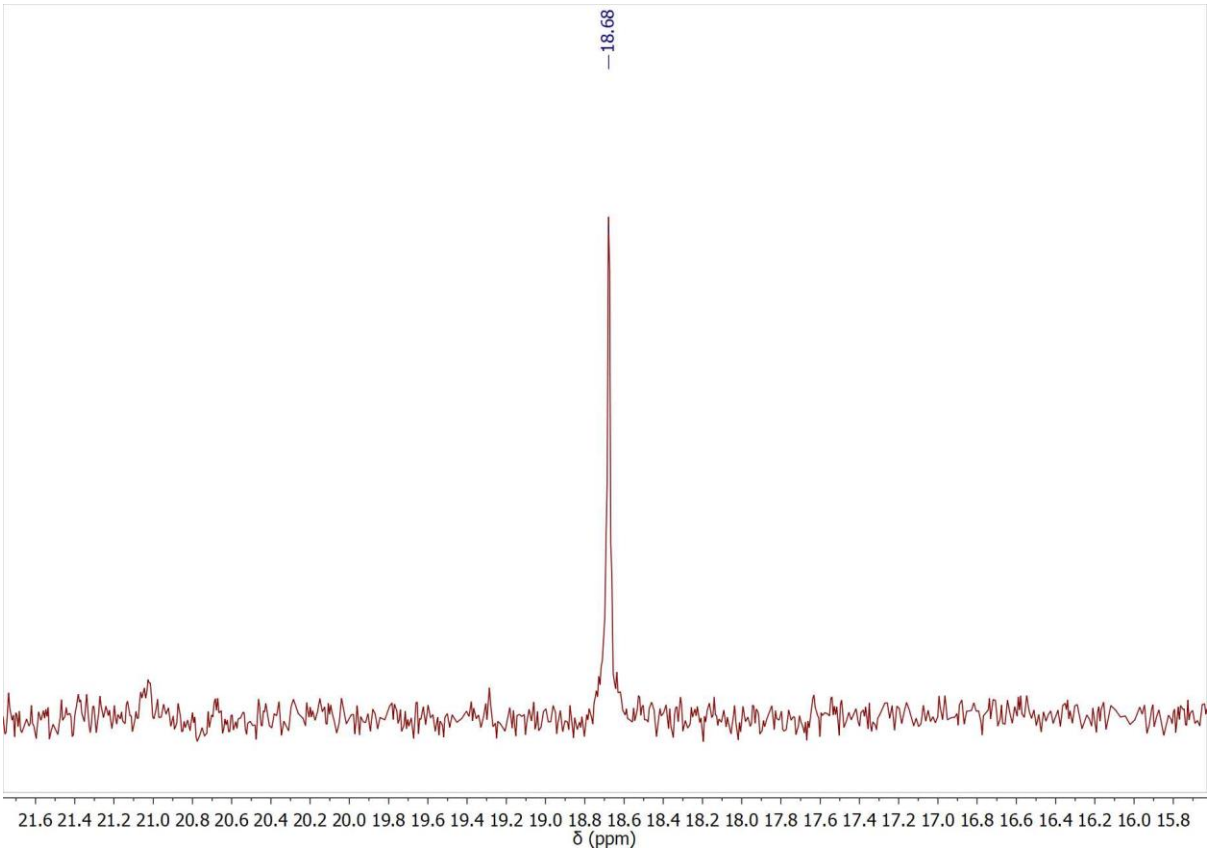

Figure S40 $^{31}P\{^{1}H\}$ NMR spectra of intermediate **VI** in CD_2Cl_2 at 298 K formed by reaction between intermediate **VII** and HCl.

NMR Spectra of complex VII

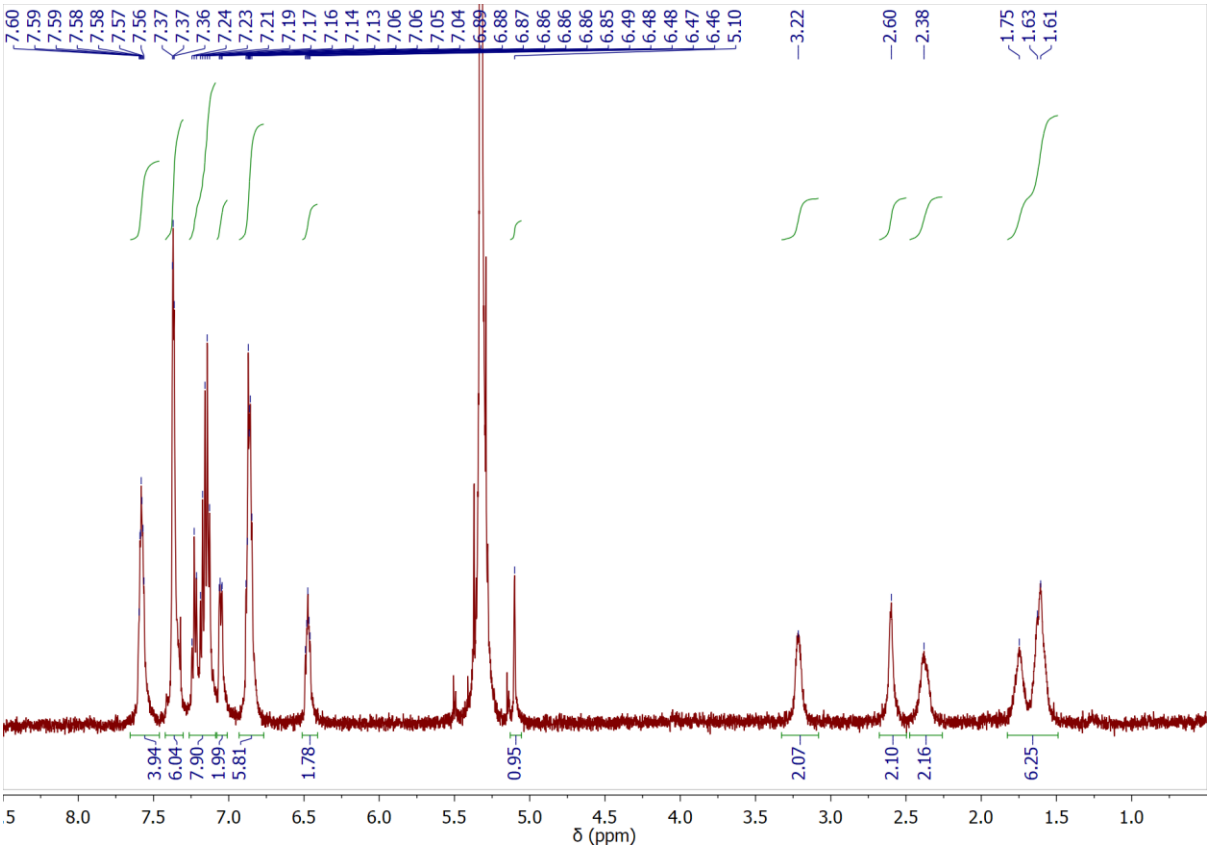

Figure S41 ^{1}H NMR spectrum of isolated complex **VII·CH_2Cl_2** in CD_2Cl_2 at 298 K.

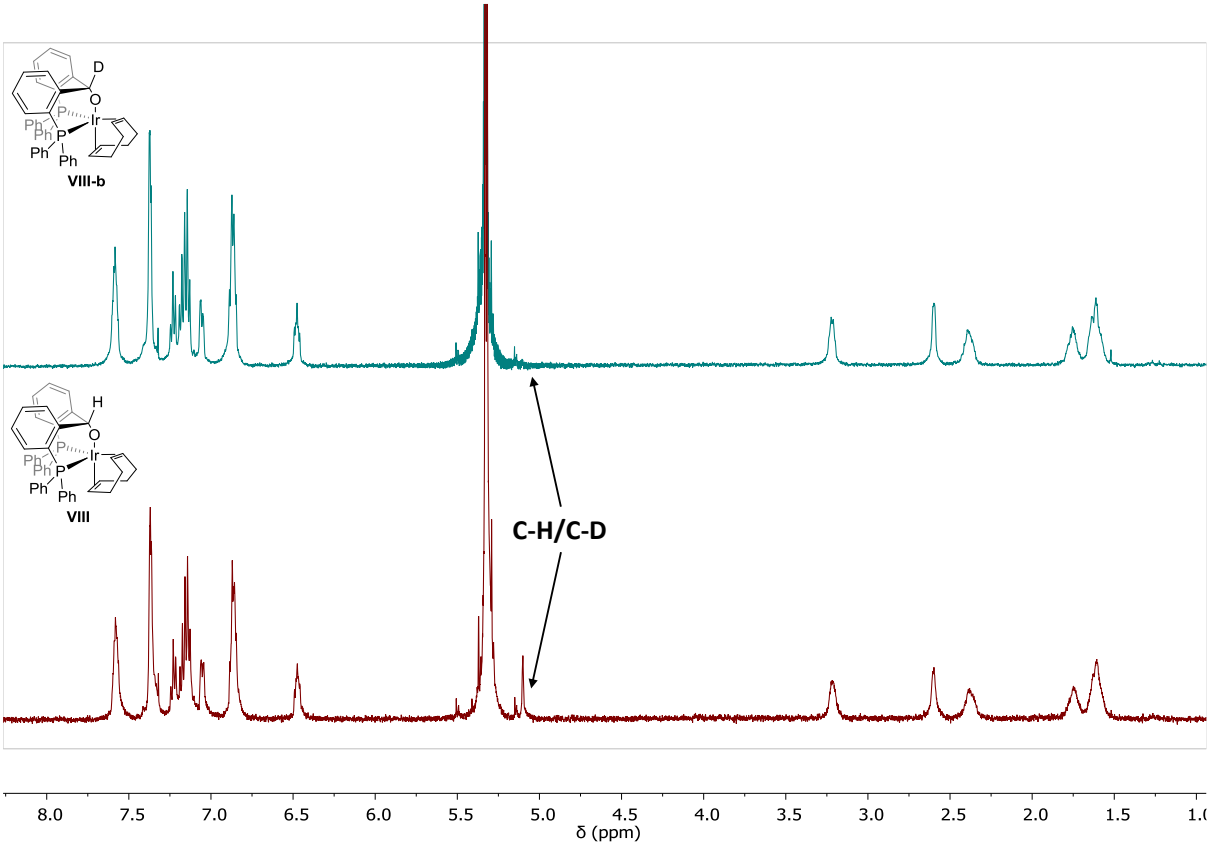

Figure S42 Comparison of ^{1}H NMR spectra in CD_2Cl_2 at 298 K highlighting the absence and presence of the methine resonance in **VII-b** and **VII** when ligands **1b** (top) or **1** (bottom) were used respectively.

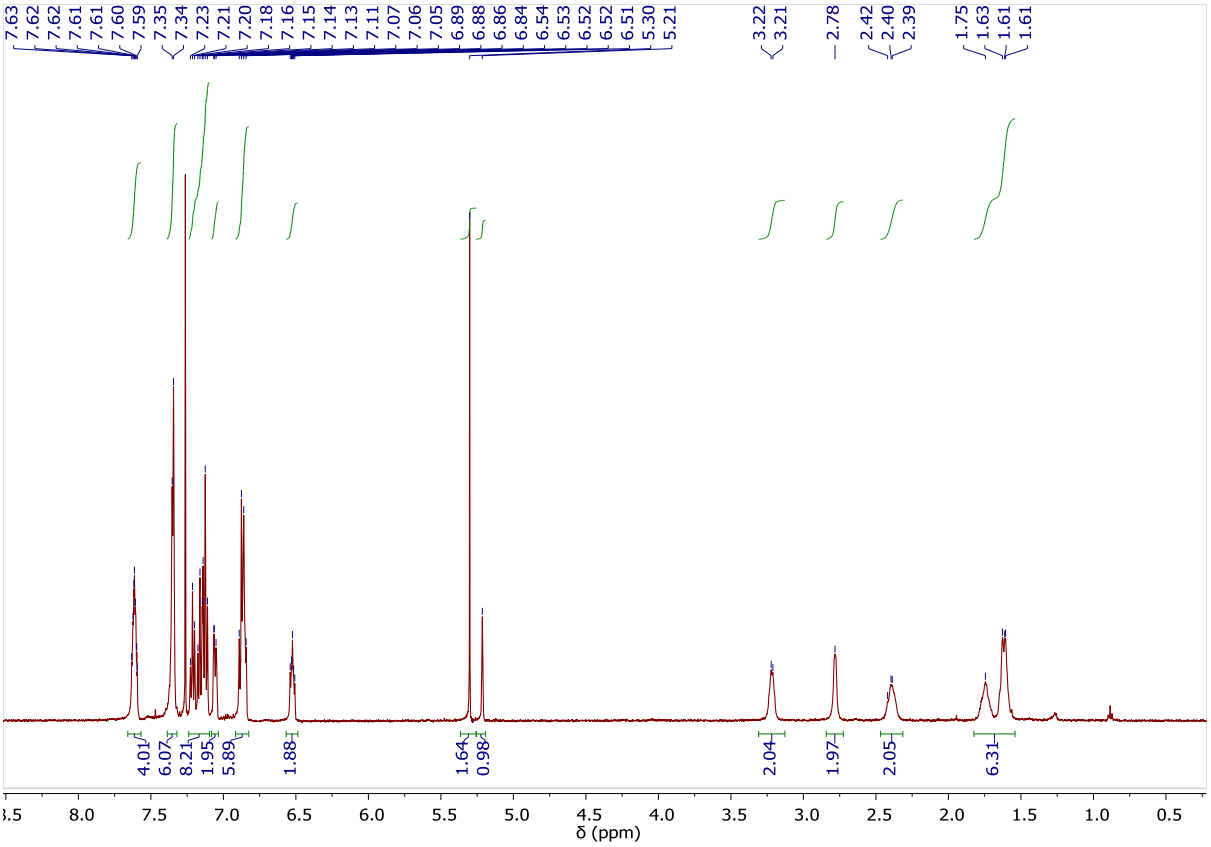

Figure S43 ^{1}H NMR spectrum of isolated complex **VII·CH_2Cl_2** in $CDCl_3$ at 298 K showing the one solvate molecule of CH_2Cl_2 at δ_H 5.30 ppm.

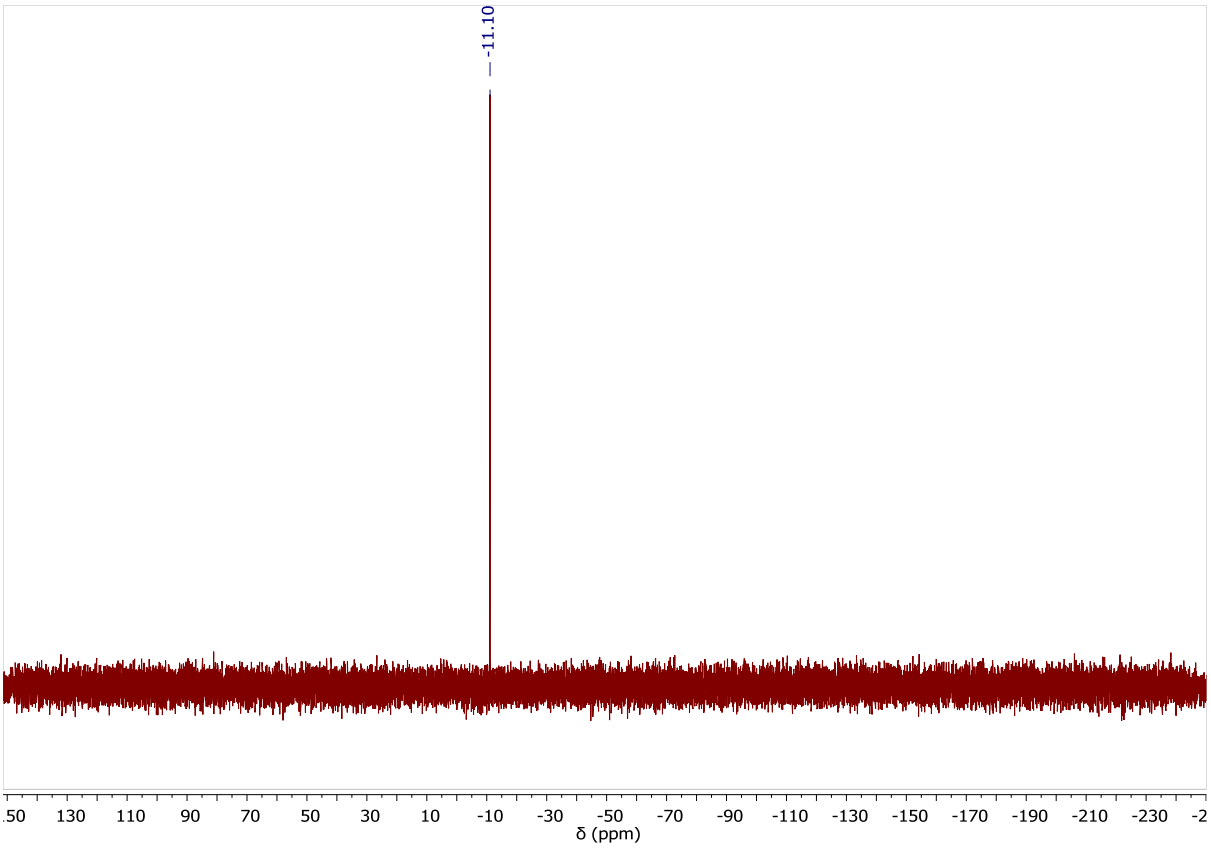

Figure S44 ^{31}P{^{1}H} NMR spectrum of complex **VII·CH_2Cl_2** in CD_2Cl_2 at 298 K.

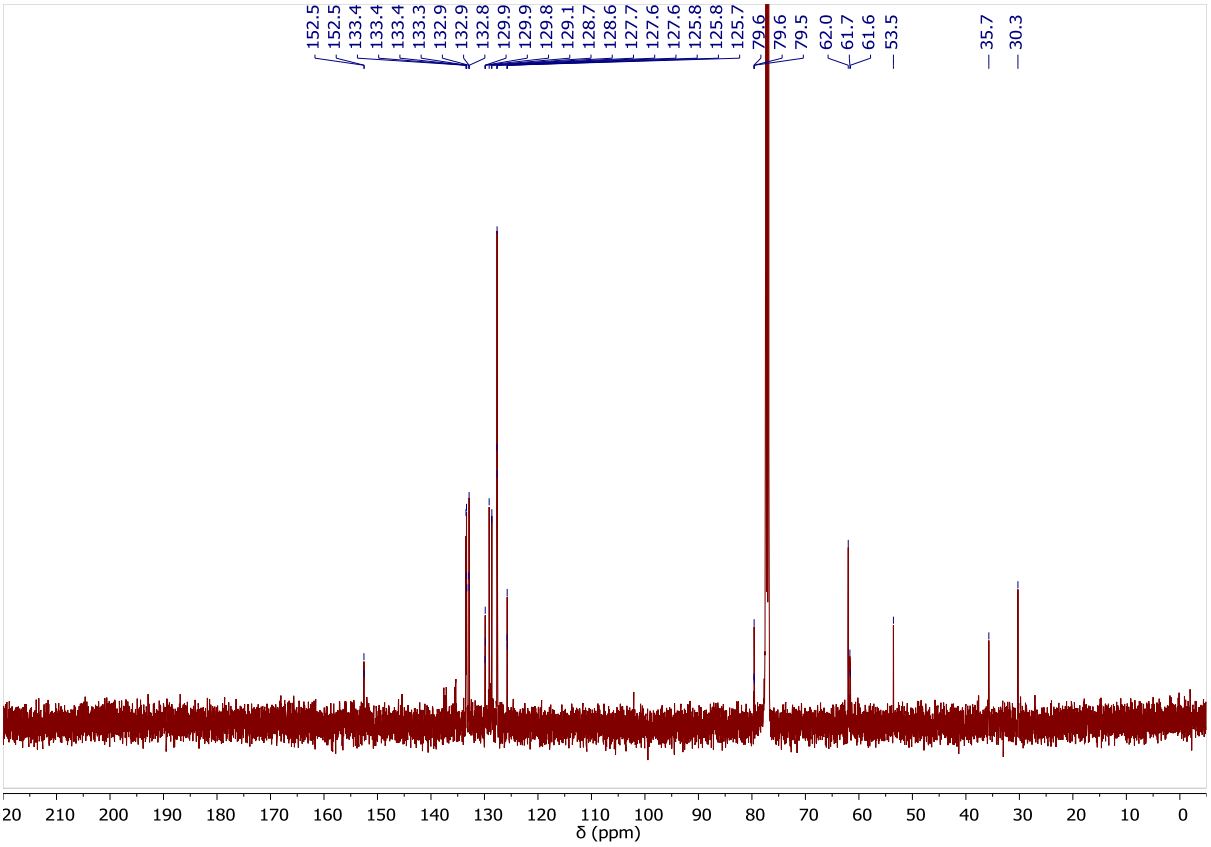

Figure S45 $^{13}C\{^{1}H\}$ NMR spectrum of complex **VII·CH_2Cl_2** in $CDCl_3$ at 298 K.

Addition of HCl to complex VII

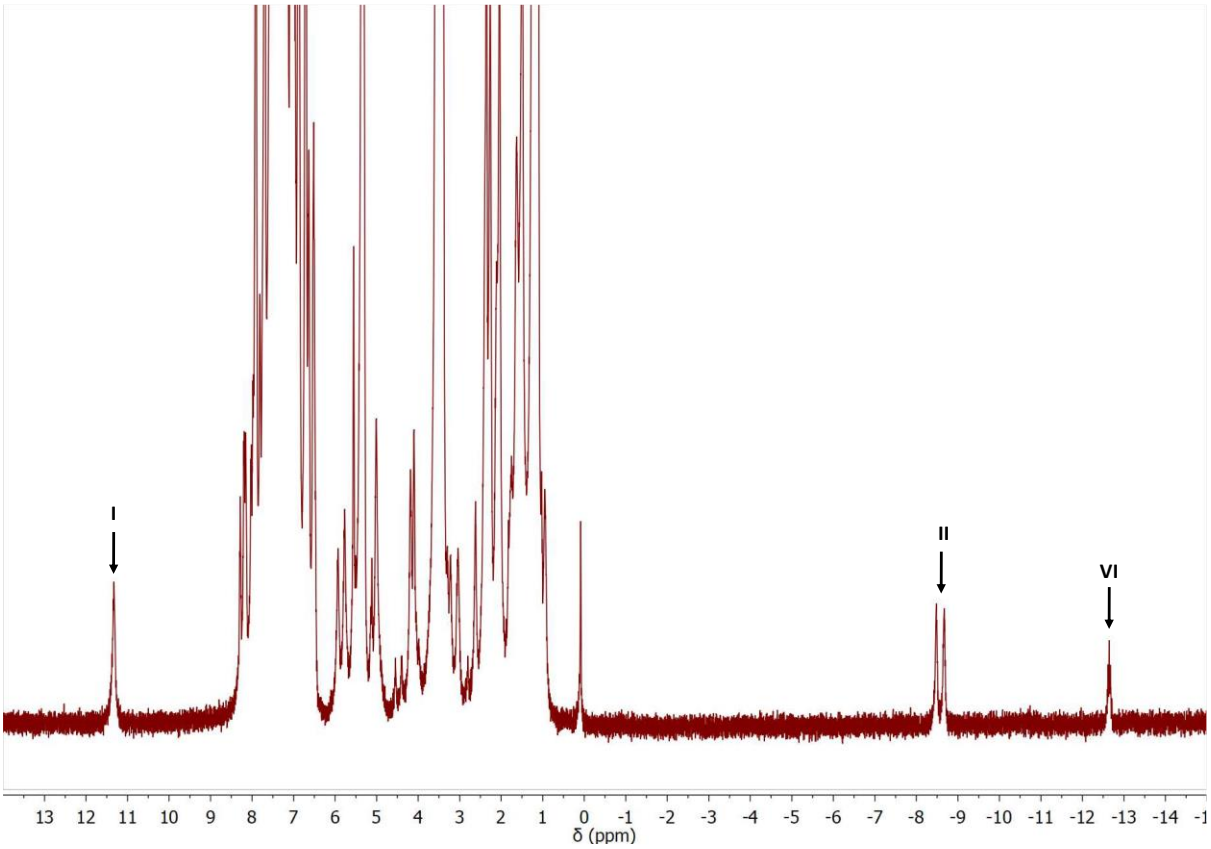

Figure S46 ^{1}H NMR spectrum at 298 K taken 1 min after reacting complex **VII·CH_2Cl_2** with HCl in CD_2Cl_2, highlighting the formation of intermediates **I**, **II**, and **VI**.

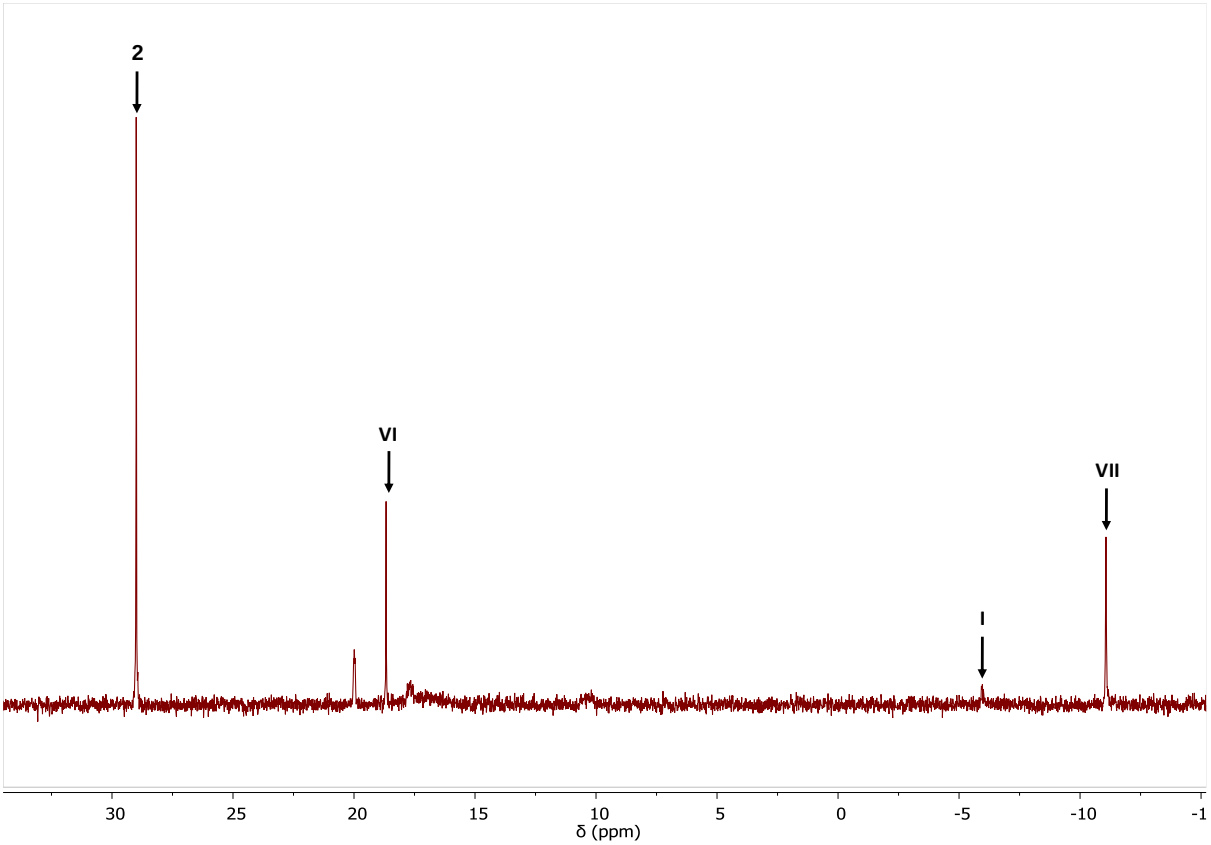

Figure S47 $^{31}P\{^{1}H\}$ NMR spectrum at 298 K taken 2 min after reacting complex **VII·CH_2Cl_2** with HCl in CD_2Cl_2, highlighting the formation of intermediates **I**, **VI**, and product **2**. Intermediate **II** is not clearly visible, likely due to fluxionality in solution.

Reaction between 1-H_2 and [IrCl(COD)]$_2$ under a H_2 atmosphere

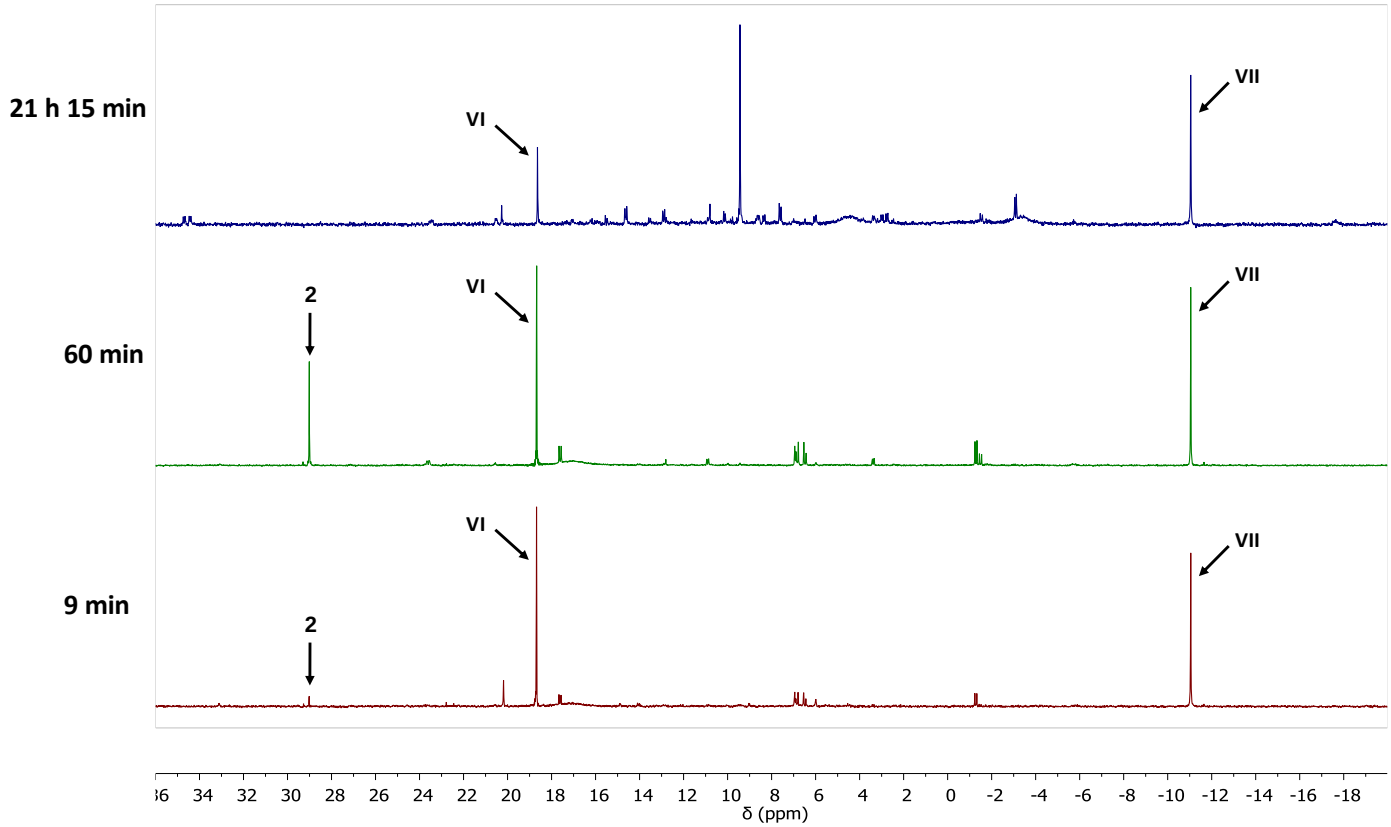

Figure S48 $^{31}P\{^1H\}$ NMR spectra at 298 K after reacting **1-H_2** and [IrCl(COD)]$_2$ under a H_2 atmosphere in CD_2Cl_2, highlighting the formation of intermediates **VI**, **VII·CH_2Cl_2** and product **2**. The absence of the peak for **2** after 21 h 15 min indicates that **2** is unstable over long periods in these conditions.

Mass spectrum of complex 2

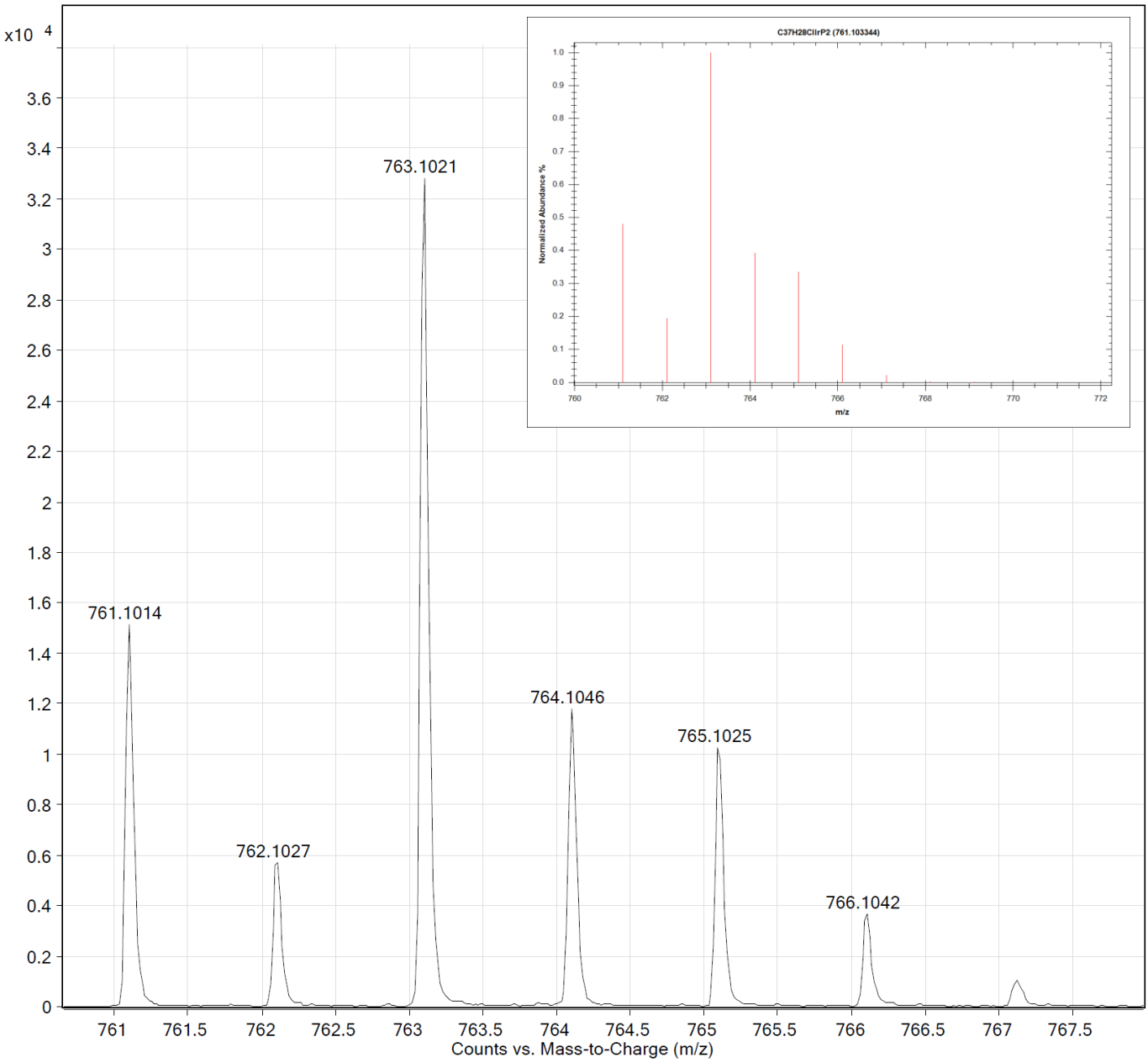

Figure S49 Positive mode HRMS (ESI-TOF) spectrum of $[M+H]^+$ ion of **2**. Inset shows expected isotope pattern.

Mass spectrum of complex 3

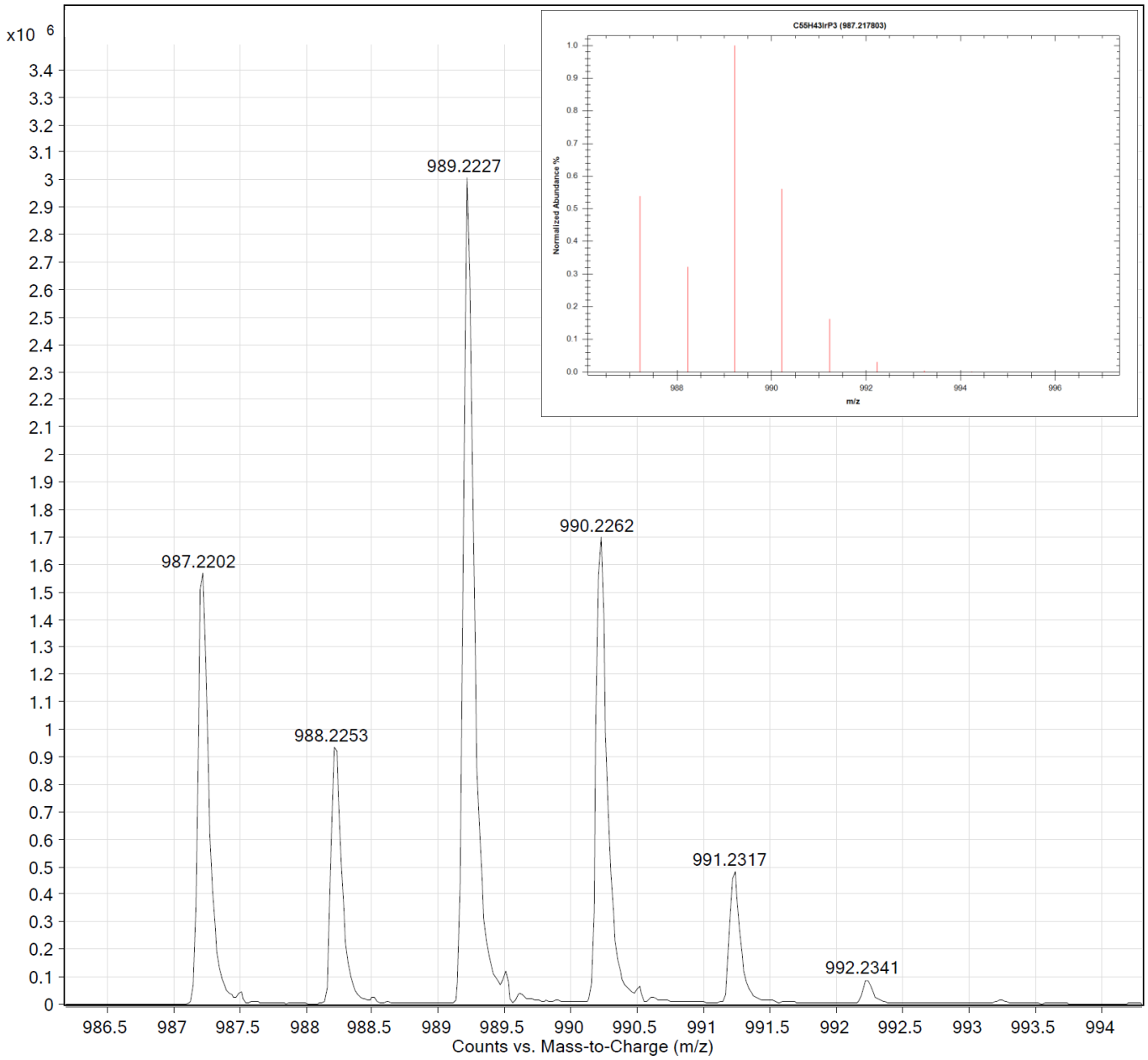

Figure S50 Positive mode HRMS (ESI-TOF) spectrum of $[M]^+$ ion of **3**. Inset shows expected isotope pattern.

Mass spectrum of complex 4

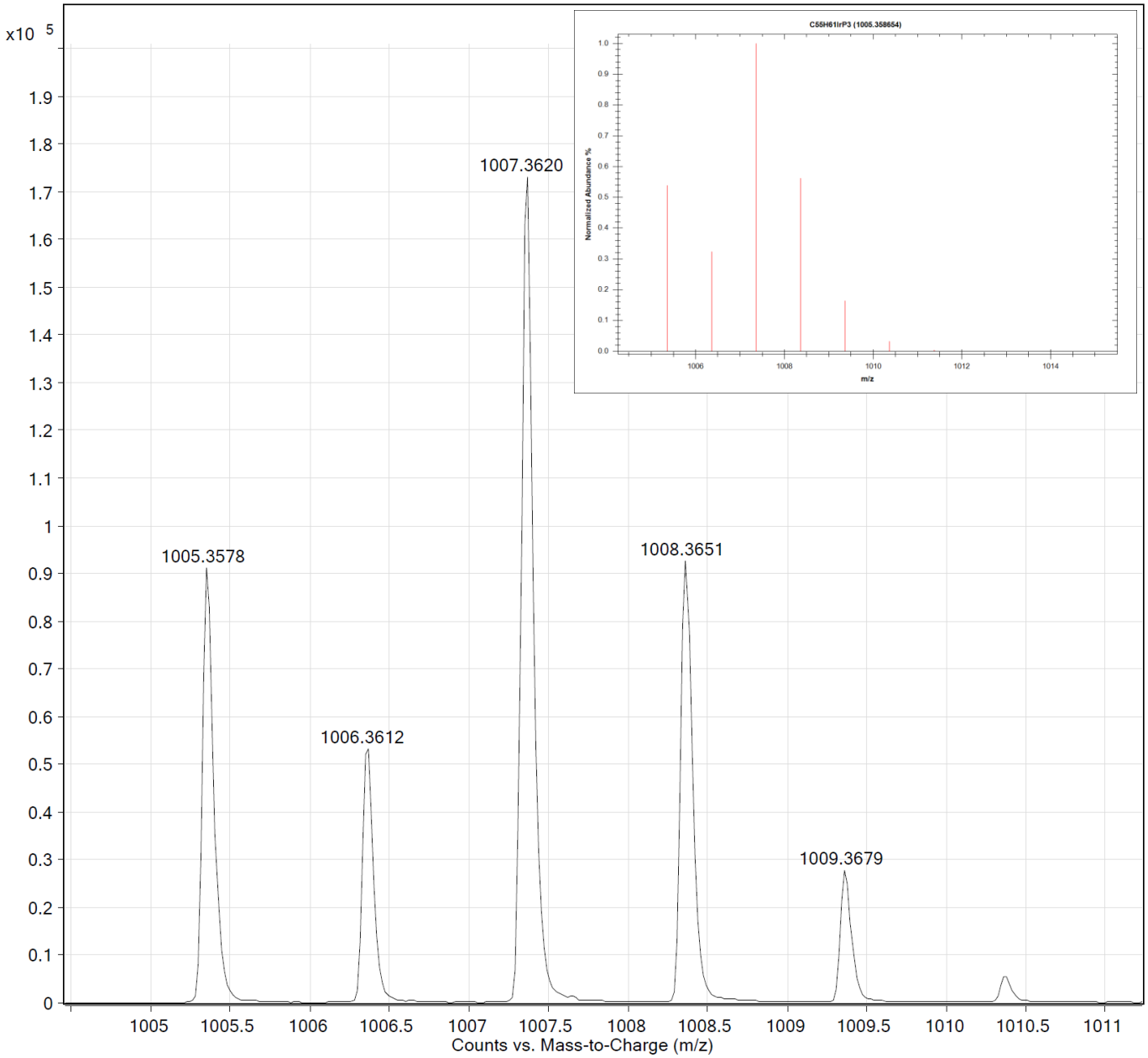

Figure S51 Positive mode HRMS (ESI-TOF) spectrum of $[M]^+$ ion of **4**. Inset shows expected isotope pattern.

Mass spectrum of complex 5

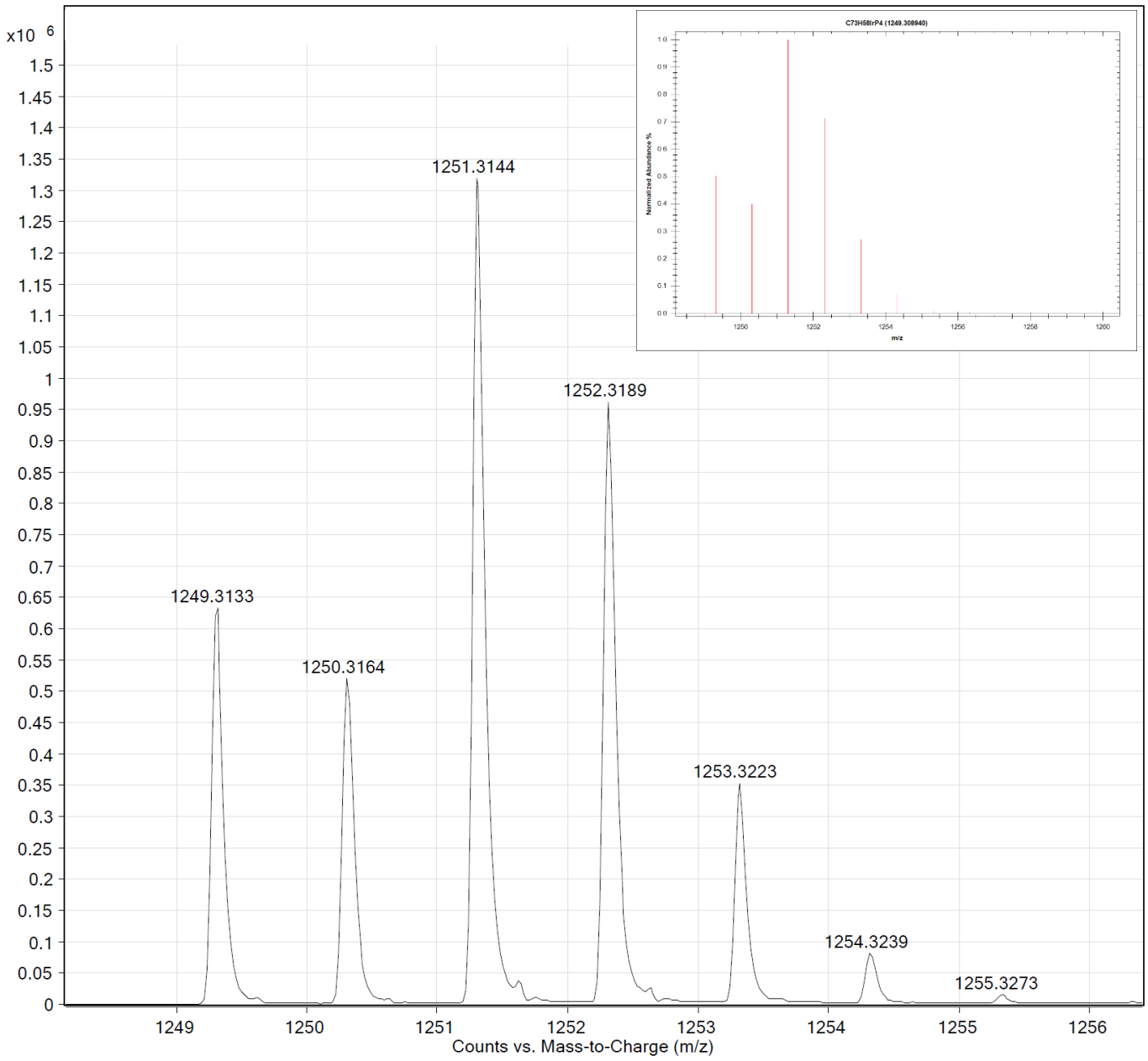

Figure S52 Positive mode HRMS (ESI-TOF) spectrum of $[M]^+$ ion of **5**. Inset shows expected isotope pattern.

Mass spectrum of complex 6

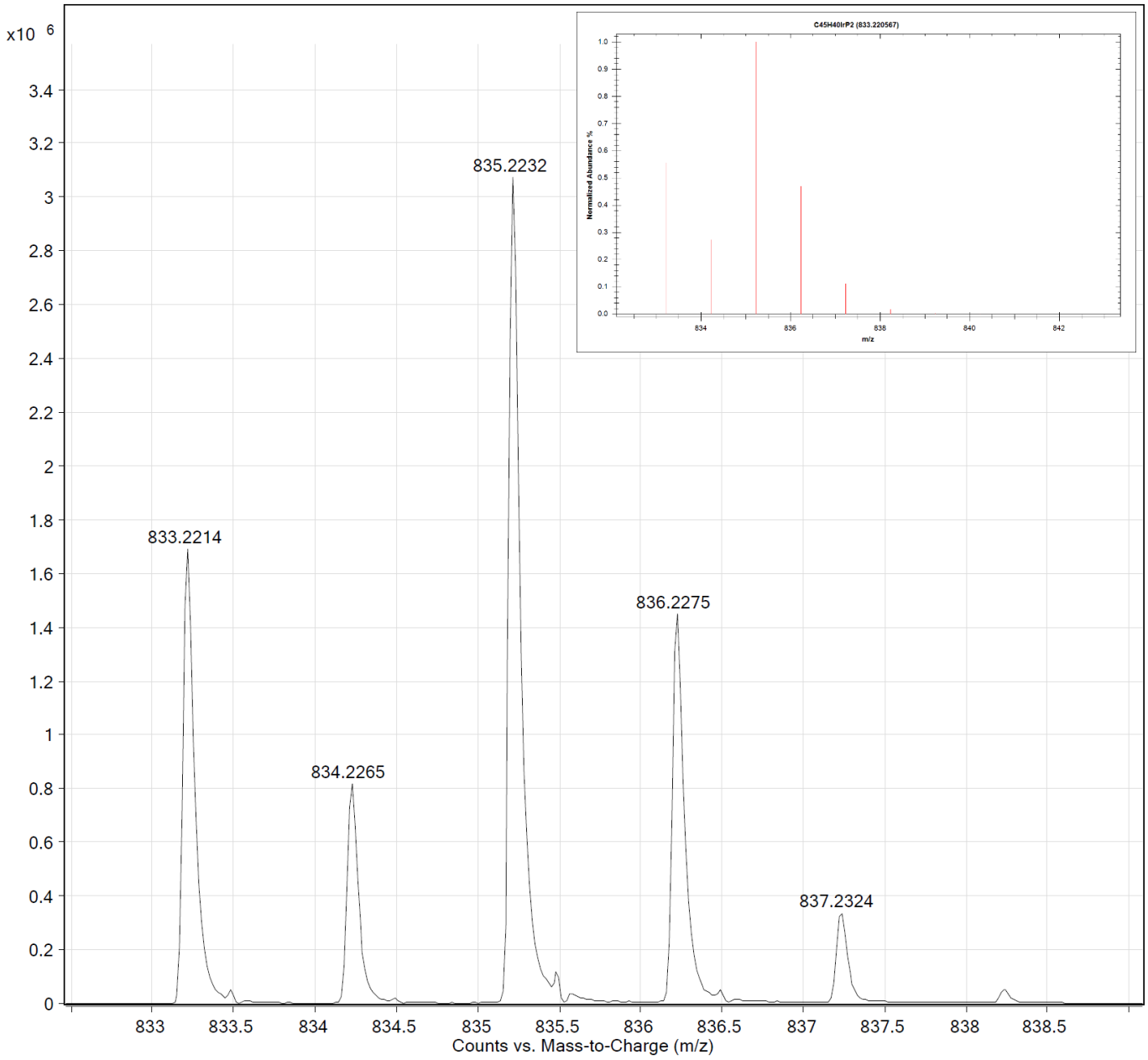

Figure S53 Positive mode HRMS (ESI-TOF) spectrum of $[M]^+$ ion of **6**. Inset shows expected isotope pattern.

Mass spectrum of complex 7a

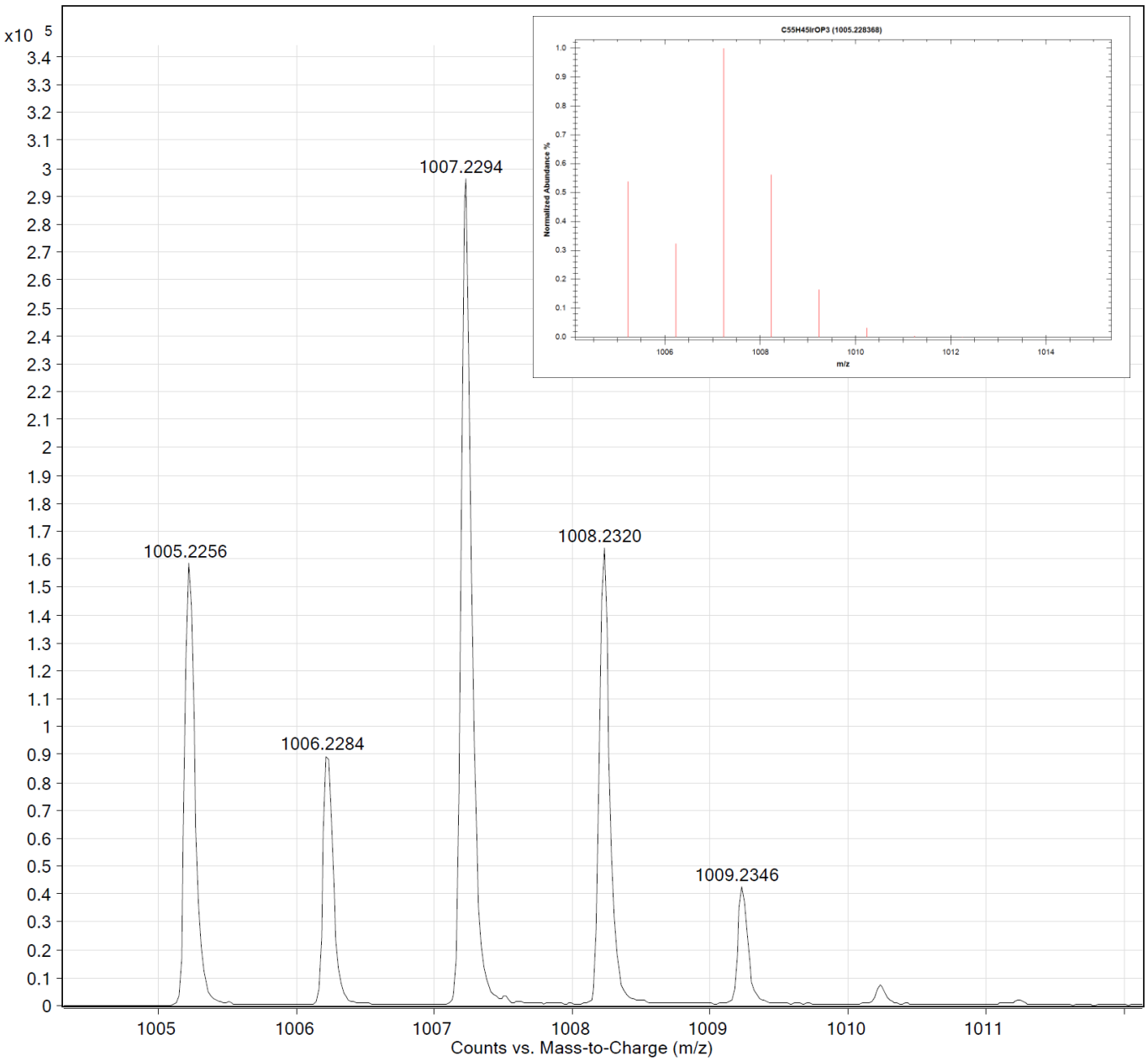

Figure S54 Positive mode HRMS (ESI-TOF) spectrum of $[M\text{-}Cl]^+$ ion of **7a**. Inset shows expected isotope pattern.

Mass spectrum of complex VII

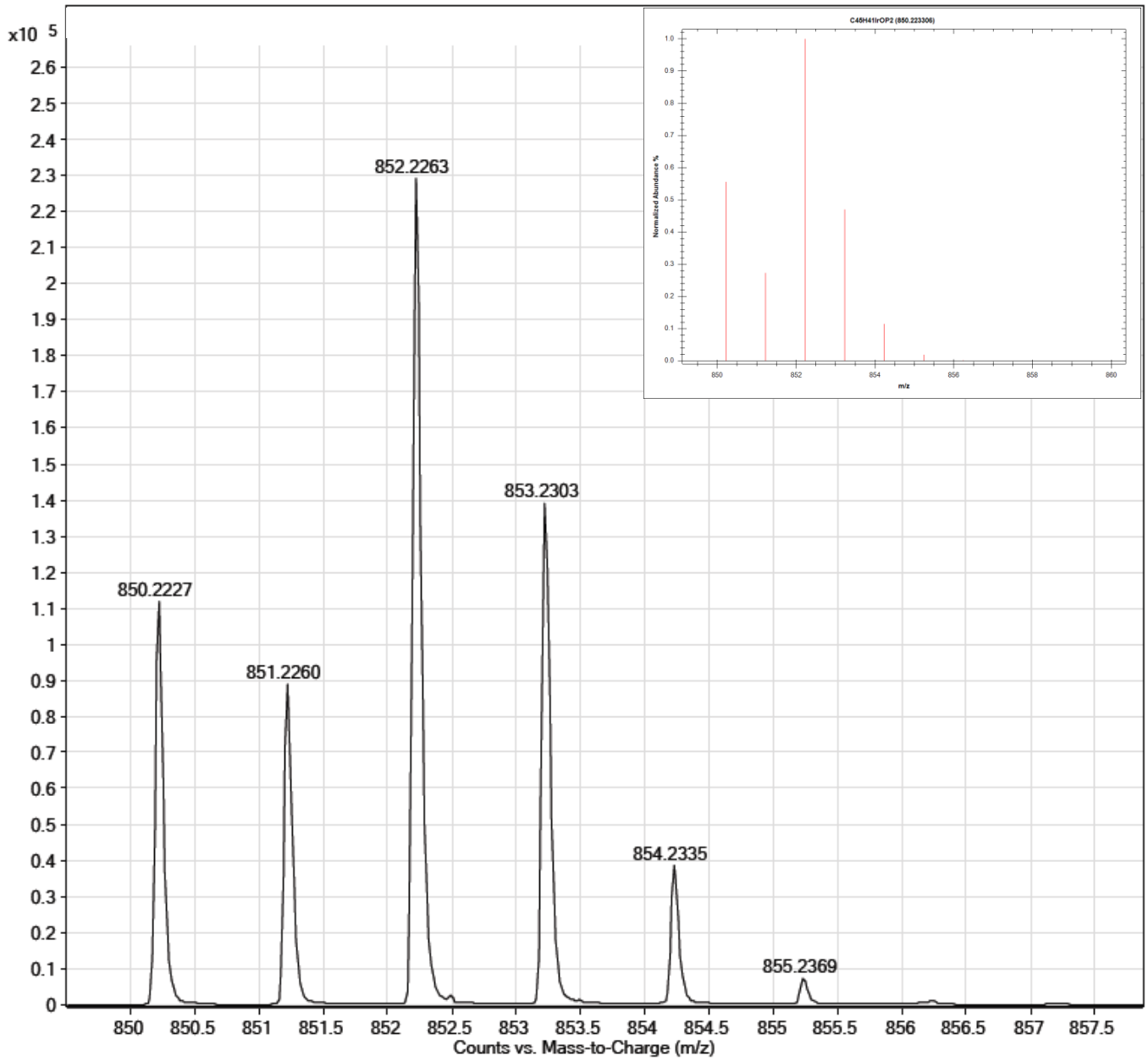

Figure S55 Positive mode HRMS (ESI-TOF) spectrum of $[M]^+$ ion of **VII**. Inset shows expected isotope pattern.

X-Ray Crystallography Data

Crystallographic data table

Data	2	3	4	5	6	7b	VII
Formula	$C_{37}H_{28}ClIrP_2$	$C_{87}H_{55}BF_{24}IrP_3$	$C_{87}H_{73}BF_{24}IrP_3$	$C_{105}H_{70}BF_{24}IrP_4 \cdot 0.5CH_2Cl_2$	$C_{77}H_{52}BF_{24}IrP_2 \cdot C_6H_{14}$	$C_{55}H_{45}ClIrO_3P_3$	$C_{45}H_{41}IrOP_2 \cdot CH_2Cl_2$
Formula weight	762.25	1852.31	1870.45	2157.06	1784.38	1042.55	936.91
Colour	Green	Dark green	Dark green	Light yellow	Colourless	Colourless	Yellow
Crystal size / mm³	0.087 × 0.112 × 0.135	0.117 × 0.119 × 0.574	0.144 × 0.223 × 0.271	0.140 × 0.200 × 0.335	0.071 × 0.113 × 0.121	0.67 × 0.084 × 0.131	0.120× 0.153 × 0.215
Temperature / K	100	100	100	100	100	100	100
Crystal system	Orthorhombic	Triclinic	Triclinic	Triclinic	Triclinic	Triclinic	Triclinic
Space group	F d d 2	P -1	P -1	P -1	P -1	P -1	P -1
***a* / Å**	32.741(2)	13.6373(16)	20.144(2)	12.7542(6)	12.8273(6)	12.6314(7)	10.5803(9)
***b* / Å**	18.6304(11)	18.2263(18)	20.626(2)	17.2595(7)	17.8318(8)	18.2527(12)	13.0617(14)
***c* / Å**	9.7858(6)	18.3369(19)	21.132(3)	22.2988(10)	18.1429(7)	21.5647(14)	15.0671(17)
α / °	90	109.090(3)	104.677(3)	73.9920(15)	61.9894(14)	102.884(2)	90.099(3)
β / °	90	93.332(4)	100.375(3)	74.3769(18)	78.9200(14)	99.609(2)	99.829(3)
γ / °	90	102.372(4)	95.711(3)	83.4459(16)	87.8968(17)	97.872(2)	112.011(4)
***V* / Å³**	5969.1(4)	4166.3(4)	8257.0(10)	4539.8(2)	3588.61(14)	4699.6(3)	1897.2(2)
Z	8	2	4	2	2	4	2
ρ_{calcd} **/ g cm⁻³**	1.696	1.476	1.505	1.578	1.611	1.473	1.640
Radiation used	Mo-Kα	Mo-Kα	Mo-Kα	Mo-Kα	Mo-Kα	Mo-Kα	Mo-Kα
***μ* / mm⁻¹**	4.696	1.757	1.774	1.670	2.013	3.039	3.781
***2θ max* / °**	53.0	52.8	52.9	52.8	52.8	52.8	55.1
No. of unique reflns	27124	16947	33744	18523	14641	19153	8714
No. of variables	396	2456	4305	1380	1744	2313	469
GoF (S)	1.00	1.00	1.03	1.02	1.04	1.01	1.09
R factor (I > 2σ)	0.025 (2816 reflections)	0.075 (13694 reflections)	0.068 (21251 reflections)	0.039 (16063 reflections)	0.040 (12972 reflections)	0.062 (12255 reflections)	0.033 (7867 reflections)

Table S1 Crystal Data, Data Collection and Refinement Parameters for the structures of **2** – **6**, **7b** and **VII**.

X-ray crystal structures

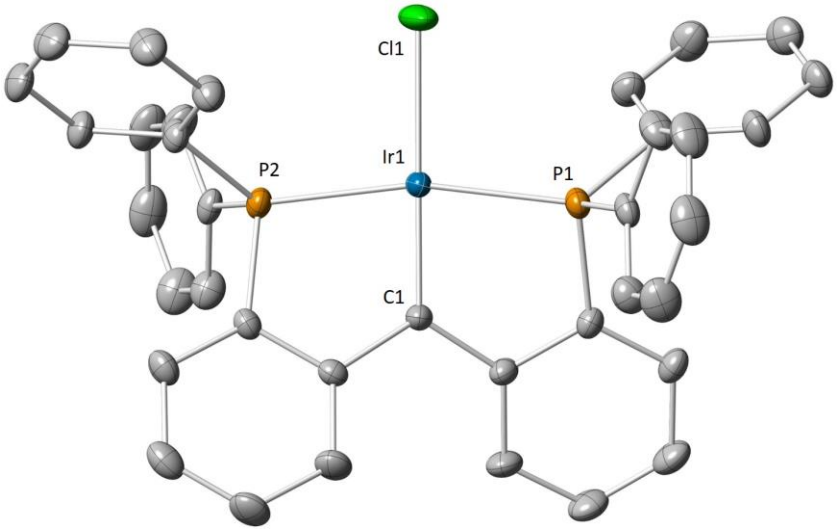

Figure S56 Molecular structure of **2** (50% probability thermal ellipsoids). Hydrogen atoms omitted for clarity.

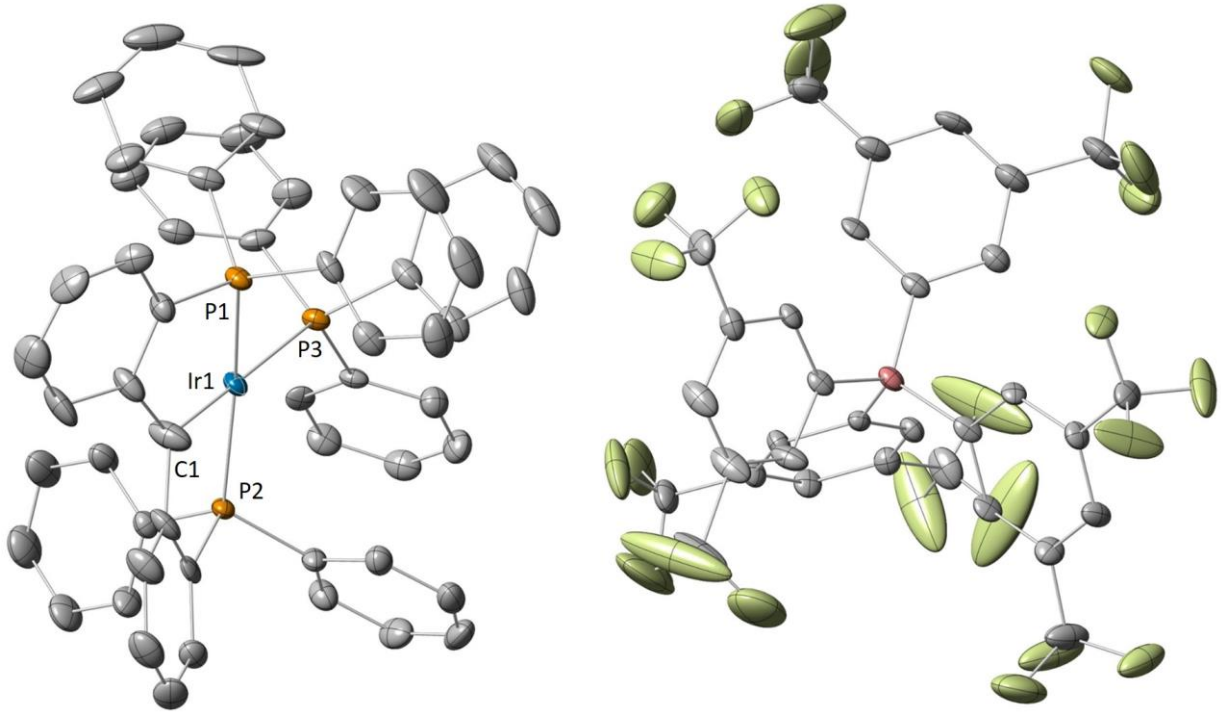

Figure S57 Molecular structure of **3** (50% probability thermal ellipsoids). Hydrogen atoms omitted for clarity.

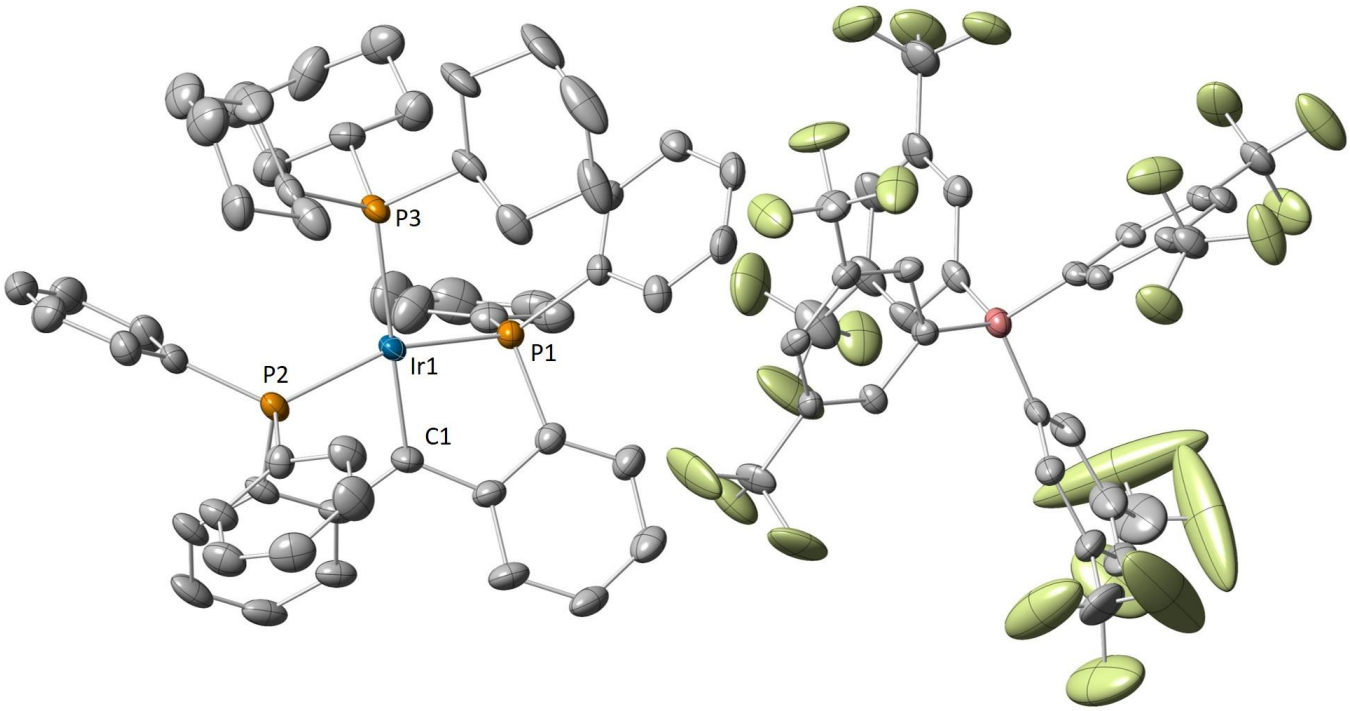

Figure S58 Molecular structure of **4** (50% probability thermal ellipsoids). Hydrogen atoms omitted for clarity.

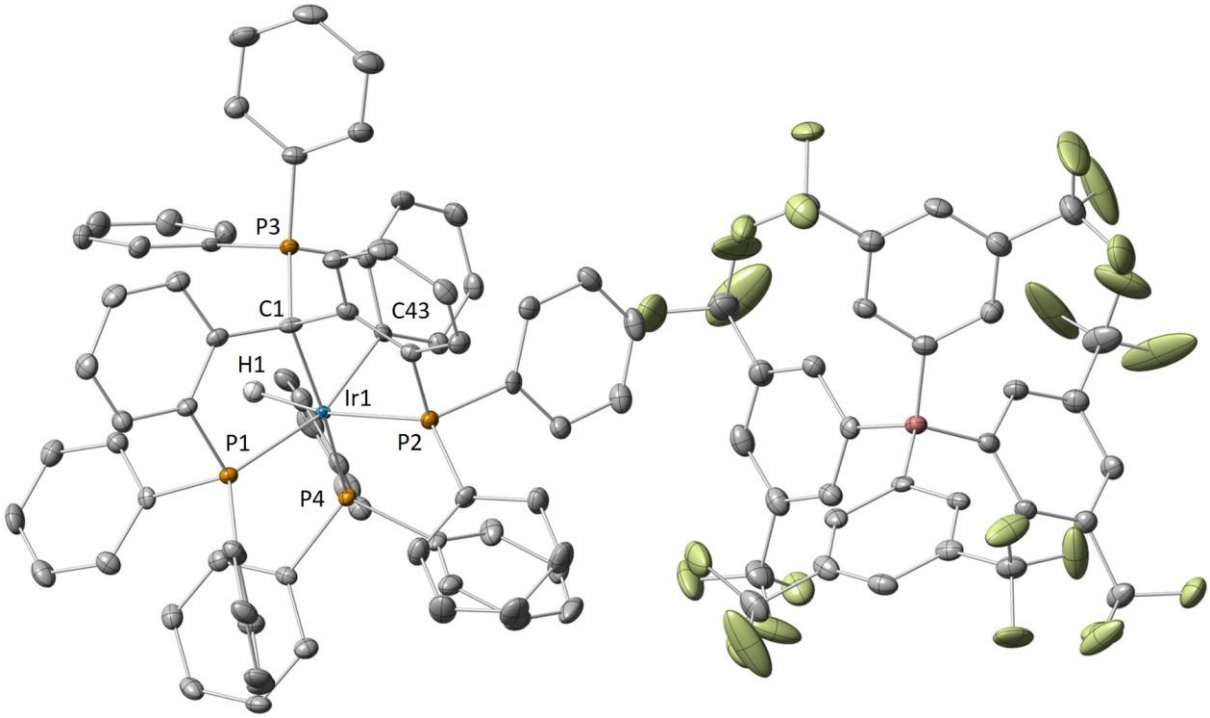

Figure S59 Molecular structure of **5·CH_2Cl_2** (50% probability thermal ellipsoids). Hydrogen atoms except for H1 omitted for clarity.

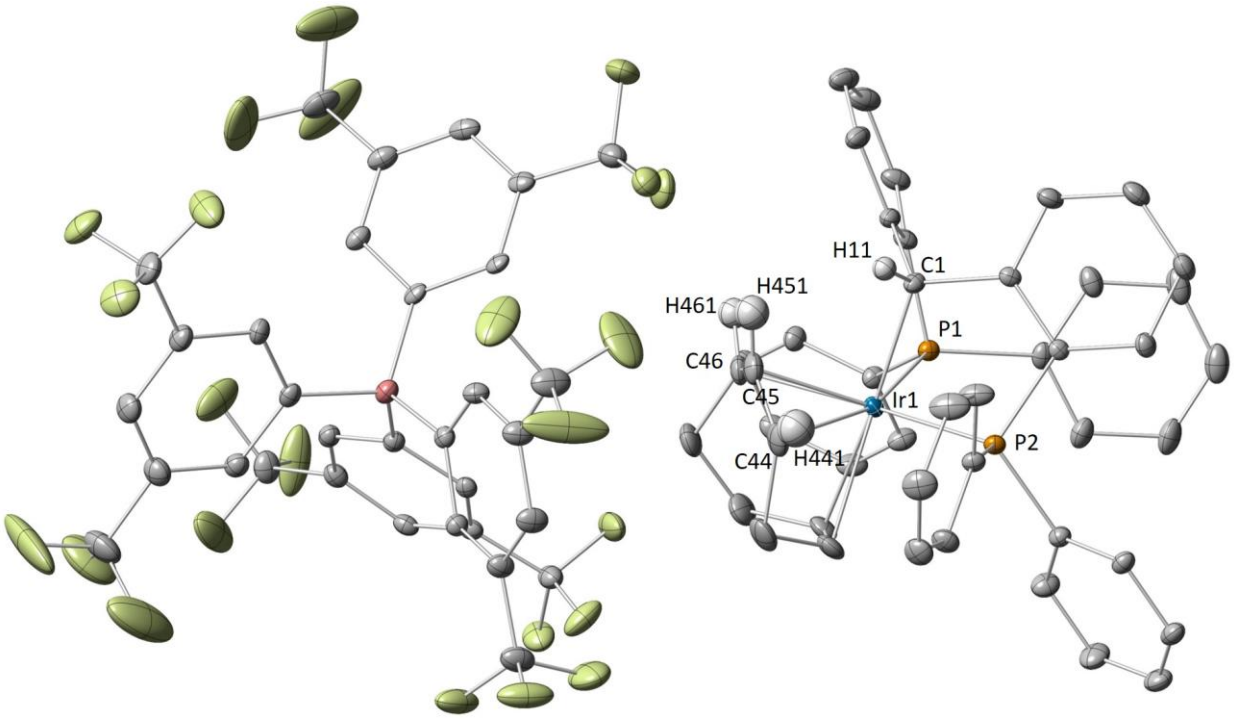

Figure S60 Molecular structure of **6·C_6H_{14}** (50% probability thermal ellipsoids). Hydrogen atoms except for H11, H441, H451, and H451 omitted for clarity.

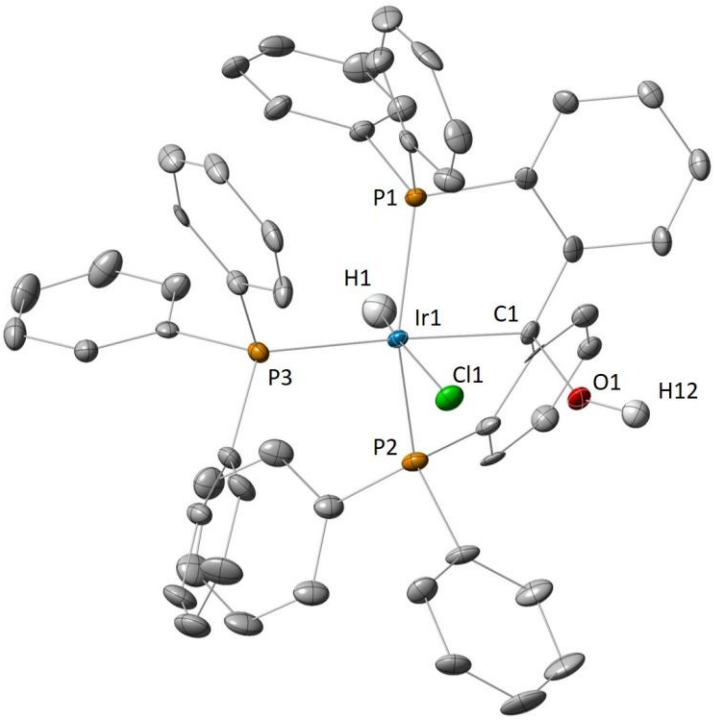

Figure S61 Molecular structure of **7b** (50% probability thermal ellipsoids). Hydrogen atoms except for H1 and H12 omitted for clarity.

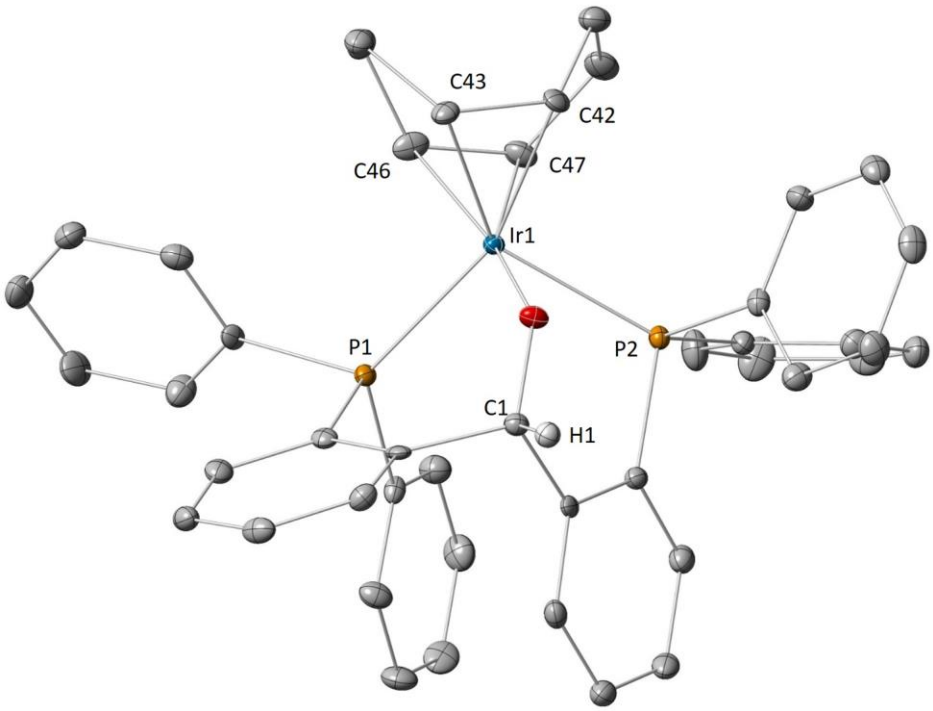

Figure S62 Molecular structure of **VII·CH_2Cl_2** (50% probability thermal ellipsoids). Hydrogen atoms except for H1 omitted for clarity.

References

(1) Y. Nakamura, N. Yoshikai, L. Ilies and E. Nakamura, *Org. Lett.*, 2012, **14**, 3316–3319.

(2) Q. Jing, C. A. Sandoval, Z. Wang and K. Ding, *Eur. J. Org. Chem.* 2006, **2006** (16), 3606–3616.

(3) S. Sung, J. K. Boon, J. J. C. Lee, N. A. Rajabi, S. A. Macgregor, T. Krämer and R. D. Young, *Organometallics*, 2017, **36**, 1609-1617.

(4) J. L. Herdé, J. C. Lamber, C. V. Senoff, *Inorganic Syntheses* 1974, **15**, 18–20.

(5) S. Chen, E. Manoury and R. Poli, *Eur. J. Inorg. Chem.*, 2014, **2014**, 5820–5826.

(6) N. A. Yakelis and R. G. Bergman, *Organometallics* 2005, **24**, 3579–3581.

(7) B. Guzel, M. A. Omary, J. P. Fackler and A. Akgerman, *Inorganica Chim. Acta* 2001, **325**, 45–50.

(8) P. J. Stang, Y.-H. Huang, *J. Organomet. Chem* 1992, **435** (1-2), 185–192.

(9) L. E. Doyle, W. E. Piers, J. Borau-Garcia, M. J. Sgro and D. M. Spasyuk, *Chem. Sci*. 2016, **7**, 921–931.

(10) A similar ^{13}C NMR chemical shift for a bound η^2-carbonyl carbon ligand was observed for a previously described rhodium complex in Reference 3.

.